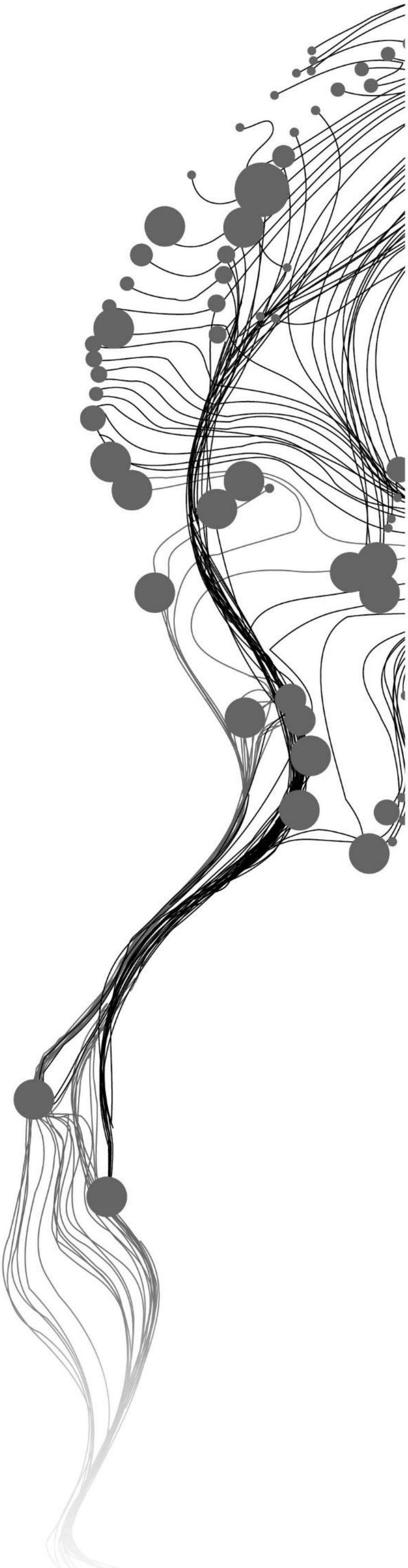

EFFECT OF CROWN SIZE AND SHAPE OF DIFFERENT TEMPERATE TREE SPECIES ON MODELLING AGB AND AGC USING UAV IMAGES

ALEJANDRA TORRES RODRIGUEZ
September,2020

SUPERVISORS:
Dr. Y.A. Hussin (ITC-NRS)
Ir L.M. van Leeuwen – de- Leeuw (ITC-NRS)

EFFECT OF CROWN SIZE AND SHAPE OF DIFFERENT TEMPERATE TREE SPECIES ON MODELLING AGB AND AGC USING UAV IMAGES

ALEJANDRA TORRES RODRIGUEZ
Enschede, The Netherlands, September, 2020

Thesis submitted to the Faculty of Geo-Information Science and Earth Observation of the University of Twente in partial fulfilment of the requirements for the degree of Master of Science in Geo-information Science and Earth Observation.
Specialisation: Natural Resources Management

SUPERVISORS:
Dr Y.A. Hussin (ITC-NRS)
Ir L.M. van Leeuwen – de- Leeuw (ITC-NRS)

THESIS ASSESSMENT BOARD:
Dr T. Wang (Chair)
Dr T. Kauranne (External Examiner, LUT School of Engineering Science, Finland)

ABSTRACT

The improvement in the quantification of aboveground biomass (AGB) and aboveground carbon stock (AGC) is highly relevant for the optimisation in forest management and conservation initiatives worldwide, like REDD+. UAV RGB images can estimate AGB/AGC in diverse forest ecosystems. The stem diameter or Diameter at Breast Height (DBH) is the most influential tree variable to determine AGB and AGC.

The measurement of some tree variables is more straightforward than others, but the relationship between them can be used to estimate one of them indirectly from the other. Crown Projection Area (CPA) and Crown Diameter (CD) have been used to estimate DBH. In the field of remote sensing, RGB images have used these relationships to estimate DBH. The advance in UAV high resolution images has rapidly improved, allowing more details in the interpretation of tree parameters like CPA or CD from which DBH can be estimated.

This study focuses on the effect of DBH acquired from the relationships of DBH-CPA and DBH-CD on the estimation of AGB/AGC. A species-specific DBH model (i.e., 6 species), as well as a General Broadleaves and Conifers DBH model, were built from both DBH-CPA and DBH-CD relationships in a temperate mixed forest in the Netherlands. The results of this study showed that both DBH-CPA and DBH-CD relationships could estimate DBH from UAV with high accuracy and with no significant difference compared to field measurements. Also, the difference between the accuracy results from both relationships was minimal.

The general Conifers and Broadleaves DBH model validation brought similar accuracy results, but broadleaves have a much higher residual, related with a higher crown size variation. In the case of the species-specific models, Spruce resulted in the highest accuracy and the lowest residuals. Moreover, in all cases, DBH-CD relationships estimated DBH with a lowest variance.

Once the DBH estimations are used to calculate AGB and AGC plot-wise, then the model has to deal with the variation from the accumulative effects of the influence of endogenous and exogenous factors on the crown size and hence, on the DBH estimation. Overall, the general models and species-specific models from both relationships were proved to estimate AGB and AGC with no significant difference compared to the biometric AGB/AGC.

A few plots presented important differences (under and overestimations), and this was proven to be highly influenced by Beech species, due to its high crown flexibility to deform itself according to the external conditions (plasticity). Consequently, the sensitivity limitations of Beech species-specific models (DBH-CPA and DBH-CD) should be acknowledged.

Both relationships lead to results with no significant difference when compare against DBH field measurements. Nevertheless, this study has found the species-specific DBH models from DBH-CD resulted in higher accuracy and less variation (except for Beech) on estimating AGB/AGC than DBH-CPA relationship.

ACKNOWLEDGEMENTS

I am deeply grateful to my supervisor dr. Yousif A. Hussin, thanks to his constant guidance, feedback, and encouraging words I was able to accomplish this research into such extraordinary circumstances. I am also grateful to my second supervisor IR. Louise M. Van Leeuwen for her support and valuable feedback.

I also want to thank dr. Raymon G. Nijmeijer -NRM programme Director- for his care during these two years of master and, mostly during the thesis phase. I am also thankful for dr. Tiejun Wang, as the Chairman of this research work, for the constructive feedback on my research work.

My sincere gratitude to the Faculty of Geo-information Science and Earth Observation (ITC), the University of Twente for supporting me financially to pursue this MSc. And to the National Council on Science and Technology of Mexico (CONACYT) for their financial help during my second year of master.

I want to thank my family and friends at Mexico for virtually holding my hand. And for the friends, I made here that became family. Their unconditionally love and encourage words made me stronger. Mainly I feel profoundly thankful to the friends that were willing to bike to the study area and help me collect the ground truth data in the middle of the COVID-19 lockdown pandemic. With a special note for Hector Tamez Garza.

Lastly, I want to thank my love, Alejandro Garcia Navarrete, for his unconditional support into all this adventure, for the laughs in the middle of the chaos and for always give me perspective.

Alejandra Torres Rodriguez
September 2020
Enschede

TABLE OF CONTENTS

ACRONYMS

AAT	Automatic Aerial Triangulation
AGB	Above Ground Biomass
AGC	Above Ground Carbon
BBA	Bundle Block Adjustment
C	Carbon
CD	Crown diameter
CPA	Crown Projection Area
COP	conference of parties
DBH	Diameter at Breast Height
GCOS	Global Climate Observing System
GCP	Ground control point
GHG	Greenhouse gas(es)
GNSS RTK	Global Navigation Satellite System Real-time Kinematic
GSD	Ground sampling distance
Ha	Hectare
LiDAR	Light Detection and Ranging
MRV	Measurement Recording and Verification
REDD+	Reducing Emissions from Deforestation and Forest Degradation
RGB	Red Green Blue
RS	Remote Sensing
RMSE	Root Mean Square Error
SDG	Sustainable Development Goals
SfM	Structure from Motion
UNFCC	United Nation Framework Convention on Climate Change
UAS	Unmanned aerial system
UAV	Unmanned aerial vehicles
VHR	Very high-resolution

ELISTOF FIGURES

LIST OF TABLES

1. INTRODUCTION

The current climate change crisis is caused by the effects of global warming, which is produced by the increment in the concentration of greenhouse gases (GHG) in the atmosphere (IPCC, 2018). Carbon dioxide is a GHG that plants absorb from the atmosphere as part of their photosynthetic process; then, they store this carbon in their biomass and soil. Forests contribute highly on local and global climatic regulation (Sanderson et al., 2012) as well as in the nitrogen and hydrological cycle. They provide numerous ecosystem services (Sanderson et al., 2012), one of them being carbon storage (Erb et al., 2018; Sedjo, 1992). Forests contain around half of the terrestrial carbon stock (Ali et al., 2020). At the same time, deforestation and forest degradation are estimated to be responsible for around 11% of world GHG emissions (FAO, 2018). Therefore, forests worldwide have a significant role in the mitigation of climate change.

Forests are distributed worldwide according to the climatic zone (Figure 1). The temperate forests are located at mid-latitude regions of the planet, between the tropical and boreal forest regions. Temperate forests are in the northern and south hemisphere at around 25 and 55° latitude, i.e. North America, Northeast Asia, North and West Europe, Mediterranean, New Zealand, Chile and Argentina (Lal & Lorenz, 2012). Temperate forest configuration and species is location dependent (the specific latitude, elevation, temperature, moisture, etc.), but generally characterised by having distinctive seasons (below 0°C at the coolest and above 10°C at the warmest) (Ali et al., 2020). They are composed of a mixture of coniferous and broadleaved trees, which are either evergreen or deciduous (Potapov, 2009).

Compared to other forest types, the temperate forest has a simpler structure since they have few layers: generally, an overstory and an understory (shrubs and herbaceous), and sometimes a soil-ground layer (ferns and forbs) (Ecology Pocket Guide, 2018; WWF, 2020). While respiration happens continuously, photosynthetic activity does not, since it is dependent on the seasonal climatic changes; and at temperatures below 0 C, photosynthesis cannot occur (Musselman & Fox, 1991). This means that carbon sequestration is also not continuous in temperate forests. The majority are secondary forests since most of them grew or were planted on an abandoned agricultural or logging area (Wilson, 1988). This forest type is also characterised by having less diversity (Wilson, 1988) Western-European temperate forests, in particular, are less diverse due to the Pleistocene ice age (Smith, 2020).

The temperate forest has been estimated between about 800 million ha (Ecology Pocket Guide, 2018), covering 25% of the world's forest extent and holding around 16% of the global plant biomass (Morin et al., 2019; D'Annunzio, et al., 2017). As a carbon pool, the temperate forest holds about 100 Gton (Heath et al., 1993), which contains 57.1 tons of Above Ground Carbon (AGC) per hectare (Heath et al., 1993). In optimal environmental conditions, average fast-growing temperate trees can gather annually around 20 Mg/ha (Lal & Lorenz, 2012).

Even when temperate forest ecosystems are highly valuable as carbon sinks, among others ecological services, they are also related to important anthropogenic carbon emissions as they face several threats (Ishii et al., 2004). The impact of human activity is marked the most within temperate region (Ishii et al., 2004). Overtime, this forest type has been intensively harvested for wood production, and their area reduced by agriculture and grazing expansion (Heath et al., 1993; Ciesla, 1995). Nowadays, and especially in Europe, this type of forest is characterised as being highly fragmented (Musselman & Fox, 1991).

In recent years, the area extension of the temperate forest is globally stable, and it has even shown a slight increase (D'Annunzio et al., 2017; Musselman & Fox, 1991). Nevertheless, forest degradation is a problem in temperate forest (Gilliam, 2016). Forest degradation is the reduction in the general health and the environmental services of forests, which affects hydrological cycles, biochemical cycles and biodiversity loss (Gilliam, 2016; Musselman & Fox, 1991). There are different factors for the degradation of these forests, i.e. being a substitute for tree plantations, air pollution or climatic stress (FAO, 1993).

The majority of temperate forests are under a certain type of management program, frequently under a sustainable timber yield production approach (and other commercial products) but, conservation and recreational goals have become gradually more critical (FAO, 1993; Potapov, 2009)(Figure 1). It is estimated that 75% of the world's industrial wood products are coming from the temperate forest (Musselman & Fox, 1991).

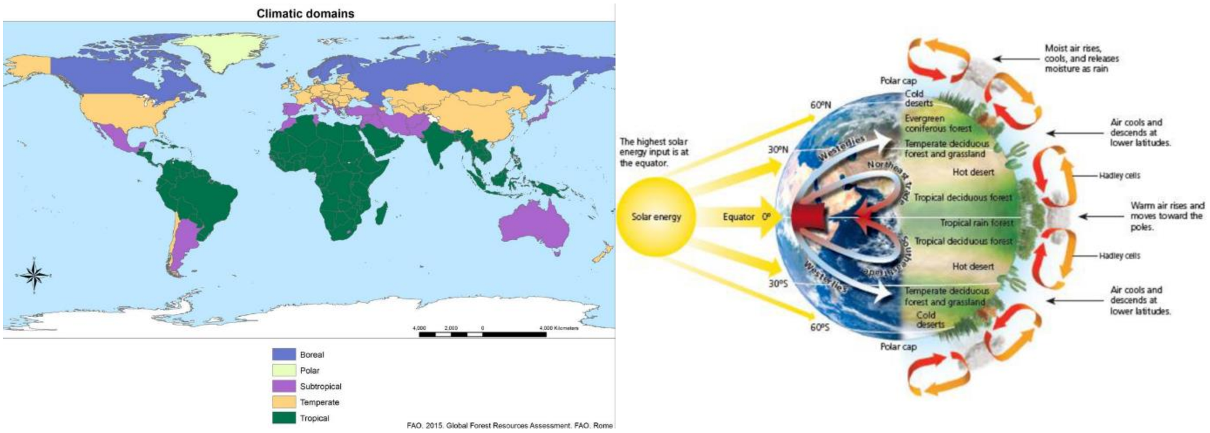

Figure 1. Distribution of the world's forests and grasslands on the left (Miller, 2019) and climatic domains on the right (FAO, 2015a).

Fortunately, initiatives to protect forests have become a worldwide priority, such as the international conservation program on Reducing Emissions from Deforestation and Forest Degradation (REDD+) set by the conference of parties (COP) of the United Nation Framework Convention on Climate Change (UNFCC) (IPCC, 2018). Moreover, the Sustainable Development Goal (SDG) number 15 aims to "*Protect, restore and promote sustainable use of terrestrial ecosystems, sustainably manage forests, combat desertification, and halt and reverse land degradation and halt biodiversity loss*" (United Nations, 2018).

To accomplish all international targets related to protect and improve forests it is essential to keep developing and refining quantitative methods to monitor them and, particularly, its carbon stocks and carbon losses over time. With this, we could better understand the function of these types of ecosystems and to have more information about their dynamic changes for better management decision-making.

Forests must be managed on local, national and global levels. Stakeholders need to have access to the spatial distribution of forest variables: i.e. tree species, height (H), Basal Area (BA), Diameter at Breast Height (DBH), Crown Diameter (CD), Canopy Projection Area (CPA), Aboveground Biomass(ABG) and Aboveground Carbon stock (AGC).

According to the Global Climate Observing System (GCOS, 2020), AGB is considered as an essential ecological variable (ECV) to understand the planet's climate system. Still, it is complicated to measure it along with AGC on national and local levels. The carbon stock is estimated by assuming that it is 50% of the AGB (Hirata et al., 2012). An accurate estimation of AGB and AGC and its distribution at different scales is essential to a truthful carbon balance. Moreover, these estimations can enable a better understanding of the forest ecosystems and their ecological services, their role in climate change mitigation and ultimately to help improve the certitude in climate scenarios.

Until now, there has not been direct measurement method of AGB or AGC applicable to a large area (Gibbs et al., 2007; Lu, 2006). In this sense, the development of Remote Sensing (RS) has been a technological milestone since it brings accurate, efficient and repetitive estimations and measurements of forest attributes (such as biomass and carbon stock) through different sensors and methods-(Rodríguez-Veiga et al., 2017). REDD+MRV (Measurement Recording and Verification) have recommended some remote sensing techniques and methods, with different characteristics, applicability, cost, and estimated accuracies (Hirata et al., 2012). They suggest to the participant countries to apply a reasonably accurate, inexpensive operation and practical technique for the quantification of carbon sequestration. Because of this, trustworthy ABG and carbon stock estimates approaches and methods are of enormous societal relevance.

Optical remote sensing has been commonly applied in AGB/carbon stock mapping. Low and medium resolution satellite optical remote sensing has been used for AGB and AGC stock. The struggle with species discrimination and biomass variation makes the low and medium resolution not accurate to estimate AGB (Pham et al., 2019). Contrary, high spatial resolution (HR) and very high spatial resolution (VHR) images (below 5 m) have shown favourable results to extract biophysical variables and relate them to AGB through allometric relationships and regression analysis (Gibbs et al., 2007; Hirata et al., 2012; 2013; Lu, 2006). Among the disadvantages are the data occlusion and spectral variation by clouds or shadows, as well as the high cost of acquisition and time to process (Lu, 2006; Pham et al., 2019).

1.1. Research problem

As previously mentioned, forests are important carbon pools, meaning that they are a system that collects and releases carbon (a carbon reservoir). They can also be considered as a carbon sink if, during a given range of time, the amount of carbon sequestered by them is higher than the amount flowing out. The carbon stock is the amount of carbon which is held within a pool in a determined time (IPPC, 2018).

The global climatic crisis along with the threat to the forests has increased the need to research for more accurate and accessible methods and techniques to quantify carbon while supporting the REED+ and other world objectives (Hirata et al., 2012). Intending to reach zero net deforestation, all participant countries of the United Nation Framework Convention on Climate Change (UNFCC) have to present an update report of their carbon balance periodically, as well as compensation actions of REDD+ program. In 2020, REDD+ compensation payments should start to be implemented along with the compensation actions in which money from emission countries should be paid to carbon stock countries (mostly developing countries) (FAO, 2018).

Therefore, accuracy, transparency and accessibility of the carbon quantification processes are essential to achieve REDD+ objectives and ultimately the conservation and enhancement of forest carbon stocks. MRV is the mechanism to make sure that the countries who claim that they have more carbon stock than emitted are correct.

In terms of sustainable forest management, local and global policies and management measurements are made and applied to protect worldwide forests. Hence, monitoring of aboveground carbon (AGC) using innovative techniques is essential for evaluating the efficiency of these policies. Remote sensing allows forest managers and decision-makers to have access to biophysical properties information necessary for the AGB and AGC estimation. The variables used are mainly: Crown Projection Area (CPA), Crown Diameter (CD), Diameter at Breast Height (DBH) and tree height (H). The process is done based on the statistical relationship between the biophysical variables from the remote sensor compared to ground measurements (Gibbs & Herold, 2007).

In this respect, the latest developments of UAV have opened the possibility to estimate AGB and AGC efficiently and accurately, with economic accessibility and Spatio-temporal control on the data acquisition. Regarding their potential pros and cons, more research needs to be done on the relationships of both CPA and CD with DBH between species and, its subsequent influence on estimate AGB and AGC. Coniferous and broadleaves in general as well as each species in particular, have specific canopy shape and size, which would affect the assessment of AGB/AGC. Very high spatial resolution (e.g., 5-15cm) UAV images can capture these differences. The effect of these differences on the assessment of AGB and AGC using very high spatial resolution images of UAV has not been studied.

This study aims to investigate the detection of these difference between coniferous and broadleaf species in a temperate mix forest using UAV images. We want to compare the morphology of the canopy architecture between species and its effect on the DBH estimation and the accuracy of AGB and AGC estimation from UAV images. This research would explore which specific species of the coniferous and which particular species of Broadleaves has the highest correlation with DBH. Thus, how the DBH-CPA and DBH-CD relationship affects the assessment of AGB and AGC using allometric equations that use DBH as a single explanatory variable.

1.2. Research Objectives

1.2.1. Main objective

The main objective is to evaluate the ability of UAV RGB images to estimate aboveground biomass (AGB) and aboveground carbon stock (AGC) of coniferous and broadleaves tree species in general and their specific species. This research deals with the effect of shape and size of canopy projection area (CPA) and crown diameter (CD) on the accuracy of assessing DBH of various coniferous and broadleaves tree species. Ultimately, it aims to contribute to the efforts to mitigate climate change.

1.2.2. Sub-objectives and research questions

Table 1 presents the sub-objectives and the research questions of this research.

Table 1. Sub-objectives and research questions of this research.

Sub-objectives	Research questions
1. To assess, and compare, the canopy size and shape of tree general categories and specific species, and its effect on the relationship between CPA and DBH.	1.1 What is the relationship between CPA and field measure DBH of conifers and broadleaves species in general categories and specific species?
	1.2 Which specific specie presents the highest accuracy in assessing DBH from CPA?
2. To assess and compare the relationship of CD (derived from CPA) and its effect on DBH-CD relationship in both conifers and broadleaves categories and specific species.	2.1 What is the relationship between CD and field measure DBH of conifers and broadleaves species in general categories and species-specific?
	2.2 Which specie presents the highest accuracy in assessing DBH from CD?
3. To analyse the effect of both DBH estimation models on the plots ABG and AGC.	3.1 What is the accuracy of modelled AGB and AGC derived from UAV images compared to field measurements?
	3.2 Which plot type (broadleaves, conifers or mixed) specie shows higher accuracy in estimating its AGB and AGC from species-specific DBH models?
	3.3 Which DBH estimation model performed better on the AGB and AGC estimations?

Hypothesis

1. H0: The biometric DBH and DBH estimated from DBH-CPA relationship, from UAV-RGB images, has no significant difference.
   H1: The biometric DBH and DBH estimated from DBH-CPA relationship, from UAV-RGB images, has a significant difference.
2. H0: The biometric DBH and DBH estimated from DBH-CD relationship, from UAV-RGB images, has no significant difference.
   H1: The biometric DBH and DBH estimated from DBH-CD relationship, from UAV-RGB images, has a significant difference.
3. H0: The estimated AGB and AGC from DBH-CPA species relationship and biometric-AGB and AGC have no significant difference.
   H1: The estimated UAV- AGB from DBH-CPA species relationship and biometric-AGB and AGC has a significant difference.
4. H0: The estimated AGB and AGC from DBH-CD species relationship and biometric-AGB and AGC have no significant difference.
   H1: The estimated UAV- AGB and AGC from DBH-CD species relationship and biometric-AGB and AGC have a significant difference.

2. THEORETICAL BACKGROUND AND RELATION TO PREVIOUS WORKS

This chapter will briefly clarify some concepts, and the links between them, which are essential for this research.

2.1. Unmanned Aerial Vehicle and AGB

Unmanned Aerial Vehicles (UAV), or remotely piloted aircraft systems, is a type of lightweight aircraft that can fly without an onboard pilot. Instead, they are remotely piloted from a ground control station. The aircraft can be a fixed-wing or rotary-wing. The rotary-wing needs a small take-off and landing area. The system is composed of GPS and an inertial measurement unit (IMU) and, the camera or sensor for the image capturing (Torresan & Wallace, 2016). Initially built for military proposes, UAV have expanded their uses and applications. Since it can give high spatial resolution images with good quality and at a low-cost, it offers a high potential for UAV applications in earth observation as a remote sensing tool. It has been increasingly used in recent years in forestry and agricultural monitoring, as well as for supporting quick responses to natural disasters (Giri et al., 2011).

With the photogrammetry and the computer vision methods applied on Structure from Motion (SfM), RGB-UAV can almost automatically create a 3D point cloud model from a set of 2D overlapping images (Kachamba et al., 2016). The 3D model is built by identifying matching points on the consecutive overlapped images and allowing it to recognise and refine the objects structured in the image according to the camera movement (Figure 2). The more matching points, the denser the point cloud - hence the finer the object details. Bundle adjustment is also an important part of the process since it estimates the location of the object in the image (image calibration), as well as the camera position and this, is done by taking the GCP as reference (Nex & Remondino 2014). Then, the Check Points (CP) are used to assess the accuracy of the absolute orientation (Nex & Remondino, 2014).

a **b**

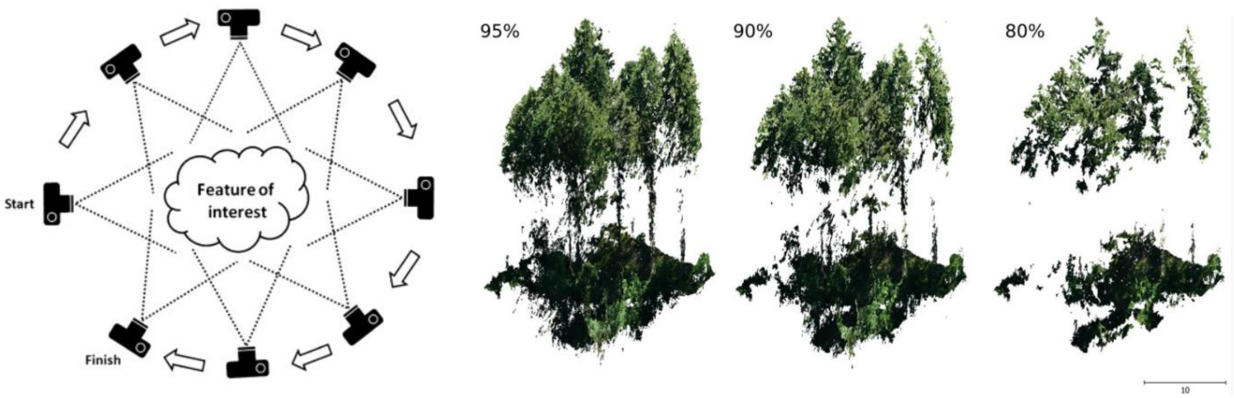

Figure 2. Example of a 3D reconstruction with structure from motion (SfM).(a) SfM uses multiple overlapping stereo pair images taken from different angles (Westoby et al., 2012). (b) It uses that information as input to recreate the feature of interest as a 3D point cloud scene. The image is from Frey et al. (2018) research, the higher the overlapping percentage of the image, the more tie points hence, the denser the point cloud and more detail can be appreciated.

An advantage of UAV with SfM is that they can deliver spectral data complementary to the point cloud (Fritz et al., 2013). The 3D point cloud can be derived in a high-resolution orthophoto as well with the terrain and digital surface model (DTM and DSM). The digital surface model (DSM) include those points cover the surface of the objects, i.e. tree canopy. The digital terrain model (DTM) represents the topography of the terrain without any objects or features (it is produced based on the pixels classified as ground pixels) (Figure 8). An orthophoto is a geometrically corrected (ortho-rectified) aerial photograph; the 3D image gets into an orthogonal cartographic projection. The orthophoto has a uniform scale along the pixels; without projection distortions, making possible to get the real position and size of the objects in the scene (it is made from the DSM, not DTM) (Kraus, 2007).

This way, tree structure parameters can be efficiently acquired on a lower cost and faster processing of intense data collection, compared to other alternatives (Dittmann et al. 2017; Kachamba et al., 2016). UAV has proved to acquire an assessment of AGB and carbon stock efficiently, and forest data collection in general at a relatively low cost (Otero et al., 2018; Torresan & Wallace, 2016). UAV images, with photogrammetric and SfM, have reported promising results, comparable with ground measurements and LiDAR measurements for AGB and AGC stock estimation in different forest types (i.e. Alonzo, et al., 2018; Jayathunga, et al., 2018; Kachamba et al., 2016; Messinger, et al., 2016).

Another significant advantage is that the image acquisition can be space and time planned according to the objectives and to minimise weather conditions that could affect the data quality (Messinger et al., 2016). The UAV is capable of recreating orthoimages with such a resolution that tree canopy textures can be appreciated and make species recognition much more straightforward. The data is relatively easy to acquire and to process in comparison to other remotely sensed data, but it is also easier to do so with high frequency allowing, for example, seasonal changes analysis (Alonzo et al., 2018; Lisein et al., 2015). The combination of structure (3D- point cloud, DSM and DTM) and colour information allow a wide range of research and practical applications in different fields (Alonzo et al., 2018). When compared with LiDAR 3D point cloud, UAV SfM creates a greater point density giving a higher detail level on forest structure on the DSM (Alonzo et al., 2018; Dandois & Ellis, 2013).

Apart from the climatic conditions (i.e. wind, rain, clouds), the quality of the UAV outputs depends: on the images overlapping percentage, the amount and distribution of the ground control points (for the bundle block adjustment process), focal length and flight altitude, camera sensor characteristics, flight pattern and speed (to minimise motion blur) (Nasrullah, 2016).

Some of the UAV disadvantages is that it can cover a limited area extension: their altitude and time flight depends on the battery power and legal regulations, such as the UAV should be visible to the pilot at all times during the flight. Legal rules and restrictions can also vary between countries and between land-use types. When talking about the 3D point-cloud, another disadvantage compared with LiDAR is the SfM is limited to visible crown surfaces from a bird-eye view, and more sensitive to shadow and light environment (Alonzo et al., 2018). Also, SfM has less penetration capability than LiDAR; thus, as we will explain further on this document, contrary to the DSM from UAV-SfM, the DTM accuracy tends to decrease when canopy density is high.

2.2. Temperate forest in the Netherlands

About 10% of the Netherlands area is covered with forests. Still, the human influence along history has made them fragmented, with forest patches of frequently less than 5ha (van der Maatek-Theunissen & Schuck, 2013). Most of the forested area in the Netherlands has a plantation origin with wood production as a principal objective (FAO, 2010). Most of the times, these forests are composed of various sections of a single or two species trees even-aged and even-spaced.

Nowadays, the management has evolved into a multi-purpose forest (i.e. recreation, nature conservation and wood production). According to The Netherlands 2015 Country report for the Global Forest Resource Assessment (FAO, 2015b), by the year 2000, 74% of the forests area of the country was multi-purpose forest. The primary management of the 24% of Netherlands forests area is focused on nature conservation, denominated "Bos accent natuur". As part of their management, wood in this areas is harvested only during a specific period and mainly exotic species to propitiate a forest with just natural species. The rest of the forest cover are productive plantations.

The ownership of the forest is split by the state and private, with 50% each (van der Maatek-Theunissen & Schuck, 2013). Although it is not compulsory, 62% of the forests in the country have a management plan. There are different types of protected areas according to their conservation level and legal status: National Parks, National Landscapes, National Ecological Network (EHS), Natura 2000, Nature Monuments and Forest Reserves (FAO, 2015b; FAO, 2010).

In terms of species distribution, 57% of the national forest extension are coniferous and 43% broadleaves. Half of the national forest area consists of a single species, 31% of which are conifers, and 21% are broadleaves (van der Maatek-Theunissen & Schuck, 2013). Dominating species within the country are Scot Pine (*Pinus sylvestris*) and Oak (*Quercus robur* and *Quercus petraea*). Other main coniferous species are Douglas fir, Larch and Norway Spruce, along with Beech and Birch among the broadleaves (FAO, 2015b; van der Maatek-Theunissen & Schuck, 2013).

2.3. Conifers and broadleaves characteristics

According to trees physiology and structural properties, there is a significant tree categorisation on broadleaves and coniferous. While both species groups usually grow even in the same places, each has several distinguishing features.

Conifers, or Gymnosperame, are characterised by their conical crown shape of many overlapping levels of branches with a dense needle or scale shape leaves on a spiral arrangement (Walker & Kenkel, 2000). They have an excurrent branching, meaning that the stem is the thickest at its lowest and slimmest at its highest mend (Pretzsch, 2014). They tend to have a smaller crown diameter than broadleaves since their canopy gets more compact, denser and pointed as they mature; and they grow skyward and triangular rather than outward (Figure 3).

The leaves of conifers are regularly replaced, giving them evergreen foliage all year (with the exception for Larch). They are characterised as a cone-on-cone since they produce their seeds inside cones (with shapes of short, cylindrical or egg-shaped) that release the seeds when it scales opens (Walker & Kenkel, 2000). They are called softwood forest because of their less dense fibre in comparison to broadleaf. Their wood is widely used in the production of timber and paper (Samanthi, 2011).

Their canopy architecture (conical anechoic or without echo) make the solar energy to scatter inside the canopy by several rebounds, so the leaves intercept and absorb the radiant energy (Walker & Kenkel, 2000). Their energy capture strategy makes them more shadow tolerant, gives them lower near-infrared radiance and allows them to continue photosynthesis activity during low sunshine availability (Walker & Kenkel, 2000). They tend to have a darker green colour and, in warmer and sunnier places, their leaves display more yellow-green tones.

Conifers can be adapted to different environmental conditions, and they are also found more commonly in colder weather compared to broadleaves (Walker & Kenkel, 2000). Their conical canopy makes them more wind adapted and helps them to remove the weight of the snow from accumulation. Some of the species also have resins in their sap as antifreeze protection, to diminish water loss and protect them from pest(Offwell Woodland & Wildlife Trust, 2000; Ciesla, 1995).

Broadleaves trees, also known as Angiospermae or hardwoods, have leaves in a wide variety of shapes and sizes with a tendency to be flat (but never needle-like). These big horizontal leaves create laminar canopies which aim to directly capture as much radiant energy as possible during the few months that the broadleaves have leaves, making them more efficient and with higher photosynthesis activity - hence why it is said that they work like "solar panels" (Walker & Kenkel, 2000). In their early years, their buds tend to grow with 'apical dominance' where the main stem is strongly dominant over the side branches (Loreti & Pisani, 1990). Since they try to absorb as much sunlight as possible, broadleaves canopy tend to grow spreading outward on a roundish shape, so they tend to have deliquescent branching – meaning branches grow outward, spreading in different directions with lateral buds (Figure 3) (Pretzsch, 2014). However, as the canopy density increases, they can adapt their growth to any direction where they have space availability (Blanchard et al., 2016).

At the same time, their leaves and canopy shape make them less capable of overcoming windy and winter weather. By losing their leaves, typically by the end of their growing season, they can adapt to these challenging or stress conditions. Therefore, most of the broadleaves shed their leaves during autumn (so-called deciduous) and grow new ones in spring. But there are also evergreen broadleaves(Loreti & Pisani, 1990).

Differently from conifers, broadleaves do not necessarily have a common way to produce seeds (Offwell Woodland & Wildlife Trust, 2000). Most deciduous broadleaves have flowers, and they tend to blossom before the leaves re-grow to become easier to spot by insect and to improve the pollen spread by wind (Ciesla, 2002). Generally, a broadleaf temperate forest can be found in between the coniferous forest and tropical forest. Their wood is of high economic value (Offwell Woodland & Wildlife Trust, 2000).

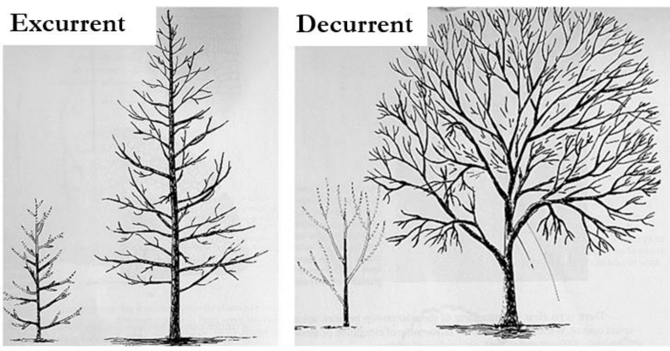

Figure 3. Typical excurrent and decurrent canopy shapes (Loreti & Pisani, 1990).

2.4. AGB and allometric relationships

Tree biomass is defined as the total biological matter within a unit area. Normally it is considered just the weight of dry matter, and the units used are usually tons per hectare (Ton/Ha) (Hirata et al., 2012). The amount of carbon that is into that biomass varies between species but as an acceptable standard is 50% of the biomass (Hirata et al., 2012). The carbon storage is often subdivided into below-ground biomass, BGB (the root system and, sometimes also considers the carbon in the soil and dead wood parts) and above ground biomass – AGB - consists of the leaves, branches, stem, and bark (Gibbs et al., 2007; Gschwantner et al., 2009) (Figure 4).

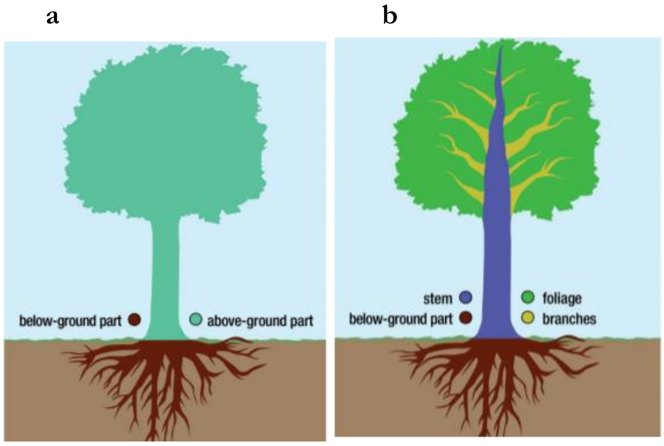

Figure 4. Tree elements. (a) Aboveground and belowground distinction. (b) Elements that constitute aboveground part of a tree into foliage, branches and stem (Gschwantner et al., 2009).

An almost completely reliable measurement of any forest biomass (besides the instrument error) would be to cut every tree, dry all the sections and then weigh them. This is called destructive method or direct method since it is necessary to sacrifice the trees to get the data. It is expensive, time-consuming and unpractical for conservation proposes (Bouillon et al., 2008; Dittmann et al., 2017; Sinha et al., 2015). On the other hand, any time of extensive field data collection is costly, time-consuming and some field location can be just inaccessible (Jayathunga et al., 2018; Puliti et al., 2017).

The non-destructive, indirect methods are then estimations methods, and as Dittmann et al., (2017) said: "*tree mass estimation procedures are always a trade-off between accuracy and efficiency*". Usually, these methods are based on mathematical relationships among the biomass (as the independent variable) and one of the forest biometric variables that are easier to measure (independent variable) (Sousa et al., 2017). The monitoring and change of forest biomass are estimated by a regression model through an allometric relationship based on forest biometric parameters such as DBH (Lu, 2006). In recent years, optical remote sensing has evolved and improved on the estimation of forest biometric parameters; meanwhile, scientists have built an extensive inventory of allometric equations for more and more species.

Optical remote sensors, also called passive sensors, register the optical reflectance of what is on the earth surface (Sousa et al., 2017). Optical remote sensing methods have focused on estimating structure parameters of an individual tree or a plot area and, use these estimations as input to calculate AGB through allometric equations. The result can be assessed against field measurements as truth. (Lu, 2006, Gibbs et al., 2007). As the possibilities of image resolution get better, the current high spatial resolution allows species recognition as well as the possibilities of better individual crown identification and delimitation (Sousa et al., 2017). In this sense, AGB estimations from UAV remote sensing offers the possibility to acquire AGB data from a large area repetitively and to process large amounts of databases on the relationships between the spectral bands and vegetation parameters. They are categorised as partially field-independent since the process is then validated from in-situ non-destructive measurements.

The term allometry in biology refers to the scaling relationship of the size of morphological characteristics of a leaving organism with each other and/or body size of the creature. These give an idea of the growth differentials of the particular creature and the impact of this relationship on ecology and evolution (Pretzsch,2010). By allometric equation, the AGB of each tree of every plot can be calculated indirectly when some of their biophysical parameters are known (Pham et al., 2019).

AGB can vary according to the age, species and even location (Ketterings et al., 2001). Researchers have developed many allometric equations throughout the years, regarding most of the tree species or family species, for the non- destructive estimation of AGB. All these equations consist of regression coefficients (which can differ among sites and species) with DBH alone or with height as biometric parameters that must be introduced by the user. It is also worth mentioning that AGB can also be derived from tree volume allometric equations by multiplying their value with the wood density. As an example, Zianis et al. (2005) made a robust recompilation of biomass and volume allometric equations for tree species in Europe.

There are many AGB allometric equations, even for the same species. In all of them, the DBH is always the most influential variable, which commonly is expressed as Equation 1. Even when height can increase the accuracy, it can also increase the variation as an error. Therefore, it is acceptable to use DBH as the only explanatory variable for the accurate AGB estimation (Ketterings et al., 2001; Magnussen & Reed, 2015; Picard, 2012; Zianis et al., 2005). The allometric equations used for this research are developed from data collected close to the study area and with a good accuracy reported(Zianis et al., 2005, Novak et al., 2011; Suchomel et al., 2012;)

$$AGB = aDBH^b \qquad \text{(Equation 1)}$$

Where *a* and *b* are constant value calibrated for a specific specie or group of species.

By having important forest parameters, either by direct measure (such as fieldwork or from forest inventories) or estimated from remote sensors, AGB allometric equations are generally used to estimate the AGB of each tree and then, summing all the tree biomass [kg] within the plot area, commonly expressed in tons/ha. Later, with an extrapolation method for its application on a larger scale (which there are several and beyond the boundaries of the focus on this research) is possible to map the AGB And AGC of an entire forest area (Sousa et al., 2017).

As already mentioned, Above Ground Carbon stock (AGC) refers to the amount of carbon contained in a carbon pool area, so it is expressed in mass per area units, generally ton/ha. It is generally accepted that 50% of AGB is carbon storage (Hirata et al., 2012).

2.5. Overview of crown structure

The tree branches and foliage constitute what is known as the crown (Gschwantner et al., 2009). The trees crown structure determines the characteristics of a forest canopy. As it shows in Figure 3, temperate conifers and broadleaves have an excurrent and decurrent canopy shape, respectively, because of the expansion rate of their leaves, bounds and branches. Loehle, (2016) and Pallardy, (2010) explained that the terminal leader, which is the vertical steam from the ground to the highest point, in the case of conifers has a continuous growth getting longer (higher) than the branches aside and below it and fomenting the conical shape. Contrary, angiosperm like Oaks, Maples, including Beech and Birch species, their lateral branches grow as much, or even faster, than the terminal leader producing a broader crown. But also, the rebranching growth pattern makes the main stem of the crown lost its identity (Loreti & Pisani, 1990; RFS, 2015).

Crown characteristics tend to be different between coniferous and broadleaves, and even among species (endogenous). However, the organism's response and adaptations to environmental influences also play an important role; hence the crown shape is also an indicator of a trees' ecological success (Paganová et al., 2015). The photosynthetic capacity and tree growth are determined by the crown structure, mainly because the sunlight access competition happens on the foliage level (Uria-Diez & Pommerening, 2017). In theory, the more sunlight access, the better. As the canopy gets denser, and to avoid the competitive pressure between the neighbouring trees to get as much sunlight access as possible, the tree responds with crown plasticity (Seidel et al., 2011).

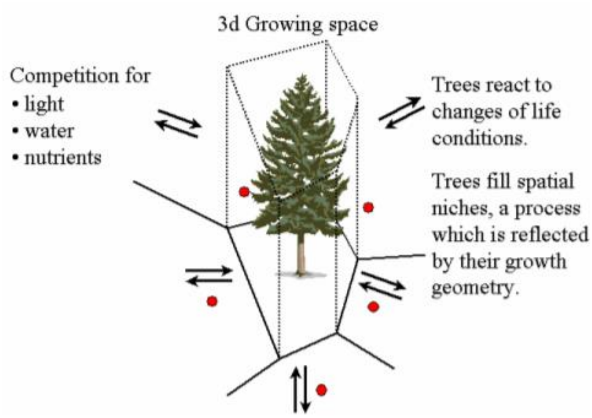

Figure 5. Graphic representation of the available tree growing space and external interactions. The location of neighbouring trees is symbolized by the red dots (A. Pommerening, 2007).

The crown plasticity is an adaptability response that some species possess, in different levels, to shift their crowns further from competition direction to improve the light interception chances and, avoid too much shade (Vincent & Harja, 2008) (Figure 5). Tree architecture depends on the processes of endogenous growth and exogenous environmental constraints. Endogenous and exogenous factors determine crown architecture. Trees in the shadow or less dominance advantage, tend to grow taller, narrower and, with few branches, sometimes just at the very top of the tree (Figure 6) In forestry science, one competition indicator is the roundness or asymmetry of the canopy shape. The more symmetry in a tree CPA shape, the less competition it is struggling with (Kikuzawa & Umeki, 1996; Seidel et al., 2011).

On the other hand, a tree with no neighbours is a tree with no competition, and this develops the highest individual stability, called an ' open-grown tree' . These trees will develop a full crown shape and wide open branches; hence it maximises the amount of light access (Pommerening, 2015). Urban trees or plantation trees with high space divisions are examples of open-grown-trees. Their crown structure has a bigger length, as it has lower branches, but they are also less tall than average forest-grown trees (Loreti & Pisani, 1990; Pommerening, 2015). When there is an open-grown-tree allows the full crown morphology of a tree species as more spreading, oval, weeping, umbrella, spherical, columnar, conical, etc. (Lenard, 2008).
In mixed European forests, depending on the light demands and shade tolerance of a tree species and their competition status, the crown will develop above the main canopy or under (often called dominant or suppressed) or at the height of the main canopy with more or less lateral competition (called co-dominant

or sub-dominant)(Pommerening, 2015). According to the literature, it seems like conifers tend to have less plasticity and among the reasons for this is because they seem to be better adapted to wind damage and shade tolerance (Loehle, 2016). Hence they have less necessity to move than broadleaves.

Depending on the mixed-species characteristics, plasticity also allows space optimization and a competition decrease (Pommerening, 2015). Pretzsch (2014), has reported that mixing species of different crown structures, such as broadleaves and conifers, besides of creating selection pressure, optimises the space as their tree architecture allows higher tree density, ampler light interception area and productivity (Figure 6). Nevertheless, this could mean that from the bird-eye perspective and the following optical image, the crowns would be seen as blocked.

Moreover, Pretzsch (2014), also found that on Beech trees the allometric relationships between crown projection area (CPA) and Diameter at Breast Height (DBH) with the even-age stands, the relationship changes according to the species that is combined with.

From all above-mentioned, even in the same species, there is not an only canopy structure (at the crown and stand-level) and estimation of the crown shape it is a complex task (Disney et al., 2010).

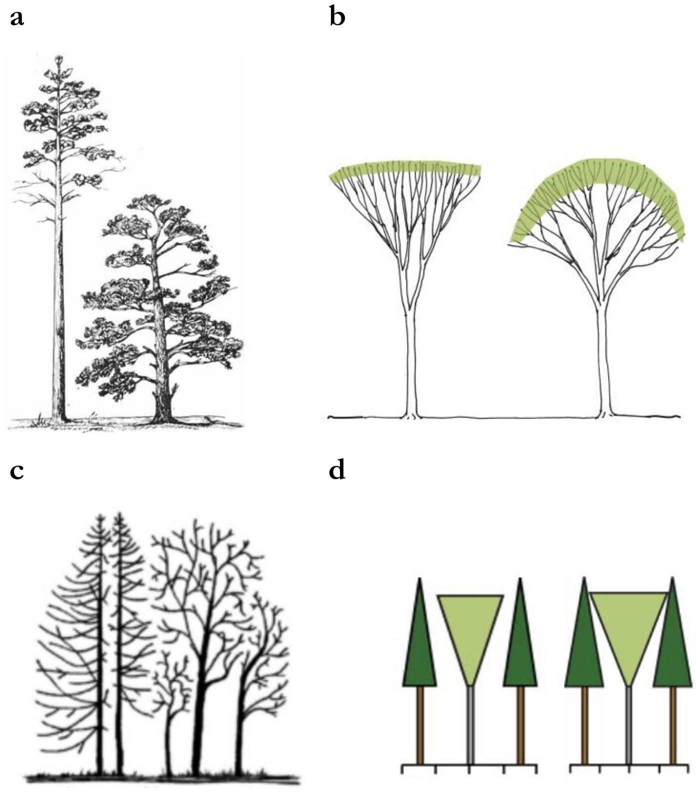

Figure 6. Tree crown shapes differences in density circumstances. (a) Morphology contrast of an open ground tree and a forest tree using scots Pine as an example (Pommerening, 2015). (b)Example of the crown of a Beech tree with more and less space competition (Pretzsch, 2014). (c) representation of the tree crowns shapes in a dense mix forest (Lenard, 2008). (d) general representation of space-filling of conifers and broadleaves crowns in different density circumstances (Pretzsch, 2014).

2.5.1. Forest structure variables

There are several forest stand variables (Figure 7), i.e., DBH, height, crown area or crown diameter, they can be either directly measured or derived from another variable. To estimate AGB and AGC, the most important ones are:

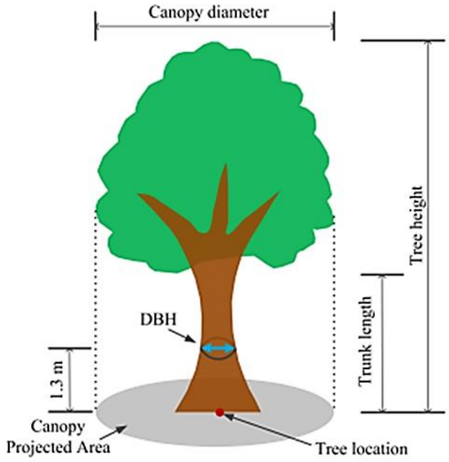

Figure 7. Tree structure variables (Wanga & Lindenbergha, 2018).

2.5.1.1. Diameter at Breast Height (DBH)

The DBH is the longitude of the cross-sectional line of the tree trunk measured at 1.3m from the ground (the base point) and is measured in centimetres (Gschwantner et al., 2009). Among other applications, constitutes an essential variable for AGB and AGC estimation. It is one of the few tree parameters that can be directly and easily measured in the field. At the same time, when using remote sensing, the DBH must be predicted since it cannot be directly extracted from the RS data such as 3D point clouds (Weng & Wang, 2013). However, DBH value can be estimated base from the direct relationship of DBH-CPA (Brown, 2002; Lisein et al., 2013) and DBH-CD (Panagiotidis et al., 2017). It is worth mentioning that, for most of the time, these DBH estimations models are built-in general for all species in the study area.

2.5.1.2. Crown Projection Area (CPA)

Viewed from an above horizontal plane sight(bird-eye view), the vertical projection of the canopy area of a tree is known as Canopy Projection Area (CPA). CPA is the area that covers the crown of a tree and whose boundaries can be identified on an image and is a variable not practical to measure from the ground for it is time-consuming (Gschwantner et al., 2009). It is considered as a multi-purpose variable in ecology, for example, result in an essential biometric parameter since it is strongly related to DBH (Shimano, 1997).

To define individual horizontal CPA, the higher the resolution, the better CPA delineation. In this sense, VHR is an advantage for accurate CPA. The CPA is relatively easy to acquire from the UAV orthophoto by manually digitising on-screen each of the canopies or automatically segmenting by several techniques (we did not use segmentation on this research). The relationship between DHB-CPA has been popularly used for the DBH estimation (i.e. Brown, 2002; Lisein et al., 2013; Shimano, 1997). It is worth mentioning that in the process of acquired CPA shape boundaries, what we are measuring is the horizontal 2D CPA from the orthophoto.

2.5.1.3. Crown diameter (CD)

As its name implies, the Crown diameter (CD) is the diameter of the tree canopy and measured in meters. When measured in the ground, the CD is the average from two perpendicular axis measurements of crown width, usually in N-S and W-E direction; this is to get a more accurate measurement of the crown shape. Measuring the CD from the ground is a time-consuming task and impractical (.i.e. could be an ambiguous measurement that relies on the person's experience). Therefore, the CD is often not considered in the forest inventories(Gering & May, 1995).

By assuming a round shape canopy, the CD can be derived from the CPA extracted from optical images (Equation 3) (Bauhus et al., 2017). Previous research has proved that there is a strong relationship between DBH and CD across forest types and have used this relationship to model and estimate DBH from CD (i.e., Panagiotidis et al., 2017; Song et al., 2010; Gering & May, 1995).

$$CPA\ [m^2] = \pi * Radious^2 \qquad \text{(Equation 2)}$$

$$Radious = \sqrt{\frac{CPA}{\pi}} \qquad \text{(Equation 3)}$$

$$CD = 2 * \sqrt{\frac{CPA}{\pi}} \qquad \text{(Equation 4)}$$

2.5.1.4. Tree height

Tree height is considered from the ground to the highest point of the tree crown. (Figure 7). The SfM process gives as an output the DSM and DTM from where the tree height can be estimated. The Digital Surface Model (DSM) is the representation of all the objects above the ground - trees in this case(Figure 8). On contrast, the Digital Terrain Model or Digital Elevation Model (DTM or DEM) is the digital representation of the topography of the terrain without any objects or features, meaning that DTM is made by an interpolation of the points from the point cloud classified as ground (Nex & Remondino, 2014).

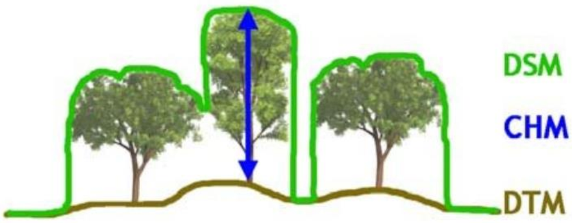

Figure 8. The Distinction between digital surface model (DSM), digital terrain model (DTM) and canopy height model (CHM) (Perko et al., 2010).

The tree height can be estimated from Canopy Height Model (CHM) by subtracting the tallest point of the DSM within the canopy area from the DTM (Lisein et al., 2013) (Figure 8). The quality of the DTM, DSM and their subsequently CHM, depends on the point cloud density, which also depends on the forest density. As the canopy gets denser and, spaces between canopies get reduced, this impedes the creation of ground points on the 3D point cloud. Low density on the grounds points makes the interpolation less accurate when building the DTM. This is why the DTM from UAV tend to have worse resolution than the DSM, even when both are created from the same point cloud. Moreover, and for the same reasons, sometimes points can be wrongly classified as ground points. Therefore, UAV tree height is often underused since its accuracy is highly dependent on the quality of the DTM, which likewise decreases as the canopy get closer (Huang et al., 2019).

Depending on the forest type and conditions, researches have reported a tree height accuracy at the most around R^2= 0.70 (Goodbody et al., 2017; Panagiotidis et al., 2017), higher accuracy is possible in agriculture or on young trees forest plantation where canopy density is not a problem (Zarco-Tejada et al., 2014a). In general, research has proved that RGB-UAV it is not a good option in the dense canopy (Lizuka et al., 2017). The season in which the UAV flight take place has also been proved to affect the DSM and DTM quality (Dempewolf et al.,2017). Alonzo et al., (2018) concludes that a sufficient and spatially distributed amount of gaps among canopies are needed to get enough terrain points at the point cloud and hence a good DTM quality and tree height estimations.

Tree height from UAV is an inferential measurement and not as accurate as LiDAR, which is a measurement. Also, LiDAR can acquire more ground points in closer canopy than UAV. That is why LiDAR is often considered as the most accurate sensor assessing tree height (Salach et al., 2018). LiDAR ALS and TLS generate a denser and more accurate DTM from its point cloud and its independent from vegetation density and height (Fritz et al., 2013; Salach et al., 2018). For all the above mentioned, most frequently, the UAV DSM is used in combination with LiDAR DTM (Jayathunga et al., 2018; Lisein et al., 2013). Nevertheless, the LiDAR technology cost makes them less suitable for REED+ proposes.

Originally, it was thought to use DTM and DSM from the UAV images and use the tree height estimation as a complementary variable for the AGB and AGC calculations. But, since we are dealing with plots of different canopy densities, the tree height estimations were not always good. There have been numerous research works around the tree height estimation from UAV and possibilities to improve them (i.e. Alonzo et al., 2018; Salach et al., 2018). Since the tree height is not the main focus of this research, it was decided not to be considered for the AGB and AGC estimation.

3. MATERIALS AND METHODS

3.1. Study area

Haagse Bos covers a total of 334 ha (Tenaw, 2011). It is located in Overijssel province of The Netherlands, 7km from the city of Enschede and 4km from Looser city (Figure 9). The whole forest area was borne as a private conifers timber production area in the 1890's as most of the current forest in The Netherlands (Kloek, 2014). Since then, the management of Haagse Bos has evolved into a multi-purpose forest: nature conservation and recreation proposes (Natuurmonumenten, 2020). The ownership and management of the forest are by Natuurmonumentent and a private company, , called Takkenkamp (Natuurmonumenten, 2020). Selective thinning activities remain on some private ownership sections; these are around every six years and proportional to the rates of re-growth within the area. The management of the Natuurmonumentent section consists of natural regeneration without any human intervention (Tenaw, 2011). For this study, we focused on a 57ha section of the forest, which covers the Natuurmonumentent area (mostly broadleaves) and just a small private section which has mostly conifers trees.

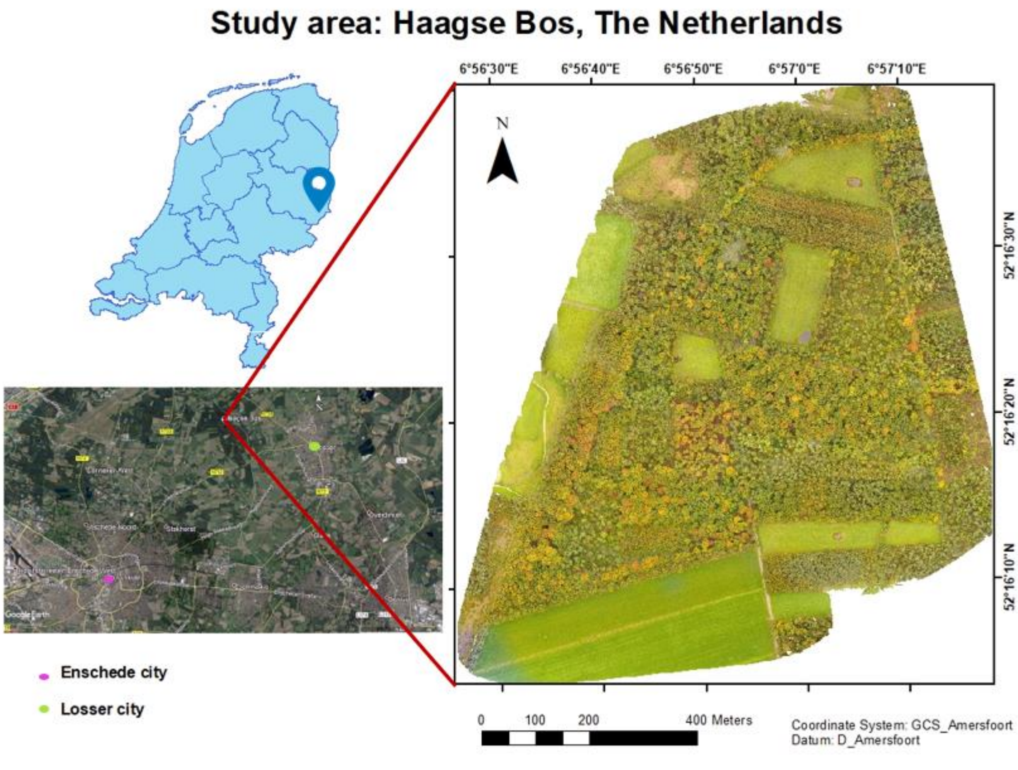

Figure 9. Location of the study area: Haagse Bos. Images sources: InfoGISMAP (2020) and Google Earth (2019).

3.1.1. Tree species

Nowadays, the forest is considered as a mixed temperate forest with native and exotic conifers and broadleaf species. As in other forests in the Netherlands, efforts have been made for the re-establishment of original species to protect wildlife habitat. Species dominance is changing. Most frequent species are Scots Pine (*Pinus Sylvestris*) and Oak (*Quercus robur)*. Other documented species are among the Conifers: Norway Spruce (*Picea abies*), Douglas fir (*Pseudotsuga menziesii*), Eastern hemlock (*Tsuga Canadensis*) and European Larch (*Larix* *decidua*, *Larix kaempferi*). Broadleaves species are European Beech (*Fagus sylvatica*), Birch (*Betula species*) and Alder (*Alnus incara*).

A previous study in Haagse Bos Natuurmonumenten and private area (Primasatya et al., 2016) has reported on the distribution of species in the forest were Spruce (37.5%), Pine (21.8%), Oak (11.7%) and Beech (23%) are the most frequent species.

3.2. Research Materials

The following materials were used in this research work. They were subdivided as data, field equipment and software packages. The data for this research was collected on-field utilising the equipment and later processed and analysed with several software types.

3.2.1. Data

Table 2 presents the data used in this research as well as the purpose of using each of them.

Table 2. Data required for this research.

Data	Objective
Tree locations and characteristics	To analyse and build the DBH models on a tree base according to each specie.
Ground truth DBH (Biometric DBH)	To calculate the sample plots AGB and validate the AGB estimations.
Centre plot location	To build the AGB and AGC models on a plot-level.
GCPs and CPs	To perform internal and external accuracy of the SfM process. These were given as secondary data from ITC-University of Twente.
Flight images set	To be used as input for the SfM process.
SfM generated the point cloud	To build the DSM, DTM and orthophoto.
DSM, DTM and CHM	To estimate the tree height.
Orthophoto	To extract the CPA and CD to model the DBH.
DBH estimations	To estimate AGB (through allometric equations).

3.2.2. Field equipment

Table 3 listed the fieldwork equipment used in this research and their functions.

Table 3. Fieldwork equipment and functions used in this research.

Fieldwork equipment	Objective
Measuring tape (50m)	To define the boundaries of the sample plots.
Diameter tape (5m)	To measure the tree DBH.
GARMIN GPS	To get the centre plot and trees location.
Field datasheet and pencil	To record the data (Appendix A).
Cellphone with Avenza App and the orthophoto	To record the data (Avenza Systems, 2020).

3.2.3. Software

Table 4 describes the software packages required and used in this research work. It shows the objectives of using each one of the software packages.

Table 4. Software required for this research.

Software	Objective
Arc GIS- Arc Map 10.6	Retrieved CHM, visualise the data, produce the AGB/Carbon stock map.
Pix4D software	Photogrammetry processing: 3D point cloud, orthophoto building, DTM, DSM.
Pix4Dcapture app & DJI GO app	To program and operate the flight of UAV
Avenza mobile app	Display the orthophoto and an approximation of the user location, store the tree location manually assigned.
Mendeley Desktop	To manage the references used
Draw.io	To draw the flowchart and the conceptual map
Microsoft excel	To perform the data analysis and plots layout
Real Statistics Excel software	To perform the statistical analysis (Zaiontz C., 2020)
Microsoft word	To write the thesis report
Microsoft PowerPoint	To build the project presentation

3.3. Research Methods

3.3.1. Study design

This research comprises three main phases. Figure 10 shows the flowchart of the method followed. The first part was the UAV and ground data collection and retrieving the UAV secondary data. The second phase was the processing of the data by treating the UAV collection of images into the SfM outputs (Orthophoto, DSM and DTM). As part of the processing, field data was convert into a digital format and CPA of every tree was manually digitised. The third part was the analysis of both the UAV and ground information.

The structure of this research consists of plot-level and tree base processes. To respond the research questions and sub-objectives, the third part is subdivided: starting with the creation of the DBH estimation model, this was done based on individual trees according to their species or species category (broadleaves and conifers) and followed by a validation process. Lastly, the modelled DBH was used to estimate the plot-level AGB/AGC and an accuracy assessment.

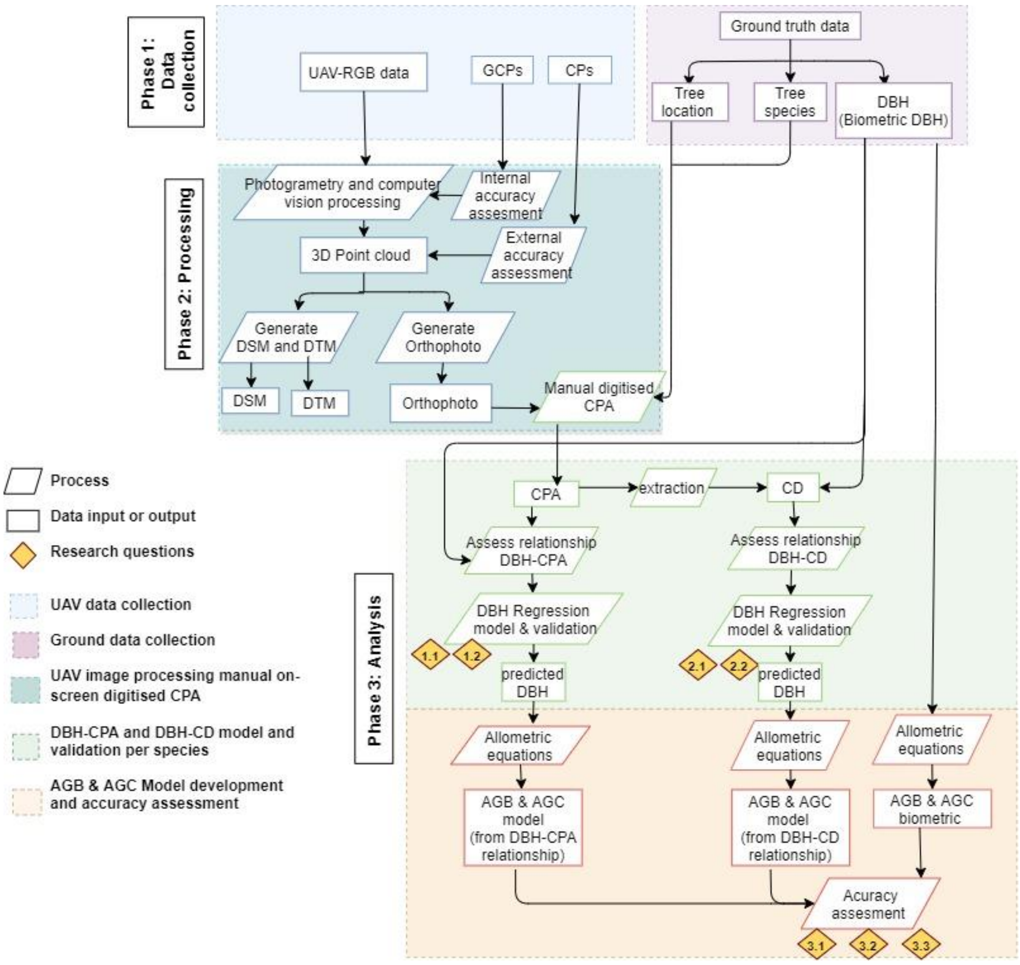

Figure 10. Flowchart of the methods used in this research work.

3.3.2. Data collection

3.3.2.1. Sampling design

To accomplish the research objectives, the data collected from the field was done in two parallel phases: on a tree base and a plot-level. Since the research objectives are related to comparisons between species, a representative number of trees per species, as well as number plots with species variation was intended. Purposive sampling was applied due to the limitations in accessibility, time and variation in the forest structure (due to its current or previous management). Nevertheless, purposive sampling is a non-probability sampling since it does not involve random selection of the sampling plots. Still, proper distribution of sample plots was aimed to get a good representation of the forest condition in the study area. In total, 39 plots were collected, and an additional 33 individual trees were measured. These individual sampled trees were collected close to the plots, to be as efficient as possible to ensure to have enough tree measurements per species for the following data analysis (Figure 11).

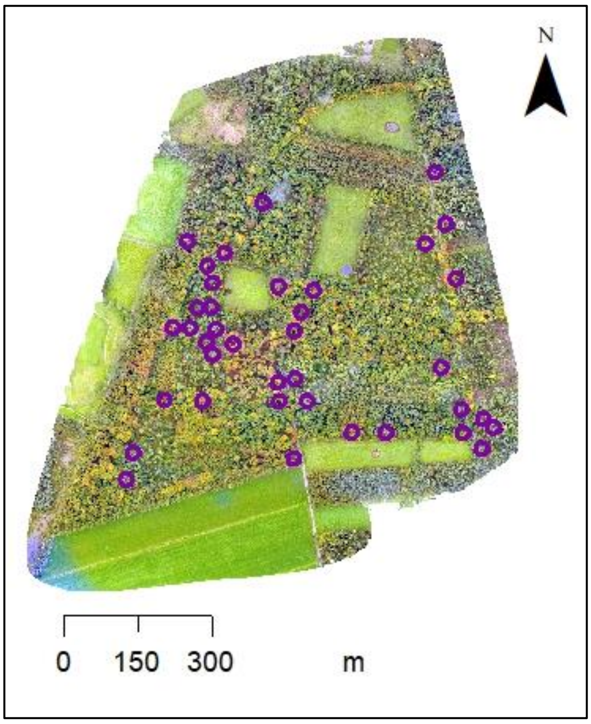

Figure 11. Map of the plots and trees sampled within the study area.

3.3.2.2. Ground truth data collection

The ground truth (biometric) measurements were performed from April 21st to 9th May 2020. Table 2 shows a list of equipment used to collect the data on the field. Every ground data was recorded on a field datasheet. Appendix A shows the table sheet of fieldwork data collection.

The measurements to acquire the individual tree data, as well as the plot-level, were done at the same time. Most of the tree base data were taken from trees within the plots but, some extra individual trees were measured to ensure a sufficient number of sampled trees per species. The biophysical parameters measured for each tree were: DBH, height, species type, distance and bearing to the plot centre, as well as the coordinates of the centre of the plot and individual tree. Just trees with a DBH equal or higher than 10cm were measured since they significantly contribute to AGB (Gibbs et al., 2007). In the case of multi-stem trees, if the dividing point of the stems less than 130 cm from the ground, then each stem considered as an individual tree. According to Chave et al. (2005) and Clough et al. (1997), the DBH was measured at 1.3 m from the ground, since the measurement must be from the stem base (Otero et al., 2018).

In other to make sure to get the most accurate coordinates of the centre of the plots and each tree location, these were recorded using GPS as well as manually identified on the orthophoto using Avenza App (Figure 12). To cross-check results, the distance of each tree to the plot centre and the bearing angle were also taken.

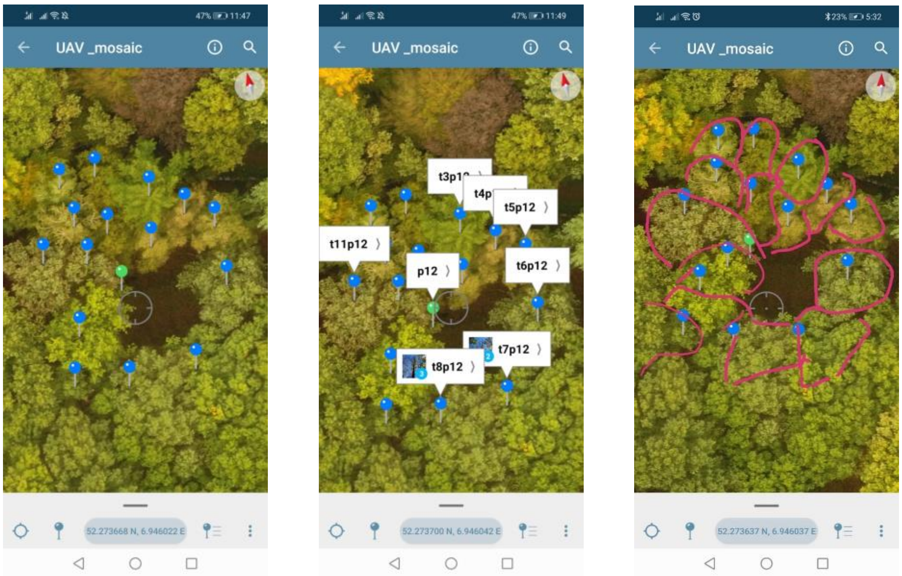

Figure 12. An example of the Avenza App display with the assigned manual tree location and an example of a plot a screenshot with an approximation of the canopy shape of the trees from ground sight.

3.3.2.3. UAV data collection

- **UAV Flight planning**

The RGB images were provided by the ITC-University of Twente as secondary data. The UAV flight and images were acquired in September 2019 using a Phantom 4 drone. A certified pilot has performed the flight.

Figure 5 shows an overview of the camera characteristics and the flight set parameters. A double grid flight was programmed, using Pix4Dcapture & Ctrl+DJI, in which the drone was set on moderate speed (5.205 [m/s]) and high overlap percentage to aim the highest point cloud density in the subsequent steps. Likewise, to achieve GSD around 5 cm, the drone flew at 100m above ground.

GSD refers to the ground sample distance, which is the distance, measured on the ground, between the centre of two successive pixels. GSD is linked with the flight hight and the spatial resolution: in general, a lower flight hight allows a smaller the GSD size; hence a bigger image spatial resolution is possible (Pix4D, 2020a).

Table 5. Flight and aerial photograph parameters (Information provided *by the ITC - University of Twente).*

Flight set conditions	**DJI Phantom 4**
Flight altitude (above-ground)	100 m
Flying speed	Moderate (Slow +)
Overlap	90% forward and 80% side overlap
The angle of the camera	On-nadir view (80° angle of the camera).
Flight mission	Polygon double grid type (North-south direction).
Picture trigger mode	Fast (5.205 [m/s])
Image Coordinate System	WGS 84 (EGM 96 Geoid
Camera characteristics	**Phantom 4 RGB camera**
Model	FC330_3.6_4000x3000 (RGB)
Sensor	1/2"3" CMOS. Effective pixels:12.4 M
Electronic shutter speed	8 – 1/8000s
Photo Formats	JPEG, DNG (RAW)
Ground control points (GCPs)	**9**
GCP Coordinate System	**Amersfoort / RD New (EGM 96 Geoid)**

❖ **Ground Control Points and Check Points**

Ground Control Points (GCP) and Check Points (CP) were pre-placed within the study area. The first ones were to be used to georeferenced the data, and the second ones were applied for the quality assessment of the image processing. During the flight, there were acquired a total of 9GCPs. The GCPs were located on permanent object and temporal (with GCP marks), the location was taken by using a GNSS-RTK.

3.3.2.4. Field Plots characteristics

This study tried to acquire an equal or similar number of plots with dominant conifers trees, dominant broadleaves trees and also mixed plots. Because of the current and previous management of the study area, the site is composed of defined sections with the same species or group of species; most of the time they are of a similar age class within one plantation. On mixed areas, the conifers were almost always much older and taller than the broadleaves.

Each sampling plot consisted of a circular plot of 500m² area and 12.62m radius. All the trees within the plot area (with >10 cm DBH) were measured. The size was determined since it has been highlighted to be in the optimum range of accuracy and cost-effectiveness in the measurements of forest attributes and AGB modelling (Bonham, 2013). Smaller plots showed a decrease in accuracy because of the geolocation shift, the edge effect and they can also capture less than the whole variability range that could lead to extrapolation errors(Frazer et al., 2011). However, after the optimum range, rising the plot size stops increasing accuracy significantly (Frazer et al., 2011; Gobakken & Næsset, 2008; Ruiz et al., 2014).

The circular shape of the sample plots was chosen since it has been proved to be less prone to errors and operationally easier: the boundaries are simpler to determine, fewer trees are in the borderline, and it minimises the perimeter length. Also, just one point location is needed (at the centre of the plot) compared to the four corner points of a square plot, which also takes longer to register and can increase the chances of error (White et al., 2013).

Priority was given on sample where there were mature trees of the species needed, making sure to have dominant broadleaves or conifers plots and also mixed plots. Other main criteria were to look for visual references that facilitate the link of the measured tree and its canopy identification on the orthophoto (i.e.

close to a path) and this way, minimise the difficulties with GPS error range. Preference was also given to single storey and spare trees spaces so most, preferably all, tree crowns within the plot can be seen from above.

The UAV orthophoto was ready generated, and some previous visits were also possible before starting the measurement activities. This was highly helpful to design the fieldwork as efficient as possible, by then we got an idea of the species distribution and where the orthophoto quality is at its best.

3.3.3. Data processing

3.3.3.1. Ground truth data processing

All data collected during fieldwork was recorded in a digital format using Excel. As mentioned before, making sure to recognize each tree and getting their exact location was an important issue. Therefore, there was a lot of crosschecking information to determine each tree location. All the field parameters and characteristics such as tree number, tree plot, DBH, Species, remarks, etc. were stored as part of the attribute table of the tree location point shapefile. The boundaries and coordinates of each plot were digitised and stored as shapefile as well. Moreover, the digitised CPA from the orthophoto was also used for the ground truth measurements. The CD was calculated as it is shown in Equation 4 and added to the biometric data Excel file.

3.3.3.2. UAV-RGB data processing

By applying Structure from Motion (SfM), a dense cluster was built of three-dimensional points recreating the mosaic image scene, within the camera motion, from the 2-dimensional set of overlapped images taken by the UAV (Nex & Remondino, 2014). Pix4D Mapper software was used for the process.

The matching of GCP and CP was done manually. Not all GCPs were given favourable results since the ones located on permanent places (i.e. a stone, a corner point or a wooden bar) were not always easily recognizable in all images. After several trials, from the nine available ground targets, the ones with the best quality outcomes were chosen: 3 GCPs were used at this stage to get the absolute orientation of the 3D point cloud and the camera locations. The process was followed by a quality assessment using the 3 CPs.

The processing workflow in Pix4D Mapper was done in three steps:

- **Initial processing.** On this step, the keypoints identified and matched between images, the camera calibration and point cloud densification are done thought Automatic Aerial Triangulation (AAT) and the Bundle Block Adjustment (BBA)(Pix4D, 2020b). The default options (the key points were identified on a full image scale) and a standard image calibration method were kept. This process is optimized with the integration of the GCPs to get the external orientation.

- **Point cloud and mesh.** This is where the point cloud densification and classification occurs. The optimal point density and a minimum of 3 images were each 3D point have to be re-projected. Also, the option multiscale- with half the image size was set to reduce the noise in the point cloud. In this step, each 3D point was automatically classified.

- **DSM, DTM, and Orthophoto.** The DSM resolution was set as 1 GSD to get the highest resolution possible, and the noise filtering option was kept and transformed, by inverse distance weighting algorithm to interpolate the points into a raster DSM and orthophoto. The orthophoto was created and merge in a single Geo-tiff.

3.3.3.3. CPA Manual digitising and CD calculation

The CPA of each tree was manually digitised using the UAV-Orthophoto as guidance (Figure 13). The CPA of all trees was saved as a shapefile and their area calculated in square meters. The issue of identifying the CPA boundaries and shape of every tree was crucial for the following analysis. In this sense, the tree location point shapefile, videos and photos taking on the field were of great help, as well as the quick canopy draws made on the cell phone screenshot. The UAV-images taken during fall season were a good help on distinguishing between species and sometimes even between tree crowns of neighbouring trees from same species. The challenge was that the tree crowns sometimes are not easy to differentiate among them. Hence, there is the risk of overestimating the CPA size (from several crowns clustering) but also to underestimate them (i.e. when crown is so irregular it looks like two or more crowns). Once the CPA of all trees were digitised and their area calculated (m^2), the CD (m) was derived by following Equation 4.

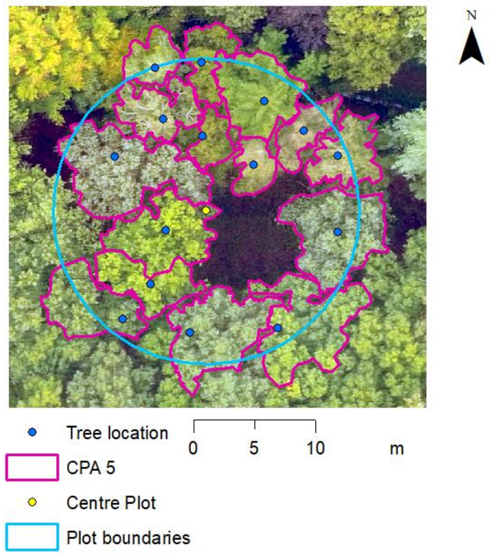

Figure 13. Example of the manual on-screen CPA digitising.

3.3.4. Data analysis

3.3.4.1. Ground truth data analysis

AGB can vary according to the age, species and even location. Various AGB allometric equations have been developed, based on destructive methods, to estimate the biomass of different tree species. To avoid wrong estimations when using allometric equations, it was selected the ones with high accuracy and that were preferably made close to our study area. The ground measured DBH of each tree was used as input for the allometric equation according to their species (Table 6) to get the biometric AGB on a plot level (Equation 5) and, derived the biometric AGC by the carbon content factor 0.5(Hirata et al., 2012) (Equation 6). The output value was used as ground truth to test the accuracy of the AGB/AGC estimations from UAV image.

*Table 6. AGB Allometric equations applied. * Species name and country where the AGB allometric equation was designed.*

Species	AGB Allometric equations	R^2	Source
Scot Pine **Pinus Sylvestris*, Czech republic.	$AGB[Kg] = 0.1182 * DBH[cm]^{2.3281}$	0.98	(Zianis, 2005)
Norway Spruce **Picea abies*, Germany	$AGB[kg] = -43.13 + (2.25 * DBH[cm]) + (0.452 * DBH[cm]^2)$	0.995	(Zianis et al., 2005)
Douglas fir **Pseudotsuga menziesii*, Netherlands.	$AGB[Kg] = -0.111 + DBH[cm]^{2.397}$	0.995	(Zianis et al., 2005)
Oak **Quercus petraea*, Germany.	$AGB[Kg] = 0.0722 * DBH[cm]^{2.5135}$	0.97	(Suchomel et al., 2012)
Alder **Alnus glutinosa*. Sweden.	$AGB[Kg] = 0.00079 * DBH[mm]^{2.28546}$	0.987	(Zianis et al., 2005)
Birch **Betula pendula*. Sweden.	$AGB[Kg] = 0.00087 * DBH[mm]^{2.28639}$	0.985	(Zianis et al., 2005)
Beech **Fagus sylvatica*, Netherlands.	$AGB[Kg] = 0.0798 * DBH[cm]^{2.601}$	0.988	(Zianis et al., 2005)
Larch **Larix decidua*, Czech Republic.	Needles branches $[Kg] = 0.027940 * DBH[cm]^{1.800410}$ Dead branches $[Kg] = 0.118280 * DBH[cm]^{1.491200}$ Live (green) branches$[Kg] = 0.027960 * DBH[cm]^{2.198240}$ Stemwood $[Kg] = 0.054380 * DBH[cm]^{2.420242}$ Stem bark $[Kg] = 0.006588 * DBH[cm]^{2.42044}$ AGB [kg] =(Needles + dead branches+ green branches+ stem wood+ stem bark)	0.98 0.85 0.99 0.99	(Novák et al., 2011)

Most of the allometric equations estimate the tree AGB in Kg. To get AGB in tons/ha, we summed the AGB of all the trees within each plot and follow Equation 5:

$$Plot\ AGB\ [\frac{tons}{ha}] = \frac{(\sum tree\ AGB\ [Kg])}{1000\ ton} /\ 0.05\ ha \qquad \text{(Equation 5)}$$

Where the summing of all trees AGB is divided by 1,000 to convert from kg to ton and then, divided by the plot area 0.05ha to get the final result in tons/ha.

Once we get the AGB, the carbon stock is calculated with a conversion factor (CF=0.5), which means that 50% of AGB is considered as the carbon stored in the above ground biomass (Hirata et al., 2012).

$$AGC = AGB\ x\ CF \qquad \text{(Equation 6)}$$

Where AGC [Mg] refers to above-ground carbon stock, ABG [Kg] is above-ground biomass, and CF [no units] is the carbon content factor, in this case, it is 0.5.

3.3.4.2. UAV data analysis

The process to estimate the AGB and AGC was done using the same allometric equations (Table 6) but this time using the DBH estimations derived from both models (DBH-CPA and DBH-CD) from the UAV-images. All the following steps in the workflow were made for each species (Spruce, Douglas, Pine, Oak, Birch and Beech) as well as for the general species category (broadleaves and conifers).

- **Assessing linear regression assumptions**

Different regression model types were be considered, but a linear regression model is usually the one considered as a starting point. Therefore, linear regression assumptions were verified (Poole & O'Farrell, 1971). As data pre-analysis, we check the normality distribution of the variables as well as the residuals of a linear regression. D'Agostino-Pearson normality test was used on all the parameters used as well as the residuals since, this normality test have proved to be more reliable in a broader range of data circumstances (Yap & Sim, 2011). We also checked on the variance of the residuals on a scatter plot. This step was useful to understand the relationships better and to spot and eliminate the outliers trees for the subsequent model building process.

- **Outliers**

Residual is the difference between the observed and predicted value, with a positive sign if the data is above the trendline and negative when it is below it. Outliers are observations with big residuals, meaning that the observed value is on a more considerable distance from the one that the regression model estimate (BU, 2016; Lumen, 2020). Histogram and Boxplot gives an idea of the general data behaviour of each variable but also to spot the outliers. A popular rule of the thumb for potential outliers identification is by Equation 7 and Equation 8 (Lumen, 2020).

$$Q3 + (1.5*IQR) < \text{observation} = \text{ potential outlier at the lower bound} \qquad \text{(Equation 7)}$$

$$Q1 - (1.5*IQR) > \text{observation} = \text{potential outlier at the upper bound} \qquad \text{(Equation 8)}$$

Where Q1 is the is the first quartile of the data, Q4 is the third quartile of the data, and IQR is the interquartile range which is the difference between Q3 and Q1.

To build each model, the criteria for outliers removal was by just disregarding the trees needed to the accomplish of normality on all the parameters (DBH, CPA and CD) and residuals distribution. It was done stating by the ones highlighted by Equation 7 and Equation 8 and by using the Q-Q plot and D'Agostino-Pearson as guidance.

3.3.4.1. Developing regression model and validation model

In this research CPA and CD are considered as the independent or explanatory variables, and DBH is the dependent variables. By taking the individual trees that satisfy the normality test and having eliminated the outliers, DBH estimation models were built by performing a linear regression model. Moreover, logarithmic, power and quadratic regressions were also built in other compare the accuracy results between them and select the regression function type that describes the relationship the best.

The process was done for both the DBH-CPA and DBH-CD relationship, randomly dividing the dataset 70/30 for model building and validation. This process was performed per conifer and broadleaved general categories, as well as for each species. From the total amount of trees, 70% were used to build the models (linear logarithmic, power and quadratic) for the relationship between the DBH-CPA and DBH- CD and select the one with the best accuracy results in terms of R^2 and Root Mean Square Error (RMSE). Residuals were graph against biometric DBH to make sure that there is a random distribution of the residuals.

As a validation process, the model chosen was applied to the 30% of the remaining (and independent) data, by plotting the estimated DBH values, derived from the chosen DBH-CPA and DBH-CD models, against the biometric DBH and create a linear regression. This way, we were applying statistical analysis to validate the consistency of the DBH models.

The correlation coefficient (r) (Equation9), coefficient of determination (R^2) (Equation 10), were used as indicators of the accuracy of the estimations. Root Mean Square Error (RMSE) (Equation 11 and 12), Root Mean Square Deviation (RMSD) (Equation 13) were calculated to know about the deviation of the estimated and observed values. RMSE tells us about how far are the estimated values from the linear regression line, and it underestimates the real error (Piñeiro et al., 2008). Therefore, the analysis was also complemented with RMSD which is the mean deviation between model estimations against the 1:1 line of the observed values (Piñeiro et al., 2008).

To answer the research hypothesis, a T-test was applied to test on the significant difference (α = 0.05) between the means of the estimated DBH results and biometric DBH; the test was done assuming unequal variance to get trustful results (Ruxton, 2006).

$$\mathrm{r} = \frac{\sum ((y_{\mathrm{est}} - \overline{y_{\mathrm{est}}})(y_{\mathrm{obs}} - \overline{y_{\mathrm{obs}}}))}{\sqrt{\sum (y_{\mathrm{est}} - \overline{y_{\mathrm{est}}})^2 \sum (y_{\mathrm{obs}} - \overline{y_{\mathrm{obs}}})^2}}. \qquad \text{(Equation 9)}$$

$$R^2 = \mathrm{r}^2 \qquad \text{(Equation 10)}$$

$$RMSE = \sqrt{\frac{\sum (y_{\mathrm{est}} - y_{\mathrm{obs}})^2}{(n - 1)}} \qquad \text{(Equation 11)}$$

$$\mathrm{RMSE}\ [\%] = \frac{\mathrm{RMSE}}{\overline{y_{\mathrm{obs}}}} \times 100 \qquad \text{(Equation 12)}$$

Where y_{obs}refers to the observed reference value (linear trendline), y_{est} is the predicted DBH from the model (from DBH-CPA and DBH- CD models) and, their average values are expressed as $\overline{y_{\mathrm{obs}}}$ and $\overline{y_{\mathrm{est}}}$. n refers to the number of observations.

$$RMSD = \sqrt{\frac{\sum (y_{\mathrm{est}} - y_{\mathrm{obs}})^2}{(n - 1)}} \qquad \text{(Equation 13)}$$

Where y_{obs}refers to the real observed value (Biometric DBH), y_{est} is the predicted DBH from the model (from DBH-CPA and DBH-CD models). n refers to the number of observations.

3.3.4.2. Plot AGB and AGC estimation and accuracy assessment

The modelled DBH was used as input to the allometric equations (Table 6) to come up with AGB and AGC. A linear regression performed as an accuracy assessment - plotted as suggested from Piñeiro et al., (2008)- taking the biomass from ground truth data, biometric AGB /AGC on the Y axis, against of AGB/AGC quantified from DBH estimations on the x-axis. They were named "AGB-DBH-CPA" from DBH-CPA relationship and "AGB DBH-CD" from DBH-CD relationship.

The assessment was made for all plots but also by dominant plot type. The evaluation was made through statistical indicators R^2, RMSE and RMSD. Residuals were graph against biometric AGB/AGC to complement the analysis of the model performance. A T-test also performed to test the significant difference between biometric and estimated AGB/AGC values (α = 0.05).

4. RESULTS

The following section starts with a statistical analysis of the fieldwork data collection as well as the analysis of the UAV data processing. Then, it exposes the DBH model building and validation results. Finally, the AGB and AGC results and accuracy assessment are presented.

4.1. Descriptive statistics from field data

A total of 477 trees were recorded from 39 plots plus, the measurements of 33 individual trees that were gathered from outside the plots to complement the number of trees per species on the DBH model building phase. Figure 14 and Figure 15 present a summary of the data collected during the fieldwork activities.

The conifers species found in the study area were: Pine, Douglas Fir and Spruce. While for the broadleaves species found in the study area were: Beech, Birch and Oak (Alder and Larch were excluded from the tree base part of this research because their number in the study area is minimal). Figure 14 presents the tree species distribution (%) as well as the number of trees collected per species (broadleaves or conifers) and individual species. The tree parameters collected were DBH, species recognition and tree location (fieldwork data sheet in Appendix A).

Table 7 presents the overall characteristics of the trees species within all the 39 plots. They are 444 trees, and each plot has between 6 and 20 trees per plot with a mean of 11.38 trees. Figure 16 presents the number of trees per plot, indicating the tree species with different colours. Plot 24 was eliminated because the bad weather didn't allow to finalize the measurements. More details on the plot configuration characteristics can be found in Appendix C.

Plots were classified as Conifers–dominated plots, Broadleaves-dominated plots and mixed according to the number of trees per species within each plot: 10 Mixed plots (plot no. 1, 3, 17, 18, 20, 25, 30, 31, 34 and 40), 18 Broadleaves plots (plot no. 2, 4, 5,6,7, 8, 10, 11, 12, 13, 14, 15, 19, 21, 27, 32, 37and 38) and 11 Conifers plots (plot no. 9, 16, 22, 23, 26, 28, 29, 33, 35, 36, 39).

Trees within the plots + individual

Broadleaves	**236**	**Oak**	97
		Beech	89
		Birch	49
		Alder	1
Conifers	**241**	**Douglas**	86
		Spruce	84
		Pine	59
		Larch	12
TOTAL	**477**		**477**

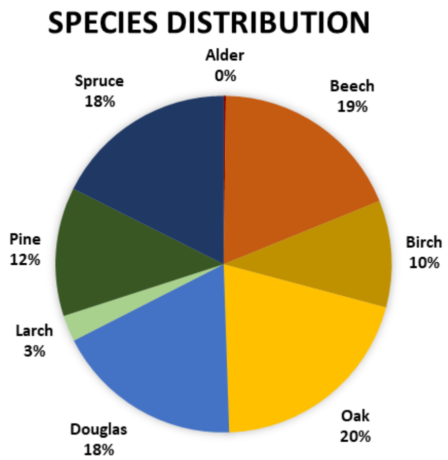

Figure 14. Trees per species and group of species (left) and species distribution (%) of the total of trees collected (right).

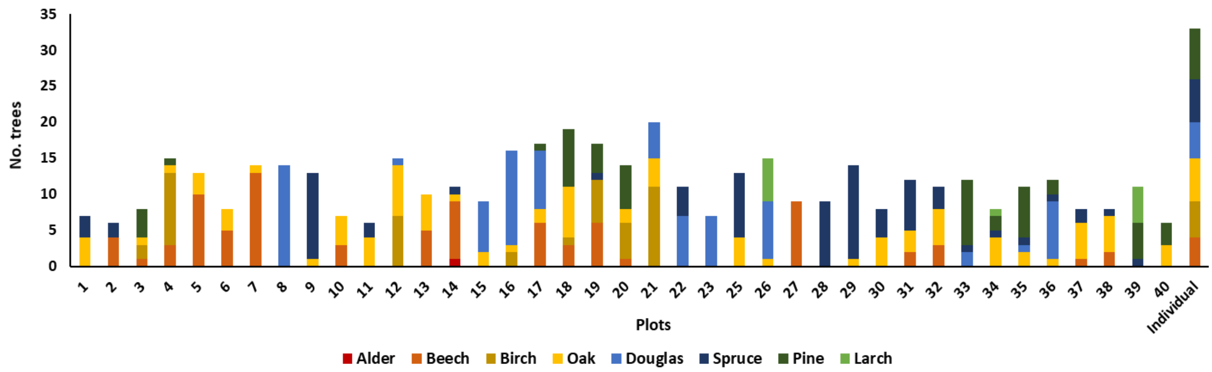

Figure 15. Distribution of the number of trees, and their species, within each plot.

Table 7. Descriptive statistics of the trees within the plots.

	No. Trees
Total	444
Mean	11.38
Std. Error	0.60
Std. Dev.	3.72
Variance	13.82
Min	6
Max	20

4.1.1. Biometric DBH descriptive statistics results

Table 8 presents the descriptive statistics of the biometric DBH from all the trees measured by species categories (broadleaves and conifers) and individual species in this research work. The range between the smallest and biggest DBH of all trees is very similar among species categories (conifers and broadleaves). Nevertheless, looking at a range of biometric DBH between species, the DBH range in Pine (11.10-65.5cm), Oak (12.60-78.90cm) and Birch (10-48.3cm) is not as wide as the rest. Worth highlight that the mean value in Birch (25cm) is noticeable low compare to any other groups. Noted that Birch doesn't tend to grow as big as the other two broadleaved species, usually, it doesn't increase beyond 60cm DBH (Hemery et al., 2005).

To complement the analysis, boxplot in Figure 16 is presented to give a visual distribution of data. The means are close between species categories (42.99cm for conifers and 42.32cm for broadleaves) and species, except for Beech (with a mean of 48.79cm) and Birch (mean of 25.61).Looking at the kurtosis and skewness, all values are considerably low which is a sign of normality; Spruce and Oak kurtosis indicate their curve is slightly flatter than the rest and the Pine skewness is slightly higher than the rest.

Figure 17 offers a visual interpretation of the data behaviour, where the general DBH histogram of all trees shows an almost symmetrical shape, were most of the trees falls in the range of 40 and 50 cm (133 trees of the 477 total). Broadleaves have an almost similar shape, 31 of the 235 total have diameters of 40-45cm and 28 trees 45-50cm. Beyond those ranges, 73 broadleaves trees have DBH above 50cm, and 103 have less 40cm DBH. In the case of conifers, from the total 229 trees, 32 have DBH between 40-45cm, 40 trees between 45-50cm, 60 trees have DBH above 50cm and, 94 below 40cm.

Overall, the biometric DBH values follow a straight line when data plotted against appropriate quantiles; a normal distribution can be assumed. It is also notable in all Q-Q plots (Figure 17) that at the ages of the line there is a light tale on both sides, but a little more pronounced in the high values. This means that the higher deviation, and possible outliers, could be at the extreme DBH rage values. Moreover, the histograms show potential outliers among the trees with the highest DBH values (above 70 cm).

D'Agostino-Pearson was also performed to look for consistency in the normal distribution assumption (Table 8). In this sense, the individual species and species categories that reported p-values below 0.05, and therefore the hypothesis of the data normally distributed, cannot be accepted. In those cases (Pine and Spruce), the outliers were spotted and discarded in the subsequent steps until the normal distribution was fulfilled.

Table 8. Descriptive statistics of the biometric DBH of all trees, from species group (broadleaves and conifers) and specific species.

DBH [cm]	All trees	Conifers	Broadleaves	Spruce	Douglas	Pine	Birch	Oak	Beech
N	477	229	235	84	86	59	49	97	89
Mean	42.59	42.99	42.32	42.97	44.37	41.01	25.61	44.81	48.79
Std. Error	0.70	0.95	1.06	1.64	1.70	1.38	1.20	1.32	1.74
Std. Dev	15.19	14.33	16.20	15.00	15.81	10.60	8.39	13.04	16.41
Variance	230.71	205.38	262.44	225.02	249.91	112.28	70.42	170.04	269.16
Min	10.00	10.10	10.00	12.50	10.10	11.10	10.00	12.60	13.10
Max	89.60	89.60	82.30	89.60	81.00	65.50	48.30	78.90	82.30
Q1	32.5	34.4	30	31.425	34.275	36.65	20.4	37.4	40.3
Q3	52.3	50.9	53.5	51.4	55.925	47.05	30.9	51.8	60.4
IQR	19.80	16.50	23.50	19.98	21.65	10.40	10.50	14.40	20.10
Kurtosis	-0.06	0.44	-0.44	0.79	-0.37	1.45	0.06	0.70	-0.35
Skewness	0.20	0.26	0.17	0.68	-0.03	-0.80	0.22	0.18	-0.24
DA-stat	3.20	4.31	3.87	8.31	0.50	9.69	0.55	2.50	1.34
p-value	0.20	0.12	0.14	0.02	0.78	0.01	0.76	0.29	0.51
Normal	Yes	Yes	Yes	No	Yes	No	Yes	Yes	Yes

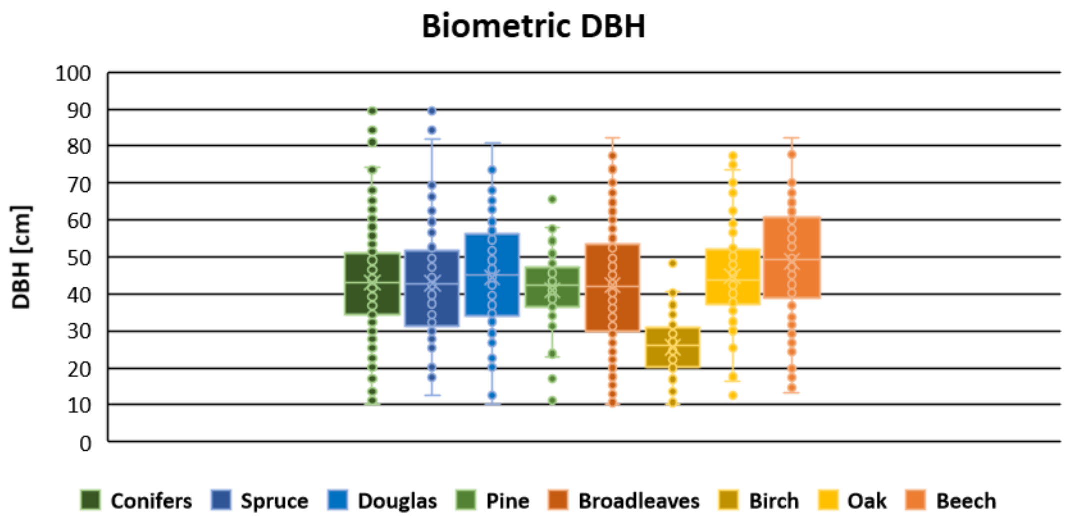

Figure 16. Boxplot of biometric DBH.

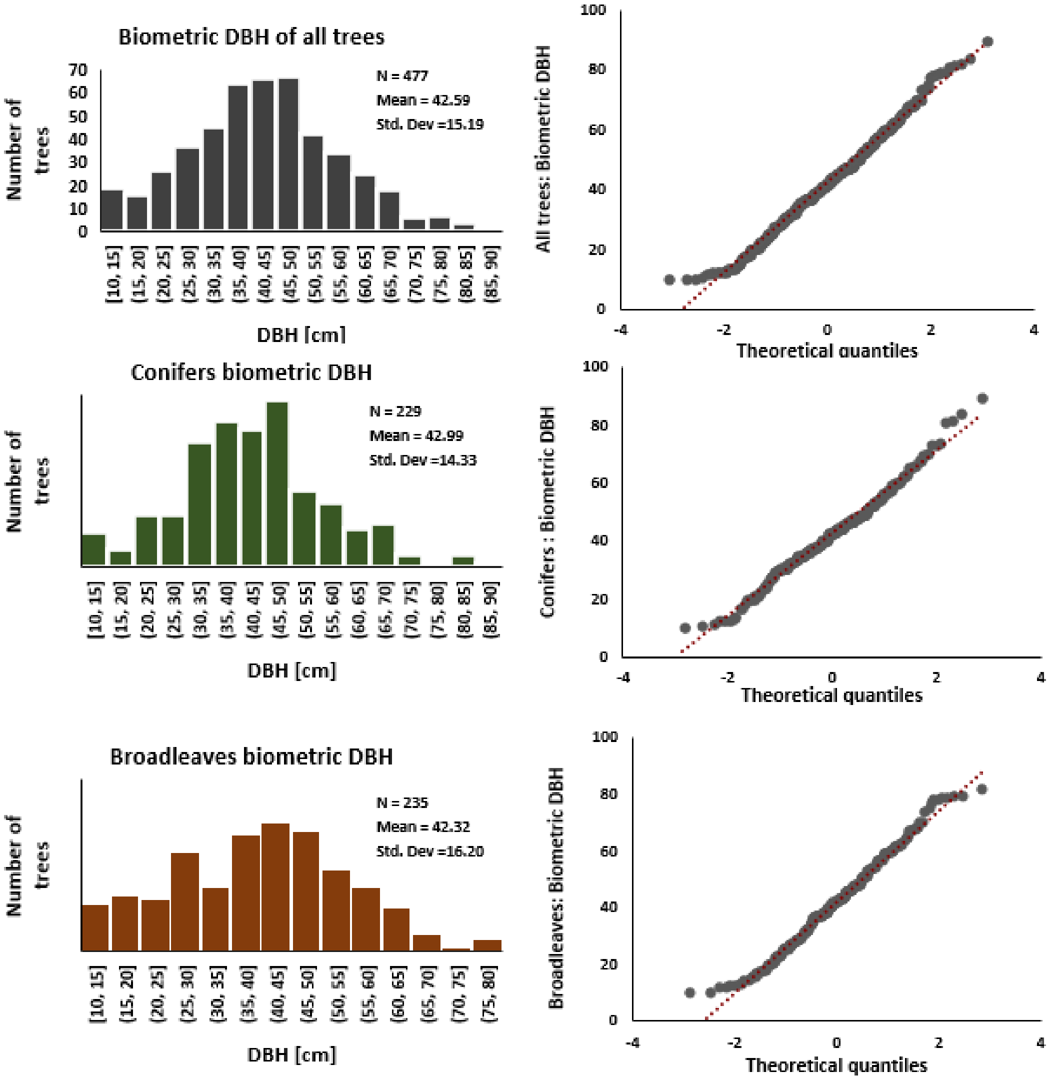

Figure 17. Histogram distribution of biometric DBH measured in the field and normal Q-Q plot .

4.2. UAV-RGB processing results

Table 9 and Figure 18 show an overview of the main steps taken by SfM to get the main tree outputs. The Dutch projected coordinate system 'RD_New' and Amersfoort as the geodetic datum was used for all spatial data. RD stands for national triangle coordinates (Rijksdriehoekscoördinaten in Dutch).

The quality report of the process is shown in Appendix B. The high overlap between the images enables 100% of the image set to be correctly oriented. A median of 57,568 keypoints and 3,122.71 matches were identified per image. From the three GCPs used, the mean georeferencing error was 0m. After the Bundle Block Adjustment, the resulted reprojection error was 0.126 pixels. Moreover, the hight overlapping percentage resulted in a 3D Point Cloud with a total of 61'138,701 3D densified points and an average point density of 30.3 points per m^3. The orthophoto acquired a spatial resolution of 4.64 x 4.64 cm/pixel and allowed a high level of detail to recognized and manual on-screen digitise each of the canopies.

The resulted DTM output was into 23.727 cm/pixel, and the DSM was 4.64 cm/pixel spatial resolution. A resample was done to the DSM to match the resolution of both before creating the CHM.

Figure 18 presents an overview of the processing procedure of the UAV images on Pix4D Mapper Software. As it can be appreciated in Figure 18g, the DTM presented some areas (blue patches) with high altitudes as if there was an elevation in the ground when there is a high tree density. In those places, the CHM reported low tree height numbers (represented with clear- brownish spots). Therefore, it was not possible to obtain a reasonable tree height quality estimations on all the plots measured in the study area.

Table 9. Summary of the UAV image processing steps.

General	
Average GSD	4.64 cm
Total area	0.790 km2/ 79.0145 ha
Dataset	807 out of 807 (100%) images calibrated and geolocated.
Georeferencing mean RMS	0 m
Bundle Block Adjustment	
Mean reprojection error	0.126 pixels
Coordinate Systems	
Image coordinate system	WGS 84
GCP	Amersfoort/ RD New
Output coordinate system	Amersfoort/ RD New
Point Cloud Densification	
Min number of matches	3
Number of 3D densified points	61'138,701
Average point cloud density	30.3 m³
DSM, Orthomosaic, and DTM	
DSM and Orthomosaic resolution	1 x GSD (4.64 [cm/pixel])
DTM resolution	5 x GSD (23.737 cm/pixel)
DTM method	Inverse Distance Weighting

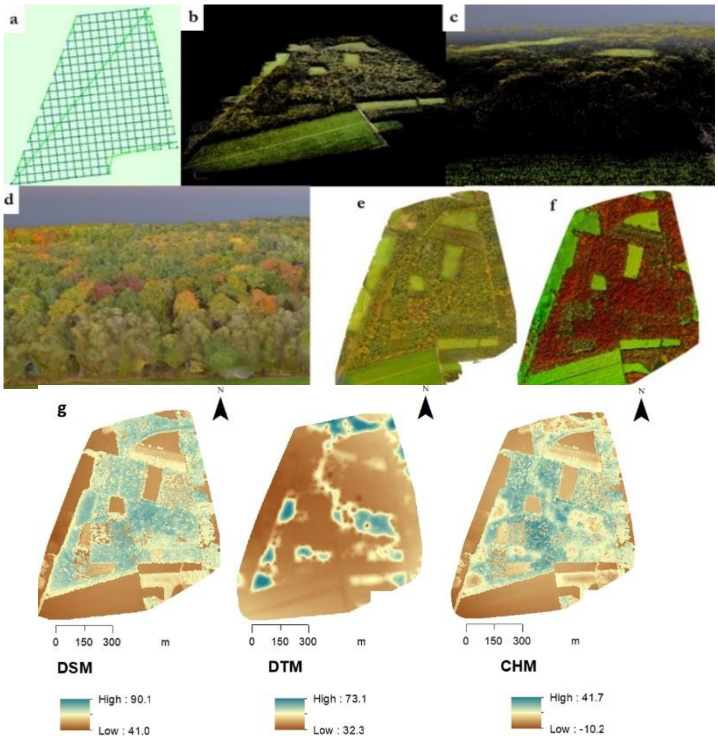

Figure 18. Overview of the UAV-RGB image processing. (a) Top view of the initial images sequence positions according to the flight path. (b) and (c) 3D point cloud from different point sight, on the image (c) can be appreciated the tree highest points as well as the ground points. (d) Triangulation modelling process. (e) Orthomosaic. (f) DSM before densification. (g) The resulted DSM [m], DTM [m] and CHM [m].

4.3. Crown Projection Area (CPA) descriptive statistics results

Table 10 presents an overall description of all the trees CPA. The general CPA tree range is between 2.86 and 100.26 m^2 and therefore with high variance. However, the majority of trees are in 18-28 m^2 range (Figure 20). Notably, the mean of broadleaves species is very different between Oak and Beech (41.37 and 38.31 respectively) and Birch (14.15 m2) while the mean value in conifer species are closer to each other. Birch and Pine presented a much lower mean but also standard deviation and variance. Looking at the boxplot (Figure 19), it can be seen that the CPA range of these two species is lower and closer than the other species.

As in the DBH histograms, in CPA cases (Figure 20), the distribution showed a slightly right-skewed that gets more pronounced in the conifers histogram, and the curve gets softer on the broadleaves. It can be seen that the conifers variance is much higher in the case of broadleaves than conifers (191.53 and 392.33 respectively). The frequency peak of the conifers histogram seems more pronounce, where 83 of the 229 conifer trees have CPA between 18-28 m^2, different from the broadleaves whose peak is peak is smoother and found between 33- 38 m^2 with 62 trees. Nevertheless, the frequency of both groups between 3-53 m^2 is pretty similar (217 of the 229 confers and 178 of the total 235 broadleaved trees fall in this range).

The Q-Q plot showed that the CPA distribution follows a straight line on their middle values as a normal distribution indication. Nevertheless, the ages of the line make a tale and this is especially notable on the highest CPA values(above 70m^2) showing an increase in variation and making an outliers warning.

In the general conifers and broadleaves categories, and the Spruce species, the kurtosis and skewness highlight that there might be a non-normal distribution. As it is showed in Table 10, in the case of conifers, broadleaves categories as well as Spruce and Beech species, they fail the normal distribution test. The boxplot in Figure 19, gives an idea of the where are some of the outliers. In those cases, the outliers were discarded during the DBH model building from DBH-CPA relationship for the fulfilment of the linear regression assumptions.

Table 10. Descriptive statistics of CPA of all trees, from species category (broadleaves and conifers) and per specific species.

CPA [m^2]	All trees	Conifers	Broadleaves	Spruce	Douglas	Pine	Birch	Oak	Beech
N	477	229	235	84	86	59	49	97	89
Mean	30.88	27.20	34.54	26.02	29.88	24.95	14.15	41.37	38.31
Std. Error	0.80	0.91	1.29	1.60	1.65	1.17	1.11	2.01	1.79
Std. Dev	17.38	13.84	19.81	14.70	15.33	9.01	7.79	19.79	16.89
Variance	302.18	191.53	392.33	216.20	235.01	81.26	60.67	391.83	285.41
Min	2.86	2.86	3.08	2.99	4.90	2.86	3.08	4.14	6.90
Max	100.26	96.03	100.26	96.03	73.14	47.25	33.49	93.47	100.26
Q1	18.52	18.56	18.03	16.12	18.83	21.00	8.33	28.23	24.40
Q3	40.95	34.17	47.73	32.22	41.89	29.43	19.81	53.73	49.27
IQR	22.43	15.61	29.69	16.10	23.06	8.43	11.48	25.49	24.87
Kurtosis	0.98	2.51	0.06	5.67	-0.40	0.50	-0.11	-0.20	1.36
Skewness	0.89	1.06	0.58	1.78	0.40	-0.23	0.74	0.34	0.67
DA-stat	58.93	49.10	12.16	44.55	3.00	1.48	4.52	2.11	10.73
p-value	0.00	2.18 E-11	2.28E-03	2.11E-10	0.22	0.48	0.10	0.35	4.67E-03
Normal	no	no	no	no	yes	yes	yes	yes	no

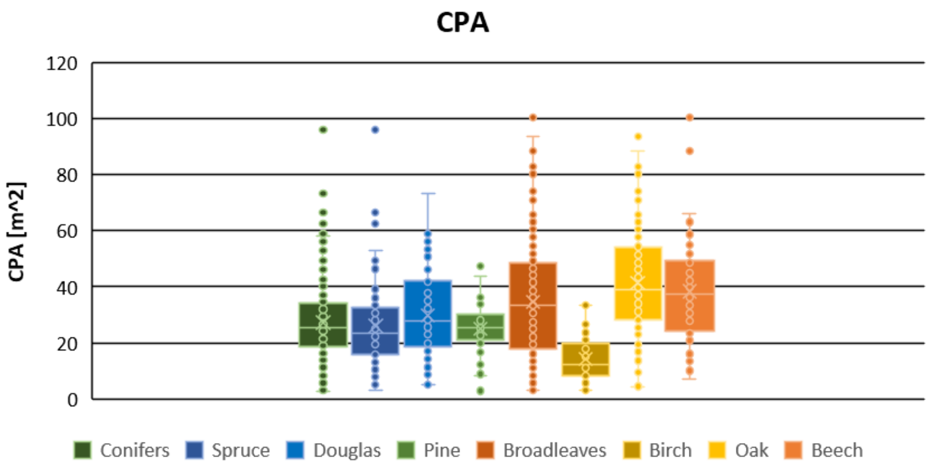

Figure 19. Boxplot of biometric crown projection area (CPA).

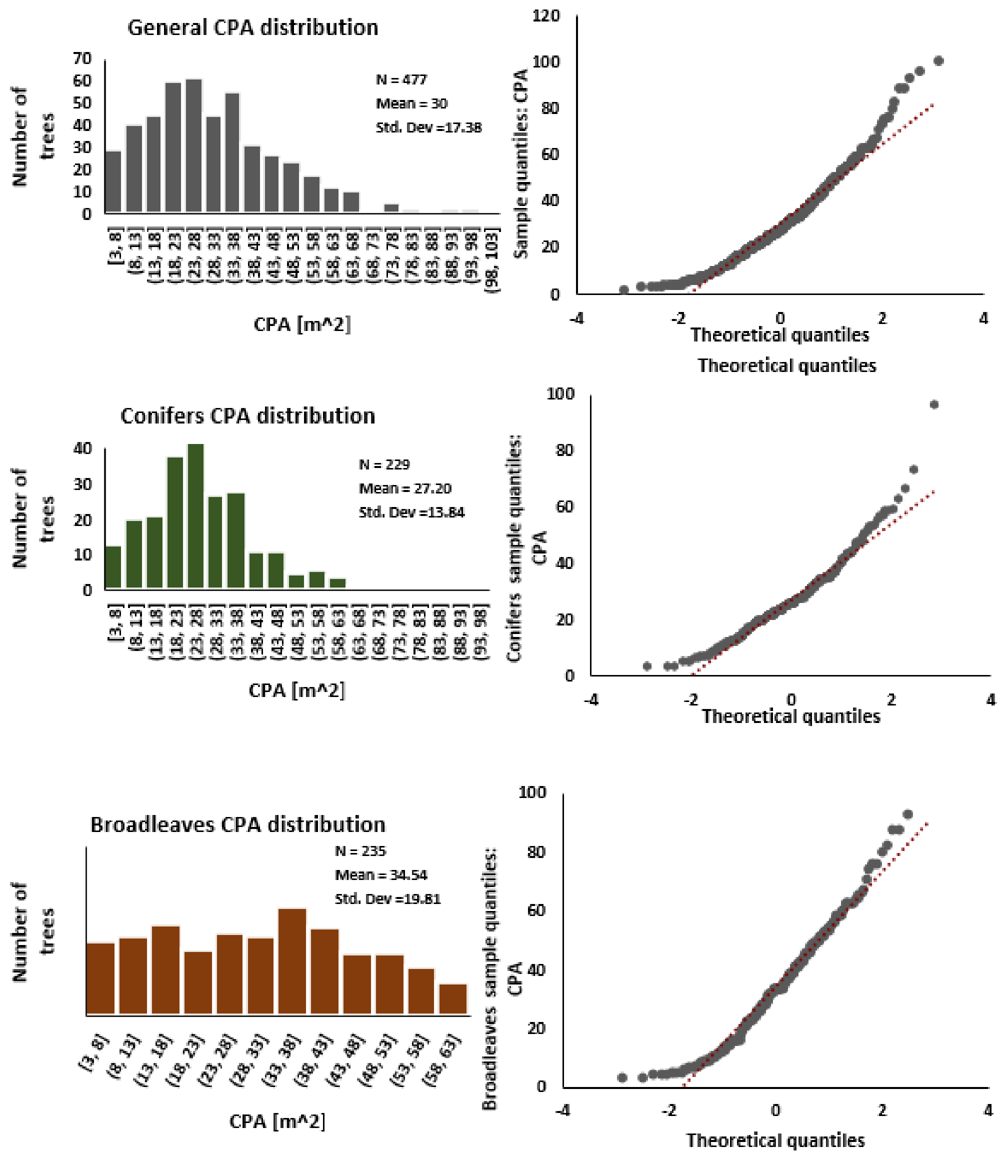

Figure 20. Histogram distribution of the crown projection area (CPA).

4.4. Crown diameter (CD) descriptive statistics results

Table 11 presents an overview of the CD descriptive statistics among the data. It can be seen that the mean of conifers and broadleaves general categories are similar (5.69 and 6.33, respectively). Among species, the conifers are also pretty consistent in their mean values, but broadleaves species have a wider difference (4.08, 7.02 and 6.81 m). Therefore, broadleaves category have a higher variance than the conifer group (3.97 and 2.25, respectively). This is also notable by looking at the boxplot in
Figure *21*.

Moreover, the standard deviation of broadleaves category is 1.99 and 1.50 for conifers category. Similar values are found between species categories (1.52m Spruce, 1.66m Douglas, 1.86m Oak and 1.57m for Beech), except for Birch and Pine which have a much lower standard deviation (1.16m and 1.15m respectively). Worth to mention that variance and standard deviation of CD [m] data are lower than CPA[m^2].

The histogram (Figure 22) shows that the CD of all trees follows a normal distribution. As in CPA, Conifers histogram peak is more pronounced than broadleaves. On the issue of normality of the CD distribution, the majority of the data follows a straight line behaviour when compared with theoretical quantiles with what looks like a slight variation on the low and high end but without serious deviation for normality (Figure 23). In general, it seems to follow better the straight line than the CPA Q-Q plots.

The kurtosis and skewness on Spruce and Pine species are highlighted and they also fail on the D'Agostino-Pearson normality test. Hence, the potential outliers were spotted.

Table 11. Descriptive statistics of the Crown diameter of all trees, from species category (broadleaves and conifers)and per species.

CD [m]	All trees	Conifers	Broadleaves	Spruce	Douglas	Pine	Birch	Oak	Beech
N	477	229	235	84	86	59	49	97	89
Mean	6.01	5.69	6.33	5.55	5.94	5.52	4.08	7.02	6.81
Std. Error	0.08	0.10	0.13	0.17	0.18	0.15	0.17	0.19	0.17
Std. Dev	1.78	1.50	1.99	1.52	1.66	1.15	1.16	1.86	1.57
Variance	3.17	2.25	3.97	2.32	2.77	1.32	1.36	3.47	2.48
Min	1.91	1.91	1.98	1.95	2.50	1.91	1.98	2.30	2.96
Max	11.30	11.06	11.30	11.06	9.65	7.76	6.53	10.91	11.30
Q1	4.86	4.86	4.79	4.53	4.90	5.17	3.26	6.00	5.57
Q3	7.22	6.60	7.80	6.40	7.30	6.12	5.02	8.27	7.92
IQR	2.37	1.73	3.00	1.87	2.41	0.95	1.77	2.28	2.35
Kurtosis	-0.19	0.43	-0.56	1.39	-0.55	1.90	-0.65	0.12	0.10
Skewness	0.09	0.09	-0.11	0.61	-0.19	-1.08	0.22	-0.41	-0.09
DA-stat	1.44	2.05	6.12	9.39	2.17	14.98	1.83	2.99	0.29
p-value	0.49	0.36	0.05	0.01	0.34	5.58E-04	0.40	0.22	0.87
Normal	yes	yes	no	no	yes	no	yes	yes	yes

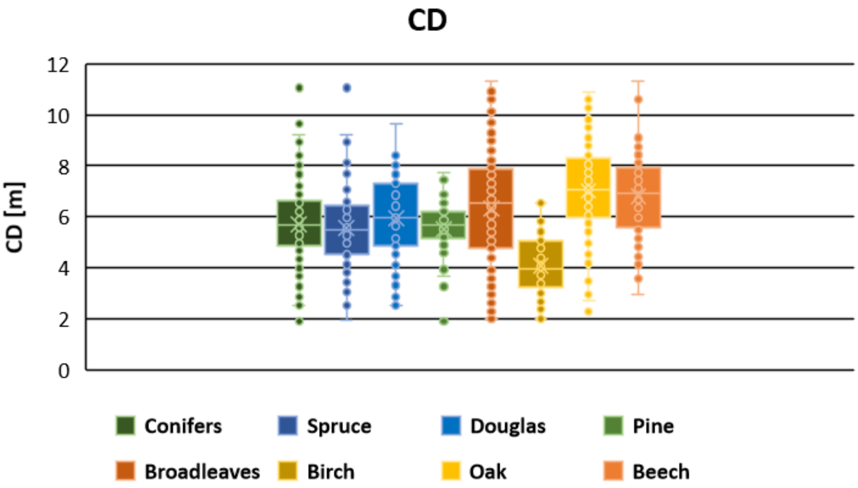

Figure 21. Boxplot of biometric crown diameter (CD).

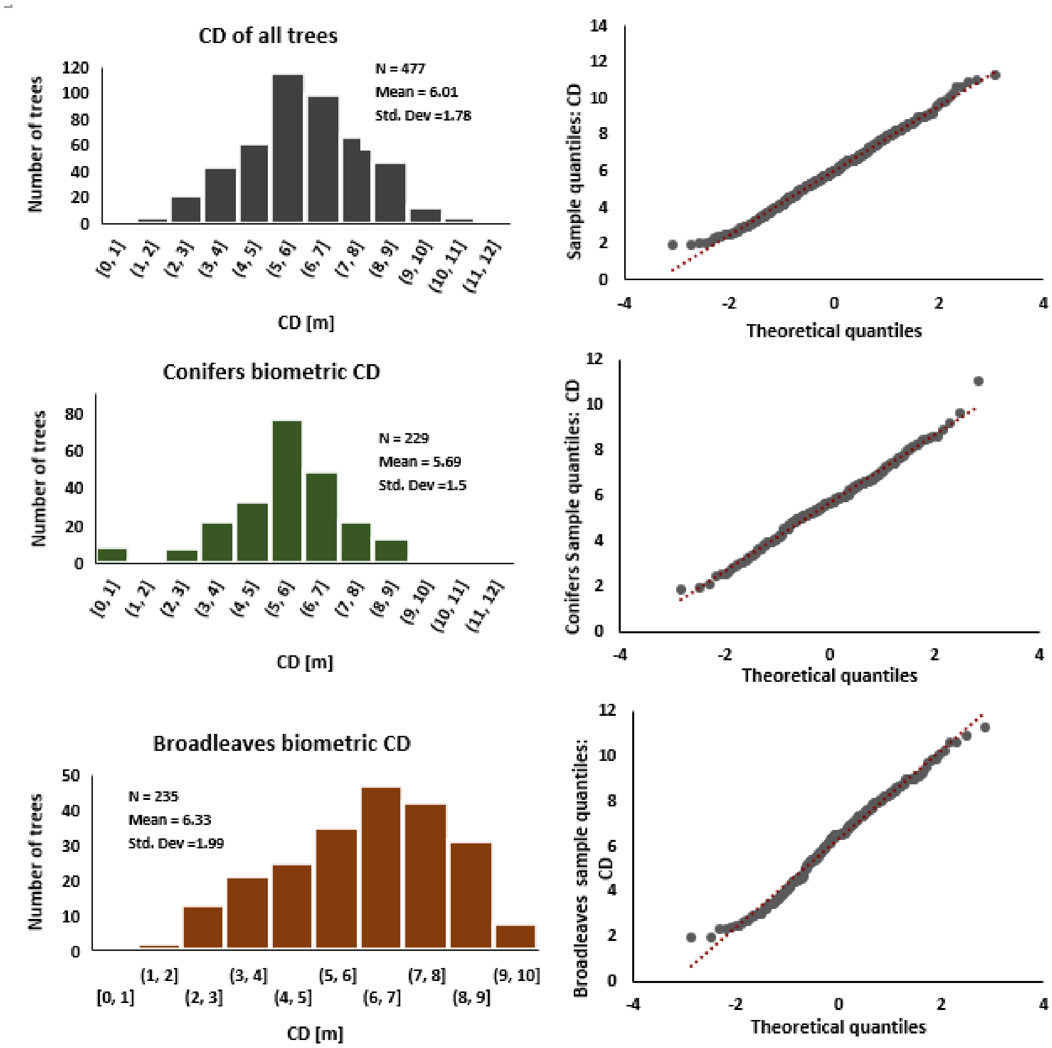

Figure 22. Histogram distribution of crown diameter Normal Q-Q plot of crown diameter (CD) distribution.

4.5. DBH model development and its validation assessment

This subsection explains first the results from the different model types derived from DBH-CPA relationship. The one with the highest accuracy was selected, and a validation process was made on a separate dataset. Then, the results of the T-test answering the research hypothesis are shown. The same process is done for the model development and validation from the DBH-CD relationship. Finally, a summary section made a recap of the selected DBH models derived from both relationships, and that were used for the AGB calculation in subsection 4.6.

4.5.1. DBH model from DBH-CPA relationship

On each species and species category, just the trees that fallowed the normal distribution were selected and randomly divided, taking 70% of the data in each case for the development of the DBH estimation model. Diverse regression models types were built to estimate the DBH (Table 12). In each occasion, the one with the best results in terms of R^2 and RMSE was chosen (Table 13). The validation was made by using the remaining and independent 30% of the data (Table 14). The scatter plot of the chosen model and their validation results can be found in Figure 23. Moreover, the variance of the residuals of the selected models and validations did not follow any patterns, so no transformations were needed (Figure 37, Appendix D).

Table 12. Overview of the DBH models development types derived from DBH-CPA. Where x is CPA [m^2] and y is DBH [cm].

Species	Model	Equation	R2	RMSE	Species	Model	Equation	R2	RMSE
Conifers	L	y = 1.0534x + 15.077	0.88	4.70	Broadleaves	L	y = 0.8002x + 14.593	0.84	6.38
	Log	y = 22.31ln(x) - 27.409	0.82	5.67		Log	y = 21.003ln(x) - 28.421	0.80	7.07
	P	**y = 5.777x^0.6184**	**0.89**	**4.56**		P	y = 5.0783x^0.605	0.85	6.17
	Q	y = -0.0061x^2 + 1.4076x + 10.85	0.88	4.57		**Q**	**y = -0.0054x^2 + 1.1938x + 9.1735**	**0.85**	**6.11**
Spruce	L	y = 1.1349x + 14.162	0.92	3.62	Birch	L	y = 1.0582x + 11.011	0.64	4.84
	Log	y = 25.149ln(x) - 35.806	0.85	5.02		Log	y = 11.517ln(x) - 3.2841	0.67	4.62
	P	y = 5.7246x^0.6284	0.90	3.75		**P**	**y = 6.072x^0.5541**	**0.71**	**4.67**
	Q	**y = -0.0032x^2 + 1.3221x + 11.849**	**0.93**	**3.56**		Q	y = -0.0401x^2 + 2.1256x + 5.3763	0.67	4.60
Douglas	L	y = 0.9637x + 15.808	0.86	5.63	Oak	L	y = 0.6549x + 18.608	0.91	3.70
	Log	y = 22.856ln(x) - 29.637	0.81	6.57		Log	y = 20.63ln(x) - 28.852	0.83	4.98
	P	y = 5.9523x^0.5996	0.86	4.68		P	y = 6.1584x^0.5439	0.89	3.79
	Q	**y = -0.004x^2 + 1.2167x + 12.635**	**0.86**	**5.56**		**Q**	**y = -0.0006x^2 + 0.7107x + 17.567**	**0.91**	**3.69**
Pine	L	y = 1.024x + 15.08	0.74	4.19	Beech	L	y = 1.0176x + 11.828	0.85	5.67
	Log	y = 23.947ln(x) - 35.445	0.73	4.26		Log	y = 31.272ln(x) - 60.51	0.83	6.05
	P	**y = 4.948x^0.6555**	**0.78**	**4.15**		**P**	**y = 3.328x^0.7499**	**0.89**	**5.58**
	Q	y = -0.0041x^2 + 1.2463x + 12.236	0.74	4.17		Q	y = -0.0055x^2 + 1.424x + 5.3722	0.86	5.55

Among the results of the regression models types, quadratic and power models were the ones that performed with the highest R^2 and lowest RMSE. Comparing the selected models, it is notable that Spruce, Oak and Beech presents the highest accuracy (R^2=0.93, 0.91 and 0.89 respectively). Spruce also has the lowest RMSE at 3.56 cm. In contrast, Birch and Pine model resulted in a much lower accuracy (R^2=0.71 and R^2= 0.78) but with an RMSE comparable with other groups (RMSE = 4.60 and 4.15cm respectively). The highest RMSE is in the Douglas model and the general broadleaves category with RMSE of 5.56 and 6.11 respectively.

The validation of the models (Table 14) confirms a strong positive correlation between the estimated and biometric DBH since all the Pearson correlation coefficient is above 0.80. Also, the linear regression results presented a similar R^2 and RMSE to the ones obtained in the model building process.

Table 13. Overview of the DBH model applied (from DBH-CPA relationship).

Species	N	Equation	R2	RMSE [cm]	RMSE %
Conifers	152	y = 5.777x^0.6184	0.89	4.56	10.69
Broadleaves	157	$y = -0.0054x^2 + 1.1938x + 9.1735$	0.85	6.11	14.56
Spruce	56	$y = -0.0032x^2 + 1.3221x + 11.849$	0.93	3.56	8.33
Douglas	60	$y = -0.004x^2 + 1.2167x + 12.635$	0.86	5.56	12.36
Pine	38	y = 4.948x^0.6555	0.78	4.15	10.04
Birch	33	y = 6.072x^0.5541	0.71	4.67	19.53
Oak	63	$y = -0.0006x^2 + 0.7107x + 17.567$	0.91	3.69	8.16
Beech	59	y = 3.328x^0.7499	0.89	5.58	10.80

Table 14. Overview of the validation results of the DBH model (from DBH-CPA relationship).

Species	N	R	R^2	RMSE [cm]	RMSE %	RMSD [cm]
Conifers	65	0.93	0.87	4.62	11.46	4.79
Broadleaves	67	0.92	0.84	6.00	15.05	6.52
Spruce	25	0.96	0.92	3.95	10.05	3.97
Douglas	26	0.91	0.83	7.29	17.01	7.31
Pine	17	0.90	0.82	4.87	11.22	5.03
Birch	14	0.84	0.70	3.67	13.32	4.19
Oak	27	0.96	0.92	3.83	8.43	4.09
Beech	25	0.96	0.92	5.0698	12.673	5.99

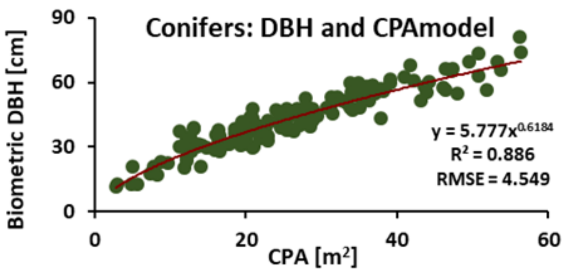

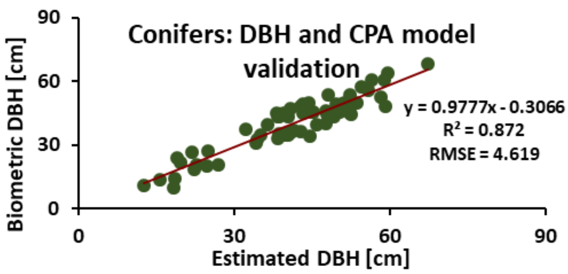

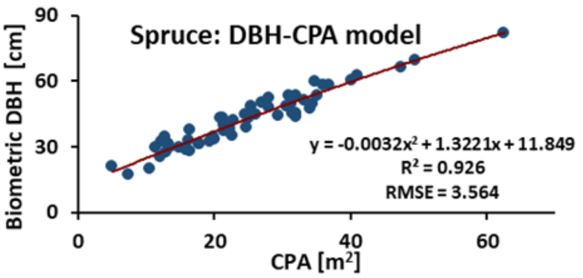

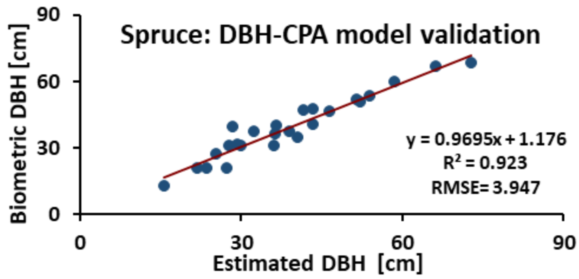

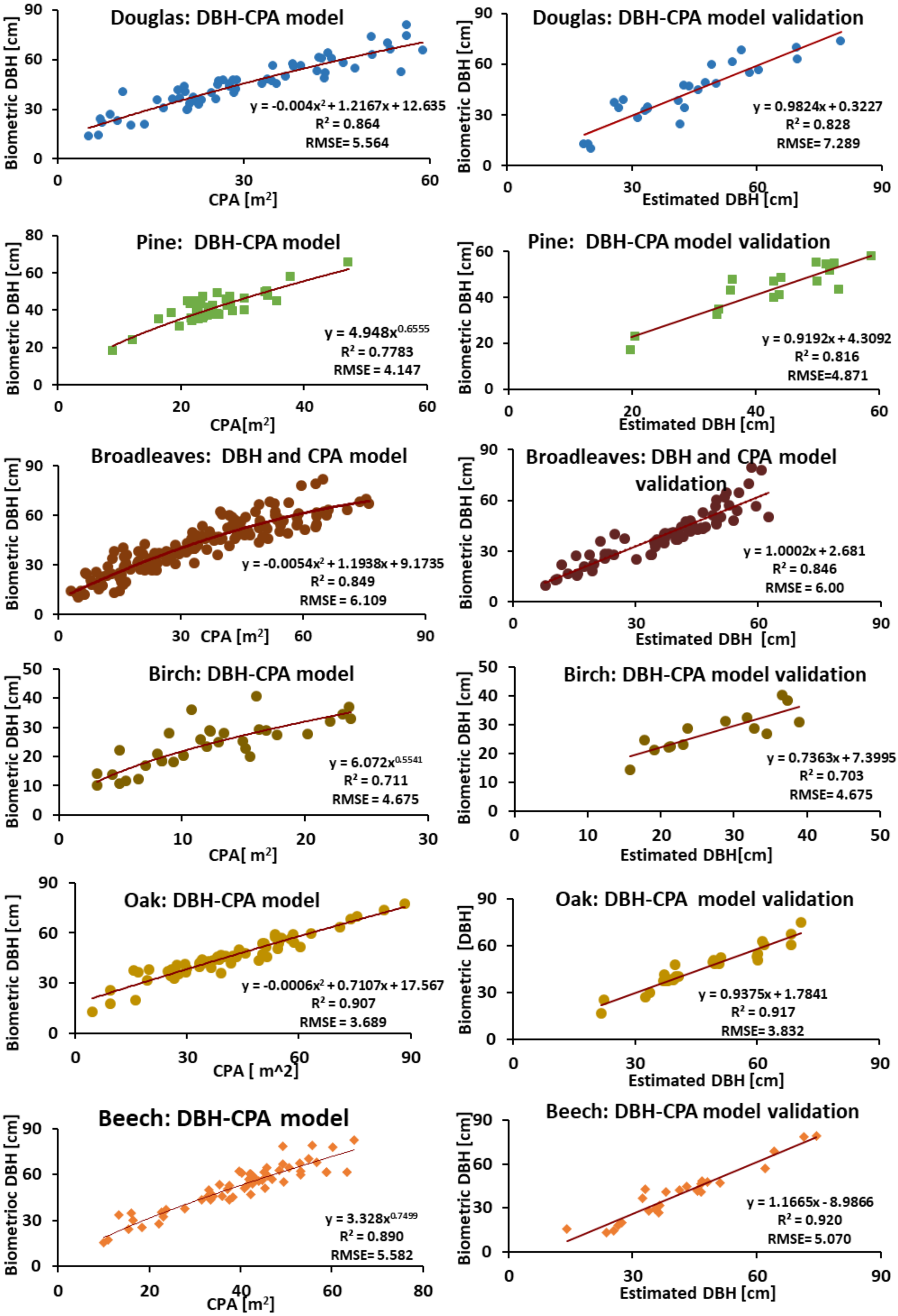

Figure 23. Model relationship DBH-CPA and model validation of the estimated DBH.

4.5.1.1. Hypothesis testing

The T-test results (Table 15) determined, for the case of every species and general species category, no significant difference among the DBH measured in the field, and DBH estimated from the CPA digitised on-screen from UAV imagery ($\alpha = 0.05$).

Table 15. Results of T-test: Two-Sample Assuming Unequal Variances from the selected DBH from DBH-CPA models and biometric DBH.

Species	df	t stat	t Critical two-tail	P(T<=t) two-tail
Conifers	129	0.56	1.98	0.58
Broadleaves	67	1.00	1.98	0.32
Spruce	48	0.01	2.01	0.99
Douglas	50	0.31	2.01	0.76
Pine	32	0.23	2.04	0.82
Birch	26	0.07	2.06	0.95
Oak	122	0.01	1.98	0.99
Beech	48	0.43	2.01	0.67

4.5.2. DBH model from DBH and CD relationship

The BHD-CD model was made by randomly taking 70% of the data (it was used the same tree selection than in DBH-CPA relationship). Different types of regression models were applied to estimate the DBH (Table 16), and the best one was chosen in terms of R^2 and RMSE (Table 17). The power and quadratic regressions presented the highest accuracy. In the case of Spruce, Oak and Beech species with R= 0.93, 0.91 and 0.89 respectively and 3.57, 3.62 and 5.63cm of RMSE respectively. Birch and Pine are again the species models with the lowest accuracy R^2= 0.71 and 0.78 respectively.

The independent 30% of the data was used for validation (Table 18), where the estimated DBH was plotted on linear regression against the biometric DBH. Except for Birch, all cases presented a strong positive correlation (R>0.80). The R^2 of the validation regression line is overall consistent with the one from the chosen DBH model. Figure 24 shows the scatter plots of the chosen model and of their validation results. Additionally, the variance of the residuals of the selected models did not show any patterns or signs of heteroscedasticity; thus, no transformation was needed (Figure 37, Appendix D).

Table 16. Overview of the DBH models development types derived from DBH-CD relationship. Where x is CD[m] and y is DBH[cm].

Species	Model	Equation	R2	RMSE	Species	Model	Equation	R2	RMSE
Conifers	L	y = 9.2442x - 9.2158	0.88	4.62	**Broadleav**	L	y = 7.8151x - 7.5613	0.85	6.19
	Log	y = 44.621ln(x) - 32.799	0.82	5.67		Log	y = 42.007ln(x) - 33.495	0.80	7.07
	P	**y = 4.9753x^1.2369**	**0.89**	**4.56**		P	y = 4.3878x^1.21	0.85	6.17
	Q	y = 0.3543x^2 + 5.35x + 0.8265	0.89	4.54		**Q**	**y = 0.1782x^2 + 5.6404x - 1.5415**	**0.85**	**6.15**
Spruce	L	y= 10.003x - 12.531	0.91	3.85	**Birch**	L	y = 6.4951x - 0.8565	0.67	4.63
	Log	y = 50.299ln(x) - 41.882	0.85	5.02		Log	y = 23.033ln(x) - 6.0661	0.67	4.62
	P	y = 4.9184x^1.2567	0.90	3.74		**P**	**y = 5.3113x^1.1082**	**0.71**	**4.67**
	Q	**y = 0.6486x^2 + 2.7736x + 6.6193**	**0.93**	**3.57**		Q	y = -0.586x^2 + 10.927x - 8.6598	0.67	4.59
Douglas	L	y =8.8326*-8.0754	0.86	**5.68**	**Oak**	L	y = 7.032x - 4.0699	0.90	3.84
	Log	y = 45.712ln(x) - 35.158	0.81	6.57		Log	y = 41.26ln(x) - 33.836	0.83	4.98
	P	y = 5.1497x^1.1992	0.86	5.62		P	y = 5.4002x^1.0878	0.89	3.79
	Q	**y = 0.4226x^2 + 3.9511x + 4.9567**	**0.86**	**5.55**		**Q**	**y = 0.3242x^2 + 2.6514x + 9.8615**	**0.91**	**3.62**
Pine	L	y = 9.0755x - 10.049	0.75	4.13	**Beech**	L	y = 10.365x - 20.197	0.86	5.60
	Log	y = 47.894ln(x) - 41.23	0.73	4.26		Log	Y = 62.543ln(x) - 68.064	0.83	6.05
	P	**y = 4.2234x^1.311**	**0.78**	**4.15**		**P**	**y = 2.7766x^1.4998**	**0.89**	**5.63**
	Q	y = 0.1979x^2 + 6.8725x - 4.0346	0.75	4.13		Q	y = 0.2824x^2 + 6.7372x - 9.1237	0.86	5.57

Table 17. Overview of the DBH model applied (from DBH-CD relationship).

Species	N	Equation	R2	RMSE [cm]	RMSE %
Conifers	152	y = 4.9753x^1.2369	0.89	4.56	10.69
Broadleaves	157	$y = 0.1782x^2 + 5.6404x - 1.5415$	0.85	6.15	14.66
Spruce	56	$y = 0.6486x^2 + 2.7736x + 6.6193$	0.93	3.57	8.35
Douglas	60	$y = 0.4226x^2 + 3.9511x + 4.9567$	0.86	5.55	12.33
Pine	38	y = 4.2234x^1.311	0.78	4.15	10.04
Birch	33	y = 5.3113x^1.1082	0.71	4.67	19.53
Oak	63	$y = 0.3242x^2 + 2.6514x + 9.8615$	0.91	3.62	8.01
Beech	59	y = 2.7766x^1.4998	0.89	5.63	10.89

Table 18. Overview of the validation results of the DBH model (from DBH-CD relationship).

Species	N	R	R2	RMSE [cm]	RMSE %	RMSD [cm]
Conifers	65	0.93	0.87	4.62	11.46	4.79
Broadleaves	67	0.92	0.85	5.98	15.00	6.57
Spruce	25	0.96	0.93	3.90	9.92	3.92
Douglas	26	0.91	0.83	7.29	17.02	7.33
Pine	17	0.90	0.82	4.87	11.22	5.03
Birch	14	0.84	0.70	3.67	13.32	4.19
Oak	27	0.96	0.92	3.76	8.28	3.97
Beech	25	0.96	0.92	5.07	12.67	5.99

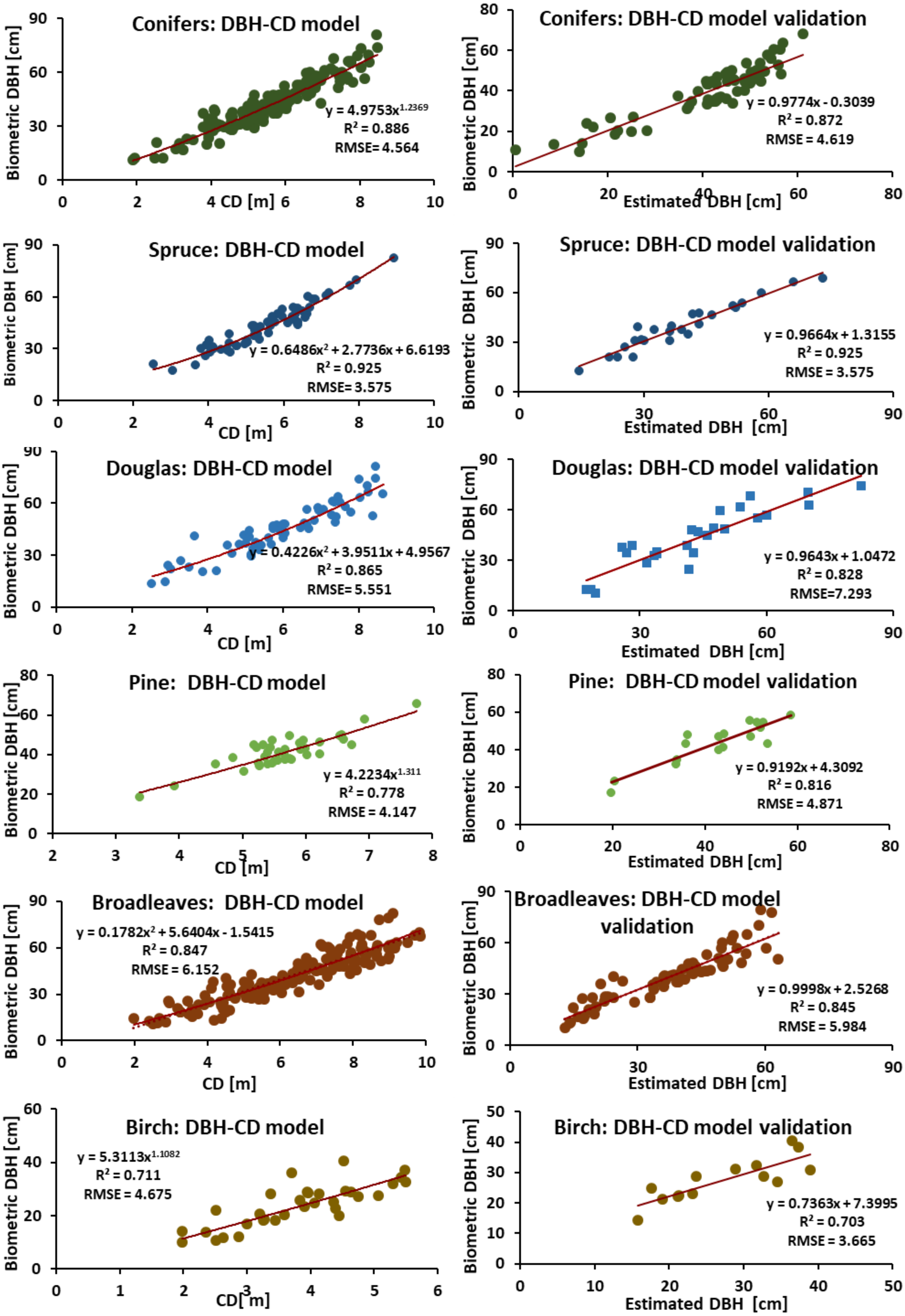
Conifers: DBH-CD model
y = 4.9753x^1.2369
R² = 0.886
RMSE= 4.564
Biometric DBH [cm]
CD [m]
Conifers: DBH-CD model validation
y = 0.9774x - 0.3039
R² = 0.872
RMSE = 4.619
Biometric DBH [cm]
Estimated DBH [cm]
Spruce: DBH-CD model
y = 0.6486x² + 2.7736x + 6.6193
R² = 0.925
RMSE= 3.575
Biometric DBH [cm]
CD [m]
Spruce: DBH-CD model validation
y = 0.9664x + 1.3155
R² = 0.925
RMSE = 3.575
Biometric DBH [cm]
Estimated DBH [cm]
Douglas: DBH-CD model
y = 0.4226x² + 3.9511x + 4.9567
R² = 0.865
RMSE= 5.551
Biometric DBH [cm]
CD [m]
Douglas: DBH-CD model validation
y = 0.9643x + 1.0472
R² = 0.828
RMSE=7.293
Biometric DBH [cm]
Estimated DBH [cm]
Pine: DBH-CD model
y = 4.2234x^1.311
R² = 0.778
RMSE = 4.147
Biometric DBH [cm]
CD [m]
Pine: DBH-CD model validation
y = 0.9192x + 4.3092
R² = 0.816
RMSE = 4.871
Biometric DBH [cm]
Estimated DBH [cm]
Broadleaves: DBH-CD model
y = 0.1782x² + 5.6404x - 1.5415
R² = 0.847
RMSE = 6.152
Biometric DBH [cm]
CD [m]
Broadleaves: DBH-CD model validation
y = 0.9998x + 2.5268
R² = 0.845
RMSE = 5.984
Biometric DBH [cm]
Estimated DBH [cm]
Birch: DBH-CD model
y = 5.3113x^1.1082
R² = 0.711
RMSE = 4.675
Biometric DBH [cm]
CD [m]
Birch: DBH-CD model validation
y = 0.7363x + 7.3995
R² = 0.703
RMSE = 3.665
Biometric DBH [cm]
Estimated DBH [cm]

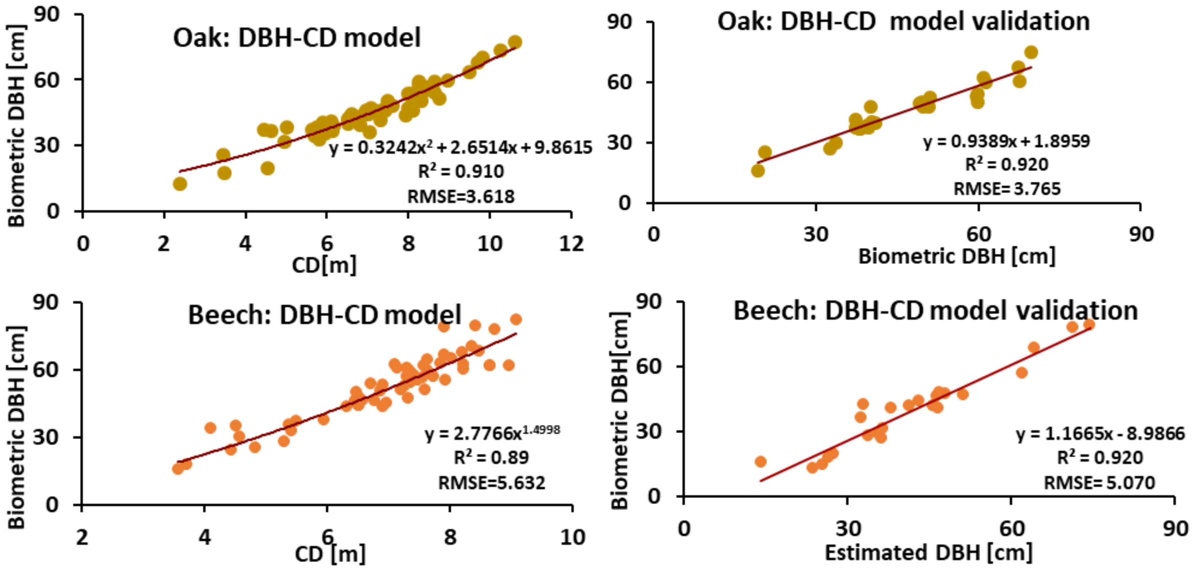

Figure 24. Model relationship DBH-CD and model validation of the estimates DBH.

4.5.2.1. Hypothesis testing

The T-test results (Table 19), for the case of every species and general species category, determined that there is no significant difference between the estimated DBH results (from the DBH-CD model) and the biometric DBH (α = 0.05).

Table 19. Results of T-test: Two-Sample Assuming Unequal Variances from estimated DBH from DBH-CD models and biometric DBH.

Species	df	t stat	t Critical two-tail	P(T<=t) two-tail
Conifers	129	0.56	1.98	0.58
Broadleaves	67	1.06	1.98	0.29
Norway	48	0.00	2.01	0.99
Douglas	50	0.25	2.01	0.81
Pine	32	0.23	2.04	0.82
Birch	26	0.07	2.06	0.95
Oak	122	0.01	1.98	0.99
Beech	48	0.43	2.01	0.67

4.5.3. Summary

Table 20 and Table 21 showed a resume of the results from both regression models by general species categories (conifers and broadleaves) and by species-specific. Comparing the validation results between both models, in most cases, the DBH-CD model presented better or slightly better accuracy results, with a higher R^2 and lower RMSE and RMDS (in some species, the difference in R^2 is found until the third or fourth decimal digit). Power and quadratic models were the model type that best describes the relationship between variables. As a sign of consistency, on every occasion, the same model type resulted as the most accurate from both relationships, DBH-CPA and DBH-CD.

RMSE tells how far is the estimated value from the regression line and is complemented with RMSD, which is the mean deviation between the estimated value and the biometric DBH; both are expressed with the independent variable units. Taking as an example the Spruce, the digitise CPA can significantly explain 93% of the DBH variation by a quadratic function model and an RMSE of 3.56 cm the typical error distance of their estimations. In the same species, the CD can significantly explain 93% of the DBH (up until the fourth digit showed a different and higher result than DBH-CPA) but, the RMSE is of 3.57 cm.

Table 20. Summary of general species category DBH estimation models and validation.

Species category	DBH model applied (from DBH-CPA relationship)	R^2	RMSE [cm]	DBH model applied (from DBH -CD relationship)	R^2	RMSE [cm]
Conifers	$y = 5.777x^{0.6184}$	0.89	4.56	y = 4.9753x1.2369	0.89	4.56
Broadleaves	$y = -0.0054x^2 + 1.1938x + 9.1735$	0.85	6.11	$y = 0.1782x^2 + 5.6404x - 1.5415$	0.85	6.15

	DBH validation model (from DBH-CPA relationship)				DBH validation model (from DBH -CD relationship)			
Species category	**R**	**R^2**	**RMSE [cm]**	**RMSD [cm]**	**R**	**R^2**	**RMSE [cm]**	**RMSD [cm]**
Conifers	0.93	0.87	4.62	4.79	0.93	0.87	4.62	4.79
Broadleaves	0.92	0.84	6.00	6.52	0.92	0.85	5.98	6.57

Table 21. Summary of species-specific DBH estimation models and validation.

Species	DBH model applied (from DBH-CPA relationship)	R^2	RMSE [cm]	DBH model applied (from DBH -CD relationship)	R^2	RMSE [cm]
Spruce	$y = -0.0032x^2 + 1.3221x + 11.849$	0.93	3.56	$y = 0.6486x^2 + 2.7736x + 6.6193$	0.93	3.57
Douglas	$y = -0.004x^2 + 1.2167x + 12.635$	0.86	5.56	$y = 0.4226x^2 + 3.9511x + 4.9567$	0.86	5.55
Pine	$y = 4.948x^{0.6555}$	0.78	4.15	$y = 4.2234x^{1.311}$	0.78	4.15
Birch	$y = 6.072x^{0.5541}$	0.71	4.67	$y = 5.3113x^{1.1082}$	0.71	4.67
Oak	$y = -0.0006x^2 + 0.7107x + 17.567$	0.91	3.69	$y = 0.3242x^2 + 2.6514x + 9.8615$	0.91	3.62
Beech	$y = 3.328x^{0.7499}$	0.89	5.58	$y = 2.7766x^{1.4998}$	0.89	5.63

	DBH validation model (from DBH-CPA relationship)				DBH validation model (from DBH -CD relationship)			
Species	**R**	**R^2**	**RMSE [cm]**	**RMSD [cm]**	**R**	**R^2**	**RMSE [cm]**	**RMSD [cm]**
Spruce	0.96	0.92	3.95	3.97	0.96	0.93	3.90	3.92
Douglas	0.91	0.83	7.29	7.31	0.91	0.83	7.29	7.33
Pine	0.90	0.82	4.87	5.03	0.90	0.82	4.87	5.03
Birch	0.84	0.70	3.67	4.19	0.84	0.70	3.67	4.19
Oak	0.96	0.92	3.83	4.09	0.96	0.92	3.76	3.97
Beech	0.96	0.92	5.07	5.99	0.96	0.92	5.07	5.99

4.6. Plot-level Above Ground Biomass and Carbon Stock results

Both DBH models (from DBH-CPA and DBH-CD relationships) were applied to estimate the DBH of every tree within the plots. The process was performed using DBH-CPA and DBH-CD species-specific modes as well as with the general broadleaves and general conifers category models. Then, the estimated DBH was used as the input variable for the AGB allometric equations according to the tree species. The AGB values of the trees within each plot were summed and transformed in tons/ha. Then, they were multiplied by the carbon content factor (0.5) to get the estimated AGC [tons/ha].

Table 22 and Table 23 present a descriptive statistics overview of the AGB estimations and AGC estimations, respectively. The estimation results of each plot can be consulted in Appendix F . The biometric AGB plots are in a range from 83 and 719 tons/ha with an average value of 266 tons/ha. The range of AGB estimations from general categories-AGB models are wider than the biometric-AGB but, the contrary situation is found when compared to the species specific-AGB. The estimations from the species-specific AGB models presented smaller standard deviation and standard error than general categories-AGB models. Moreover, the standard deviation and standard error are always lower in the estimations from CD models than the ones coming from the CPA. In the case of AGC, the biometric-AGC values were between 41 tons/ha and 359 tons/ha and a mean of 133 tons/ha. The AGC estimations presented a similar behaviour in their results as the AGB (Table 23).

Table 22. Descriptive statistics summary of above ground biomass results

		From species-specific models		From general species categories	
	Biometric [tons/ha]	**AGB [tons/ha] DBH-CPA**	**AGB [tons/ha] DBH-CD**	**AGB [tons/ha] DBH-CPA**	**AGB [tons/ha] DBH-CD**
Observations	39	39	39	39	39
Mean	266.69	285.79	276.20	302.54	291.35
Median	254.54	278.55	272.99	255.37	255.97
Standard Error	22.66	20.37	18.04	28.65	24.95
Std. Deviation	141.52	127.23	112.68	178.90	155.80
Variance	20028.09	16188.59	12697.09	32003.43	24274.59
Range	636.62	527.25	475.01	804.77	635.89
Minimum	83.14	73.62	72.26	89.40	89.05
Maximum	719.76	600.88	547.27	894.17	724.94

Table 23. Descriptive statistics summary of above ground carbon stock results

		From species-specific models		From general species categories	
	Biometric [tons/ha]	**AGC [tons/ha] DBH-CPA**	**AGC [tons/ha] DBH-CD**	**AGC [tons/ha] DBH-CPA**	**AGC [tons/ha] DBH-CD**
Observations	39	39	39	39	39
Mean	133.35	142.90	138.10	151.27	145.68
Median	127.27	139.27	136.50	127.68	127.98
Standard Error	11.33	10.19	9.02	14.32	12.47
Std. Deviation	70.76	63.62	56.34	89.45	77.90
Variance	5,007.02	4,047.15	3,174.27	8,000.86	6,068.65
Range	318.31	263.63	237.51	402.39	317.95
Minimum	41.57	36.81	36.13	44.70	44.53
Maximum	359.88	300.44	273.64	447.08	362.47

Figure 25 presents the AGB and AGC results of all plots to compare between estimations. Figure 26 shows the tree number and species constitution of each plot, along with the plot type assigned according to the species dominance within the plot as dominant broadleaves, conifers or mixed plots. The dominant conifers plots seem to have similar results than the biometrics.

In contrast, some dominant broadleaved plots have prominent differences: the values from the general models tend to have bigger values than the estimations from spices specific DBH models. This is especially distinguished on plots 2,10 and 14, notice than in this plots the species-specific models, even when they are overestimated, they still have more conservative predictions than general category models. Plot number 7, 17 and 27 showed a different situation; the general models have similar values than the biometric while species-specific are underestimated.

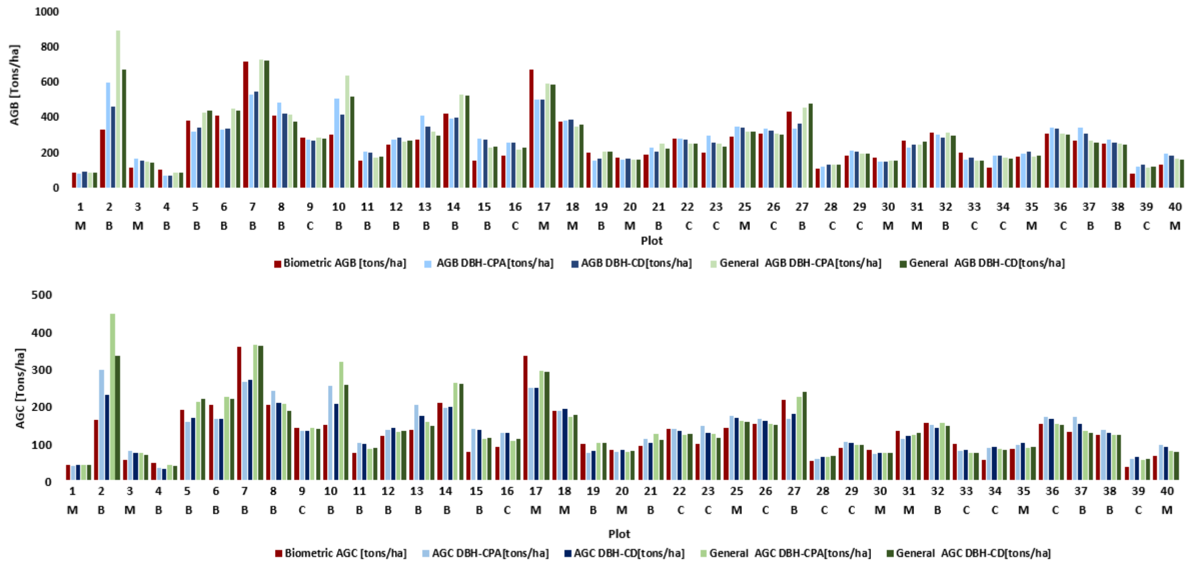

Figure 25. The AGB and AGC results per plot calculated: from the biometric DBH with a red tonne (named biometric AGB and AGC), from the DBH estimated from the species-specific DBH-CPA relationship with light blue and light green for the general tree category relationship (named AGB DBH-CPA and General AGC DBH-CPA). From the DBH estimated from the species-specific DBH-CD relationship with dark blue for the and light green for the general tree category relationship (named AGB DBH-CD and General AGC DBH-CD). A letter is placed below the plot number to identify its plot type according to its dominance was classified B (broadleaves), C (Conifers) or M (mixed).

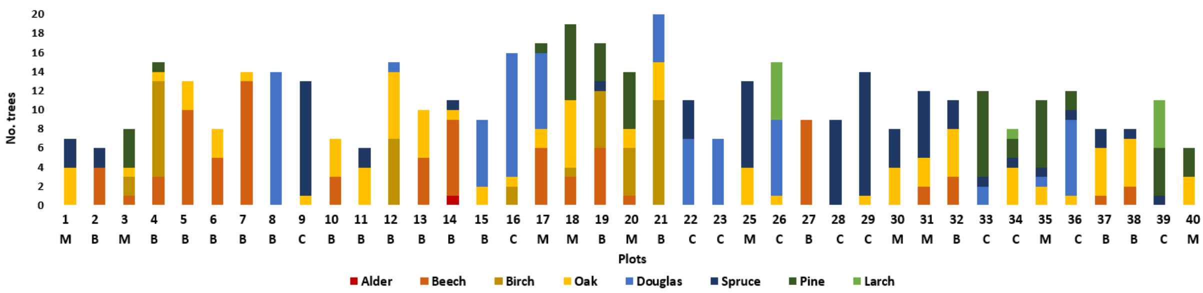

Figure 26. Total tree number per plot with colours that distinguish the tree species within each plot. At the bottom of the plot number, there is an initial of the plot type in which was classified B (broadleaves), C (Conifers) or M (mixed).

4.6.1. Hypothesis testing

To answer the third hypothesis of this research, the results of the T-test showed no significant difference between the estimated AGB/ AGC from DBH-CPA relationship and biometric AGB/ AGC (α = 0.05). Moreover, the T-test proves also no significant difference in the estimated AGB and AGC from DBH-CD species relationship and biometric-AGB and AGC answering the fourth hypothesis (α = 0.05). The T-test results for all the cases are presented in Table 24 and Table 25.

Table 24. Results of the T-test: Two-Sample Assuming Unequal Variances for AGB.

AGB model	t stat	t Critical two-tail	P(T<=t) two-tail
AGB DBH-CPA	-0.63	1.99	0.53
AGB DBH-CD	-0.33	1.99	0.74
General AGB DBH-CPA	-0.98	1.99	0.33
General AGB DBH-CD	-0.73	1.99	0.47

Table 25. Results of the T-test: Two-Sample Assuming Unequal Variances for AGC.

AGC model	t stat	t Critical two-tail	P(T<=t) two-tail
AGC S-DBH-CPA	-0.63	1.99	0.53
AGC S-DBH-CD	-0.33	1.99	0.74
General AGC DBH-CPA	-0.98	1.99	0.33
General AGC DBH-CD	-0.73	1.99	0.47

4.7. Accuracy of AGB and AGC estimates

The scatterplot of model vs biometric AGB and AGC estimations and the statistics overview of the linear regression are presented in Figure 27. All the cases presented a strong positive correlation (R>0.80) (Table 26 and Table 27). The results from DBH estimations from the species-specific DBH models performed slightly better than the general-categories DBH models. This can also be appreciated in Figure *27*, the dots from the AGB estimations that used species-specific DBH models are closer to the biometric 1:1 line than the dots from the AGB estimations that used general species category DBH models.

Moreover, the estimations made from the DBH-CD can explain a higher variance and has lower RMSE than the estimations from the DBH-CPA models, this can be appreciated on both species-specific and general category models. Taking the species-specific as an example, it presented an R^2 of 0.81 and RMSE = 62.04 ton/ha for AGB, as well as R^2 of 0.81 and RMSE of 31.02 ton/ha for AGC. Contrary to DBH-CPA model whose AGB estimations presented an R^2 of 0.65 and RMSE of 84.15 tons/ha, along with an R^2 of 0.65 and RMSE of 41.52 tons/ha for AGC. These can also be seen on the scatter plot (Figure *27*), the distance from the line tend to be less in the DBH-CD estimations (darkest dots) than the estimations made from the DBH-CPA (lightest dots).

Table 26. Overview of the regression accuracy assessment between Biometric and estimated AGB from all plots.

	R	R^2	RMSE [ton/ha]	RMSE %	RMSD [ton/ha]
AGB DBH-CPA	0.80	0.65	84.15	31.55	87.38
AGB DBH-CD	0.90	0.81	62.04	23.26	64.44
General AGB DBH-CPA	0.80	0.65	83.00	31.12	110.90
General AGB DBH-CD	0.89	0.80	62.75	23.53	73.39

Table 27. Overview of the regression accuracy assessment between Biometric and estimated AGC from all plots.

	R	R^2	RMSE [ton/ha]	RMSE %	RMSD [ton/ha]
AGC DBH-CPA	0.80	0.65	41.52	31.14	43.69
AGC DBH-CD	0.90	0.81	31.02	23.26	32.22
General AGC DBH-CPA	0.80	0.65	41.50	31.12	55.45
General AGC DBH-CD	0.89	0.80	31.38	23.53	36.70

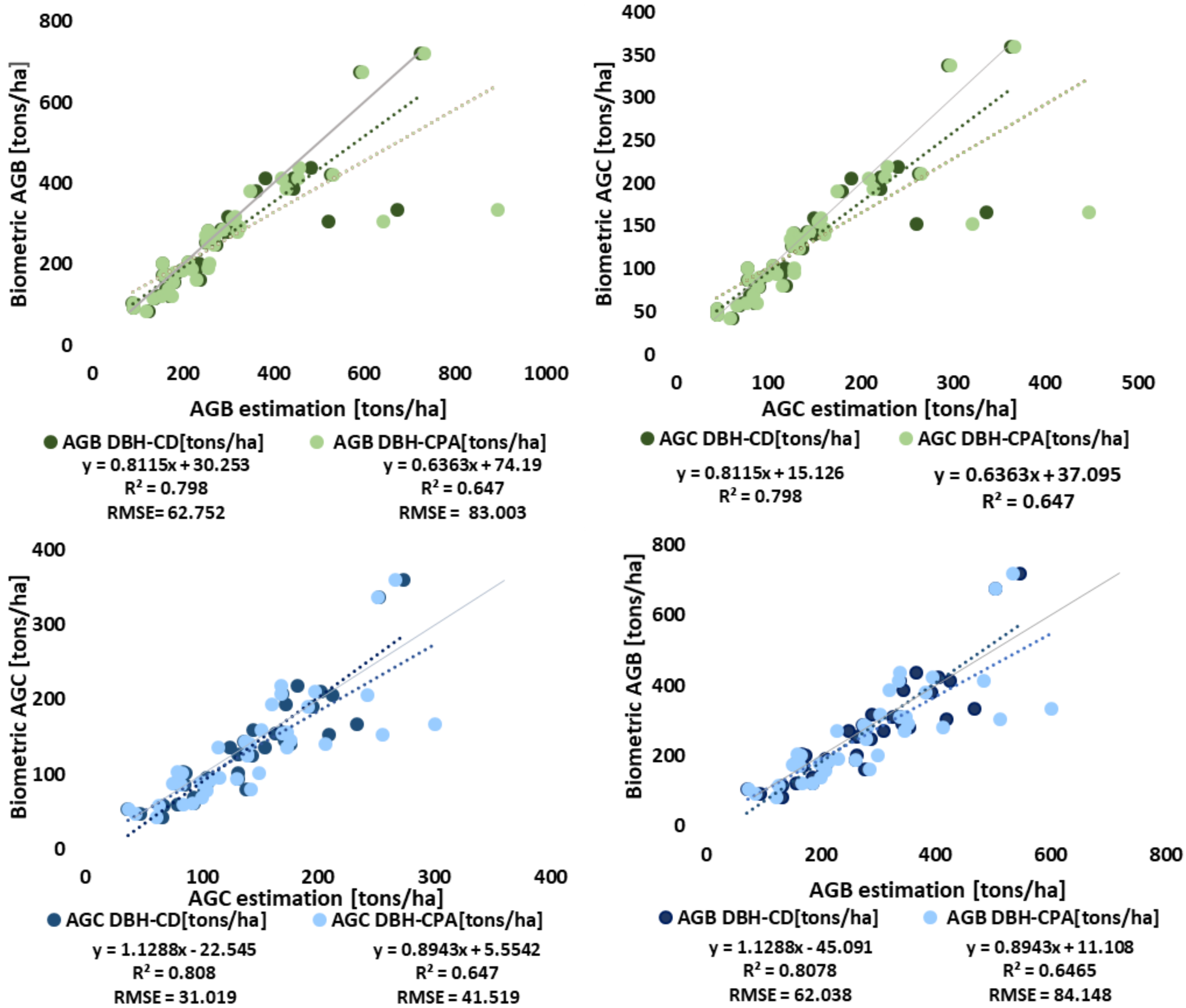

Figure 27. Biometric and estimated AGB (left) and AGC (right) linear regression. The results at the top are from the estimations using the general DBH models by tree category (broadleaves or conifers) and the bottom plots are the estimations with the species-specific DBH models. The dotted lines indicate the linear regression trend line on each model and, the grey line correspond to the biometric 1:1 line.

4.7.1. Accuracy of AGB and AGC by plot type

Table 28 and Table 29 present a deeper analysis by differentiating the AGB and AGC estimations results by plot type when applying the species-specific DBH estimation models. The dominant-broadleaves plots tend to differ the highest from the biometric AGB and AGC values. Contrarily, dominant-conifer plots, which estimation results tend to be more consistent. The mixed plots showed higher accuracy and a more consistent distance from the tendency line compare to the other plots. Also, the AGB and AGC estimations from the DBH-CD model showed a higher accuracy from all plot types (Figure 28).

Table 28. Overview of the regression accuracy assessment between biometric and estimated AGB per plot dominance type.

Estimation model applied	plot type	n	R	R^2	RMSE [ton/ha]	RMSE %	RMSD [ton/ha]
AGB DBH-CPA	**C**	11	0.89	0.79	33.58	15.76	43.80
AGB DBH-CD	**C**	11	0.91	0.83	29.77	13.97	37.62
AGB DBH-CPA	**B**	18	0.68	0.46	101.77	32.59	111.41
AGB DBH-CD	**B**	18	0.84	0.71	74.56	23.88	75.08
AGB DBH-CPA	**M**	10	0.94	0.88	57.57	23.62	67.57
AGB DBH-CD	**M**	10	0.95	0.91	51.69	21.21	63.84

Table 29. Overview of the regression accuracy assessment between biometric and estimated AGC per plot dominance type.

Estimation model applied	plot type	n	R	R^2	RMSE [ton/ha]	RMSE %	RMSD [ton/ha]
AGB DBH-CPA	**C**	11	0.89	0.79	16.79	15.76	21.90
AGB DBH-CD	**C**	11	0.91	0.83	14.89	13.97	18.81
AGB DBH-CPA	**B**	18	0.68	0.46	50.88	32.59	55.70
AGB DBH-CD	**B**	18	0.84	0.71	37.28	23.88	37.54
AGB DBH-CPA	**M**	10	0.94	0.88	28.78	23.62	33.79
AGB DBH-CD	**M**	10	0.95	0.91	25.84	21.21	31.92

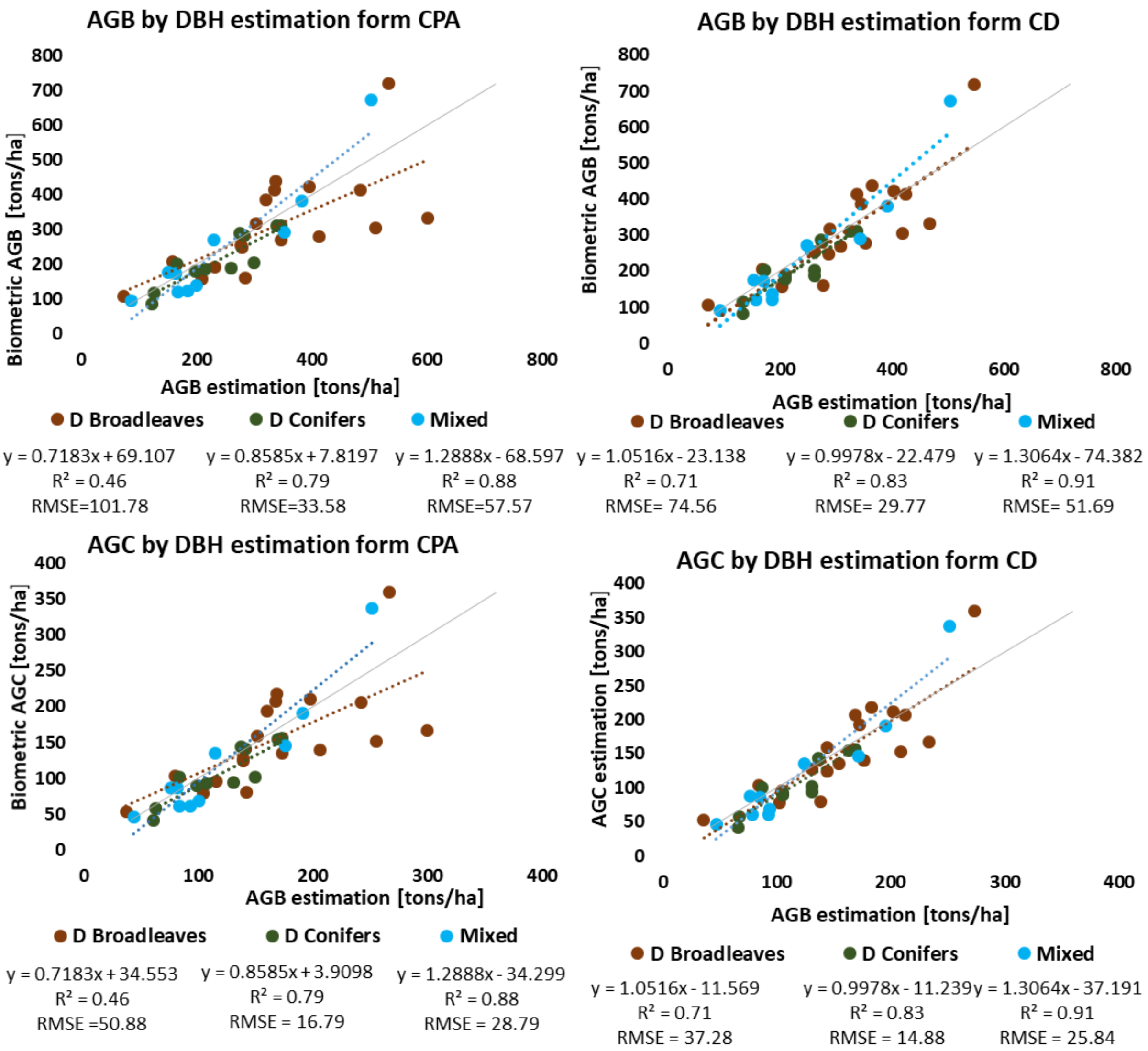

Figure 28. Regression line comparison by plot type. Biometric and model AGB and AGC per plot dominance type (broadleaves, conifers or mixed). The dotted lines indicate the linear regression trend line on each plot type and, the grey line correspond to the biometric 1:1 line.

5. DISCUSSION

5.1. Uncertainties of field-measured parameters

The COVID-19 lockdown made the data acquisition challenging, but it also allowed the innovative use of everyday technology to do science. High priority was given to the accurate tree location and the crown shape limits. This required having several sources to cross-check; GPS location lecture, bearing and distance from the centre plot, pictures, videos and Avenza App with the orthophoto charged on the cellphone. Complementary, for the tree canopy shape, video and pictures were taken, as well as a manual CPA in a cellphone screenshot of the orthophoto. We believe that having the orthophoto available on the cellphone was a big advantage because it enables a comparison with what can be seen on the ground.

5.2. Quality of UAV point cloud

The development of 3D structures (i.e., DSM, DTM and CHM) from a set of UAV images through SfM can be done as a semiautomatic process in software, such as Pix4D Mapper. It can also allow you to make some changes to improve the outcomes. In the case of this research, to achieve the desired quality on the UAV outputs, several runs were needed to process the data.

The matching of GCP and CP was done manually. Not all GCPs gave favourable results since the ones placed in permanent places (i.e. a stone, a corner point or a wooden bar) were not always easily recognizable in all images. The best quality outcomes were chosen:3 GCPs were used at this stage to get the absolute orientation of the 3D point cloud and the camera locations. The process was followed by a quality assessment using 3 CPs. A standard procedure was followed to process the UAV data (Table 9) and a high output quality accomplished with minimal georeferencing error and reprojection error (0.126 pixels) after the Bundle Block Adjustment, which allowed a good detail Orthomosaic (4.64 x 4.64 cm/pixel).

Orientation consistency and rectification were accomplished. Nevertheless, at the edges of the study area, there is a lower number of overlapping images and some with off-nadir viewing. Also, due to the close canopy and the GCP number and its distribution, there were some areas with fewer keypoints matches (Figure 29) which has an effect on the data quality translating in some blur and shift on some tree crowns. Because we did have access to the orthophoto before sampling, we tried to avoid these specific areas.

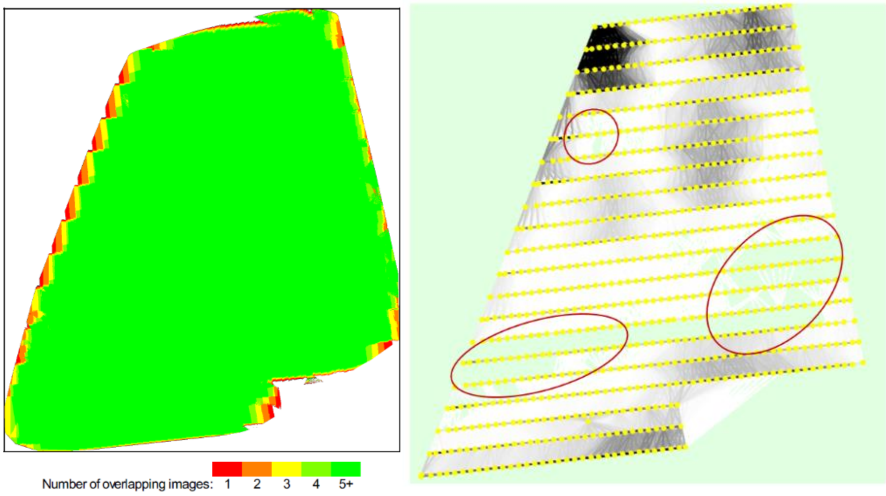

Figure 29. UAV Distribution of overlapping images and Keypoints. (a) Amount of overlapping images. (b) 2D Keypoints between the images, The more amount of matches, the darker the colour. The red circle is highlighting areas that might have low point density on the following processing steps (images from the Pix4D quality report).

5.2.1.1. Manual digitised CPA and derivation of CD

Crown diameter can be measured from the ground. Generally, the method used is by average, two measurements, from N-S and E-W direction(Grznárová et al., 2019). Nevertheless, measuring CD from the ground is time-consuming, and it could also be subjective since it relies on personal perception to identify the crown edges. It should be kept in mind that just the portion of the crown that is visible from above will be measured. Previous research has utilised CPA and CD acquired from RGB-UAV images and proved the feasibility (i.e., Grznárová et al., 2019). For this reason, this study used manual on-screen digitised CPA from the UAV-Orthophoto and, derived CD as in Equation 4. The different autumn colour tones of the trees benefit on the distinction between species crowns and the edges between neighbours crowns.

The accuracy of CPA and CD measurement from this method depends on the quality of the UAV Orthomosaic which is not completely uniform along the image. In particular sections of the image was identified some blur and shift happen (particularly at the edges of the Orthomosaic)(Figure 29). We tried not to sample in those sections, yet some Pine tree species were located closer to the edges of the images.

Caution and care were taken on how to interpret and delineate individual crown edges on the image. A group of crowns can be mistakenly considered as a single tree crown, which causes overestimation. On the contrary, the branches of one tree crown can be wrongly seen as multiple crowns (Hirata et al., 2012). Moreover, crown characteristics of some species allowed the crown outline to be easier to recognize and delineate than others. Figure 30 shows the case of Birch in which the leaves and branches architecture made the crown edges more blurry. It was also observed that the crown shapes of Beech deform into more irregular shapes than other species. Having the orthophoto on hand while being in the field complements and helps in double-checking the tree crown edges. Figure 30 presents an example of the species crown shapes found in the study area.

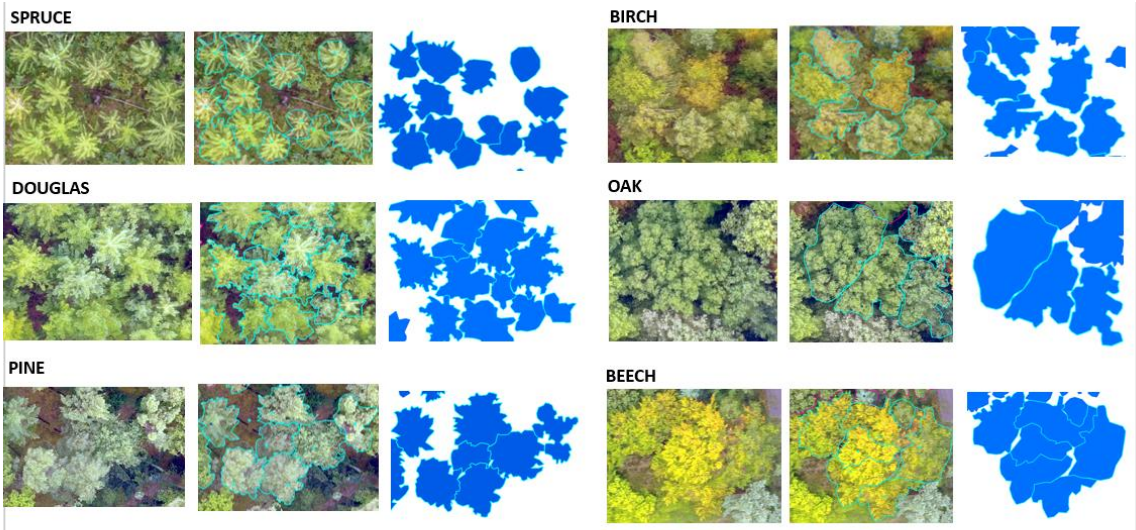

Figure 30. Examples of crow shapes and their manual on-screen digitised CPA.

5.3. DBH estimation from DBH-CPA and DBH-CD models

To build the DBH estimation models. DBH was considered as the dependent variable and is affected by the independent variables CPA and CD. Previous studies have proved the significant relationship between DBH and CD as well as DBH and CPA on different forest types (i.e., Brown, 2002; Gering & May, 1995; Kachamba et al., 2016; Lisein et al., 2013; Niklas, 1992; Panagiotidis et al., 2017; Shimano, 1997; Song et al., 2010). Many forest science fields and applied forestry activities use a CPA or CD for different situations. The relationship between them has been documented, and they are mathematically accepted as in Equation 4. No literature was found that compared the accuracy from both of these relationships on DBH estimation.

In each case, linear, logarithmic, quadratic and power functions were considered, and the best fit was selected in terms of coefficient of determination (R^2), root mean square error (RMSE), Root Mean Square Deviation (RMSD). Quadratic and power functions were the ones that resulted in the models that best describe the relationship among both parameters (DBH-CPA and DBH-CD): Quadratic for the cases of Spruce, Douglas, Oak and the general Broadleaves model, and a power function for the cases of Pine, Birch, Beech and general Conifers model. These coincide with previous studies, of Ketterings et al., (2001) in which they found that power and polynomial are the functions that most often used to describe the allometric relationship between several tree parameters. It is also worth noting that, in this study, the function type of the resulted model was applied for both broadleaves and conifer species.

Nevertheless, authors like Chave et al., (2005), Ketterings et al., (2001) and Shimano (1997) have argued that polynomial function shape models are biologically unrealistic. CPA often increases proportionally to the square of the DBH, and even though power function(Chave et al., 2005; Shimano, 1997). However, higher DBH values will lead to overestimation (Chave et al., 2005). Shimano, (1997) found that as far as the tree is growing in an open-grown situation, the growth of CPA size (and CD) will slow down as DBH continue rising, because of an increment in canopy density and competition. Shimano (1997) found that the DBH-CPA relationship is better described as power-sigmoid. According with what is been previously mentioned, it is worth emphasising that these models are an empirical relationship and that they have proved to be able to describe well the DBH variation of the study site conditions. The extrapolation beyond the DBH ranges used to build the model, and their general applicability to another site must be considered with caution.

Sometimes, logarithmic transformations are applied to power functions to linearize the models, reduce the heteroscedastic and they can even improve the accuracy of the model. In this study, transformations were not considered since it doesn't secure the same accuracy when the values are transformed back to the value that has been estimated, as it is considered to introduce bias when retransformed back to estimation results (Chave et al., 2005; Zianis & Mencuccini, 2004). Moreover, the residuals variance plot from both model and validation didn't show any patterns (Figure 37, Appendix D).

The selected models (from DBH-CPA and DBH-CD) explained between 71% - 93% of the DBH variability with an RMSE 3.56- 6.15 cm. As a sign of consistency, when analysing both relationships, the function type selected as the best fit model was the same one in all species cases as well as the general species categories (i.e., conifer and broadleaves). Also, the accuracy results showed high similarity. The DBH-CD were slightly better but notable until the third or fourth decimal.

Each of the selected models was validated using separate datasets through linear regression. The validation results were consistent with the statistical analysis on the model development. Results show a strong Pearson correlation between the DBH estimations, from both relationships, and the DBH field measurements (>R= 0.90), except for Birch (R=0.84). The differences in the statistics indicators between the DBH-CPA and DBH-CD models were not much (Table 20 and Table 21): For most of the species, the difference in the R^2 is only in the third or fourth decimal. The RMSE and RMSD have indicated that there is a less mean deviation of the estimations from DBH-CD models which can be expected by the CD since it was derived from CPA (Equation 4).

The T-test proved that there was no significant difference between the biometric DBH from ground measurements and each of the DBH estimations from DBH-CPA and DBH-CD relationships on the case of all species-specific and general species categories (Table 15 and Table 19).

5.3.1. Broadleaves and conifers general species categories.

The results from this study showed that the general conifers model is higher accuracy than the general broadleaved model (Table 20). The General conifers DBH-CPA and DBH-CD model had an R^2 of 0.89 and a validation R^2 =0.87 and RMSE=4.62cm.

The General broadleaves model was showing an R^2= 0.85 and validation results of R^2= 0.84 and RMSE=6 cm from DBH-CPA relationship, and R^2=0.85 from the model and R^2 0.85 and RMSE=5.98 cm from DBH-CD relationship. These results from general models are capable of explaining a wide variation of DBH from either CPA and CD, with similar accuracy.

The DBH results mentioned are comparable with the findings of Jucker et al., (2017). They got an RMSE of 16.6cm using ALS to predict DBH from CD from trees across species and forest types. The results are also comparable with findings of Shimano, (1997), they also reported less residual variance on conifers than broadleaves on the inverse process (482.9 and 96.6m^2) but a slightly higher correlation coefficient R on broadleaves than conifers (0.93 and 0.86 respectively). As it was mentioned before, broadleaves tend to have a more asymmetry extent in their crowns than conifers (Loehle, 2016). Getzin & Wiegand, (2007) have even found a significantly greater asymmetry between the two.

Shimano, (1997) also highlighted that after 10-20 cm DBH, there is a pronounced difference in the DBH-CPA relation, a much higher increasing rate of CPA against DBH in broadleaves while in the case of conifers, they show an earlier decrease of their CPA. Hence we would expect a pronounced difference in the slopes from our models but the results of this study did not indicate such a difference. We hypothesised that the reason relies mainly on the fact that the measured DBH range of this study is half (10-85 cm) of what they work with (0-140cm).

A t-test was run between both estimations values (the number of observations is similar). No significant difference was found between conifers and broadleaves estimations when using DBH-CPA relationship (t Critical two-tail (1.98) = 0.07, $p > 0.05$) as well as in the case of DBH-CD relationship (1.98) = 0.06, $p > 0.05$).

5.3.2. Species-specific DBH estimation models

In temperate forests, the accessibility to light limits the lateral crown growth and crowns grow asymmetrically to get as much light as possible, the level of plasticity that each species has, will allow them to adapt. The more plasticity, the more asymmetrical their crowns can deform themselves to remedy the light availability (Pretzsch, 2014).

There is a lack of consensus on how to measure crown shape flexibility (or deformation according to the space conditions). As examples, Getzin & Wiegand (2007) determined the crown asymmetry by measuring the crown radius and the length of the vector between the base of the trunk and the centre of the CPA. Pretzsch, (2014) calculates it from the quantiles 95% and 5% of the DBH-CPA allometry of several European species, they calculate a plasticity Raquin (CPL). He estimates the highest plasticity for Beech (5.1), followed by Silver Fir (4.7), Sessile Oak (4.5), Norway Spruce (4.2), Scot Pine (3.7) and at the end Silver Birch (2.6).

When comparing the results between species-specific models, the R^2 indicates the percentage of variance that can be explained by the model. The more intra-specific variations combine and the stronger the structural plasticity of a species, the more and stronger variation to the model of DBH-CPA relationship (Blanchard et al., 2016; Pretzsch, 2014) and the same resulted in the case of DBH-CD (Getzin & Wiegand, 2007; Hemery et al., 2005).

The following is a recap from best to worst DBH modelling accuracy and validation results of this study per individual species, as well as characteristics of the species that could explain those results. Starting with the broadleaves species, Oak got the highest results on the modelling results and the validation for both DBH-CPA and DBH-CD relationship (Table 21), followed by Beech and Birch at the end.

Oak got an R^2 = 0.90, RMSE = 3.67cm from DBH-CPA model and a validation of R^2 = 0.92, RMSE = 3.83cm; and from DBH-CD relationship, the model resulted with R^2 = 0.91, RMSE = 3.62 cm and a validation with R^2 = 0.92, RMSE = 3.76cm (Table 21). Our results are similar to Hemery et al., (2005) in which they reported R^2=0.92 with Beech and 0.91 for Oak from a linear regression to predict crown diameter from DBH. Beech has even higher plasticity than Oak (Pretzsch, 2014; Schröter, et al., 2012), and this can explain why Oak resulted in higher accuracy numbers than Beech. Also, the Oak crown edges tended to be easier to identify and define than Beech or Birch. Nevertheless, Oak has been highlighted to be less tolerant to shade than Beeches, with the tendency to shade their foliage and decrease their visible CPA (Konôpka et al., 2010).

The DBH-CPA model of Beech species resulted with R^2 = 0.89, RMSE = 5.58 cm and a validation of R^2 = 0.92, RMSE = 5.07 cm; from DBH-CD model with R^2 = 0.89, RMSE = 5.63 cm and a validation of R^2 = 0.92, RMSE = 5.07 cm) (Table 21). Pretzsch, (2014) reported R^2 of 0.69 and 0.62 for Beech pure stands and mix stands respectively by measuring more than 2,000 trees. Pretzsch, (2014) compares the DBH-CPA relationship of Beech, reporting that a tree with 25cm DBH is estimated to occupy 58, 27 or 16 m^2, depending on if it is without lateral restriction, medium stand density or almost in a condition of self-thinning. They also showed that the behaviour in the relationship changes when the Beech is in pure stands and even in combination with different species.

We have noted that the validation accuracy results on Beech made the species model as the most accurate, using CPA-CD, between the three broadleaves species. At the same time, and as evidence of Beech high plasticity, it also has the highest RMSE and RMDS values on its validation. This point is important to keep in mind when we analyse the AGB/AGC estimations.

Birch resulted with the lowest accuracy on the model and validation even when they are supposed to have lower plasticity compare to Beech and Oak (Pretzsch, 2014). Our results showed R^2 = 0.71, RMSE = 4.67 cm from DBH-CPA model and a validation of R^2 = 0.70, RMSE = 3.66 cm; and R^2 = 0.71, RMSE = 4.67 cm from DBH-CD model and a validation of R^2 = 0.70, RMSE = 3.66 cm(Table 21).

Our results on Birch disagree with Hemery et al., (2005), who reported a comparable accuracy with Birch and Oak (R^2=0.92 and 0.91 respectively). Since these species are not as frequent within the study area, a possible reason could be due to the small number of individual trees (n= 33 for model and 14 for validation), making the model more vulnerable to outliers. Another contribution for the low accuracy could be the human eye since the crown edges were found not as clear compared to the other species.

We used a t-test to compare the DBH estimations between species. The results showed no significant difference between the estimated DBH of Beech and Oak from DBH-CPA and DBH-CD. Nevertheless, when compared to each of these species with Birch, there is a significant difference (Table 30 and Table 31). Yet, the number of observations of Birch compared with the rest of the species might influence this result. Further analysis will be needed.

Table 30. T-test results between the species DBH estimation values from DBH-CPA.

Species	df	t Stat	t Critical two-tail	P(T<=t) two-tail
Douglas -Spruce	48	0.94	2.01	0.35
Pine- Spruce	39	0.83	2.02	0.41
Douglas -Pine	41	0.18	2.02	0.86
Birch- Oak	38	-5.73	2.02	1.33E-06
Birch- Beech	37	-4.04	2.03	2.63E-04
Oak - Beech	49	1.17	2.01	0.25

Table 31. The T-test results between the species DBH estimation values from DBH-CD.

Species	df	t Stat	t Critical two-tail	P(T<=t) two-tail
Douglas -Spruce	48	0.94	2.01	0.35
Pine- Spruce	39	0.83	2.02	0.41
Douglas -Pine	41	0.19	2.02	0.85
Birch- Oak	38	-5.68	2.02	1.59E-06
Birch- Beech	37	-4.03	2.03	2.62E-04
Oak - Beech	49	1.13	2.01	0.267

Between the Conifer species, Spruce got the highest results from the broadleaves species on both DBH model from DBH-CPA relationship from model and validation, and DBH-CD (Table 21). Followed by Douglas and lastly, Pine.

Spruce was the species with the highest accuracy model and validation values, from DBH-CPA relationship with R^2 = 0.92, RMSE = 3.56 cm from the model and a validation of R^2 = 0.92, RMSE = 3.95 cm. In the case of DBH-CD relationship, with R^2 = 0.92, RMSE = 3.57 cm from model and a validation of R^2 = 0.92, RMSE = 3.89 cm (Table 21). On the first growth stages, the biomass priorities are on growing their branches and then its foliage. As canopy closure increases, the priority is to keep on growing the diameter of the stem, and it has a high resilience when partially lose its foliage (Bayer & Pretzsch, 2017; Konôpka et al., 2010). Therefore, CPA of Spruce can growth goes more consistent with DBH. Pretzsch, (2014) reported R^2 of 0.82 and 0.74 from Spruce pure stands and on mixed stands respectively by measuring more than 3,000 trees.

Douglas Fir DBH models also resulted in high accuracy, but not as close to Spruce as expected, and it was even a bit under the general conifers DBH models. It resulted with R^2 = 0.86, RMSE = 5.56 cm from DBH-CPA model and a validation of R^2 = 0.83, RMSE = 7.39 cm along with R^2 = 0.86, RMSE = 5.55 cm from DBH-CD model and a validation of R^2 = 0.83, RMSE = 7.29 cm(Table 21). The reason can be because the species is known for its fast growth and its crown shape flexibility according to space availability (Seidel et al., 2016). Douglas Fir species also has the distinction that, as it grows, their branches get thinner and larger, creating characteristic vertical gaps (Seidel et al., 2016), hence increasing asymmetric from their bottom down view.

Pretzsch's, (2014) ranking system gives Silver Fir a higher plasticity value than Spruce and Pine (assuming the same ranking value on Silver Fir is comparable to Douglas Fir for its feature similarities. Douglas fir was not included in that study). Moreover, the variation on Douglas Fir was much higher compared to Pine and Spruce and, in general, is considered as a high plasticity species.

In the case of Pine, with R^2 = 0.78, RMSE = 4.15cm from DBH-CPA model and a validation of R^2 = 0.82, RMSE = 4.87cm; and from DBH-CD model with R^2 = 0.78, RMSE = 4.15cm and a validation of R^2 = 0.82, RMSE = 4.87cm (Table 21). Besides having a small number of Pine trees (n= 38 for model and 17 for validation) like in the case of Birch, Pine trees were located mostly in regions where the orthophoto quality was not the best. The results of this study are comparable to the study of Sharma et al., (2017) which got validation of R^2 = 0.69; RMSE = 0.66 on the opposite process, they estimated crown width of Scot Pine from DBH. They highlight Scot Pine as light-demanding but highly adaptable to different conditions across Europe and the diverse silvicultural management techniques, and their 'high' morphological plasticity gives them high variability in their stem and crown forms and size (Sharma et al., 2017). Contrastingly, Pretzsch's, (2014) gives Pine a lower plasticity ranking compare to other species.

There were no significant differences between the estimated DBH of Spruce and Douglas Fir, Spruce and Pine as well as, Douglas Fir and Pine from both DBH-CPA and DBH-CD relationships (Table 30 and Table 31).

Regardless that canopy density and competition can differ within a study site (intra-site variability), DBH species-specific models can help by describing interspecific properties in the crown morphology changes and, their response to the external factors. These DBH estimations models in this study were able to efficiently simplify the variations that affect the DBH-CPA and DBH-CD relationship to make the DBH predictions from UAV- RGB –images practical and applicable.

5.4. AGB and AGC estimates

The DBH from the trees within 39 plots were estimated from the DBH-CPA and DBH-CD models and then used as input to the allometric equations to assess AGB and AGC. To better analyse the effect of DBH estimations on AGB/AGC, all the AGB allometric equations used in this research have DBH as the only explanatory variable. Since DBH has proven as the variable that is highly related to AGB, therefore, it is considered acceptable to use this variable alone for an accurate AGB estimation (Ketterings et al., 2001; Magnussen & Reed, 2015; Picard, 2012; Zianis et al., 2005). DBH also has the advantage of being easy to be measured in the field with high accuracy and giving a highly trusted reference value to compare with when using remotely sensed data to estimated DBH.

The difference in age of trees and its density caused variation in the AGB/AGC between plots. The AGB estimations from species-specific models were on a range between 73 -600 tons/ha from AGB DBH-CPA and between and 72- 547 ton/ha from AGB DBH-CD. Also, when applied both general DBH models (conifers and broadleaves), the ranges were 89- 894 and 89-724 tons/ha using AGB DBH-CPA and AGB DBH-CD, respectively (Appendix D). Notably, there are some plots with a large discrepancy from the field AGB, specifically looking at plot 2, 7, 10, 14, 17 and 27. Except for plot 17, all of them are dominated by broadleaves trees. Further analysis was done to explain these cases.

The AGB/AGC from field measurements (observed) were plotted against the estimations, placing them on the Y and X respectively according to (Piñeiro et al., 2008)(Figure *27*). The accuracy of the AGB/AGC estimations was analysed by linear regression and the statistical indicators (Table 26 and Table 27). They showed very similar accuracy results between the estimations of General species categories and species-specific DBH models. The species-specific AGB DBH-CD model presents the highest accuracy and the less RMSE and RMSD, closely followed by the general AGB DBH-CD model. In Figure 27, the dots from the AGB species-specific estimations look closer to the biometric 1:1 line than the AGB estimations that used the general species category DBH models, especially looking at the estimation dots that are the farthest from their biometric value. The residuals variance can also be seen in Figure 38 on Appendix E.

The t-test showed no significant difference between the estimations in AGB and AGC from each of the models and the biometric AGB/AGC (Table 24 and Table 25). However, the statistical indicators show that the estimations made from the AGB estimations from species-specific DBH-CD models can explain a higher variance and has the lowest RMSE (R^2 = 0.81; RMSE = 62.04 ton/ha). Contrary, the species-specific estimations from the DBH-CPA model (R^2 = 0.65) got the highest RMSE= 84.15 tons/ha, slightly more than the general DBH-CPA model.

Moreover, since it was used a uniform conversion factor, AGC results showed the same behaviour as in AGB estimations with an RMSE was reduced around half. Where the highest estimations are also from species-specific DBH-CD models with an R2=81 and RMSE=31.02 ton/ha and 23.26% RMSE. The AGC accuracy results are comparable to Jayathunga et al., (2018), they combined UAV-SfM with LiDAR DTM reported a mean prediction of 82.0 with RMSE 15.5 [Mg C/ha] and % 18.9 RMSE% on estimating carbon stock from a fixed temperate forest.

5.4.1. Analysis by plot type

Further analysis was made on the effect of the species-specific DBH estimation models, building the regression line by plot type (Figure 28). Figure 31 presents the localization of the plots by type. The results from dominant conifer plots (R^2= 0.79 and RMSE= 33.58 ton/ha on AGB DBH-CPA and R^2= 0.83 and RMSE= 29.77 ton/ha on AGB DBH-CD (Table 28 and Table 29).

In the case of mixed plots (R^2= 0.88 and RMSE= 57.57 ton/ha on AGB DBH-CPA and R^2= 0.91 and RMSE= 51.69 ton/ha on AGB DBH-CD) resulted with the highest accuracy among the tree plot types. This is attributed to the fact that these plots have a similar number of trees per plot, and we assume less variation in CPA and CD in relation to DBH. It could be that these plots just have one or two more dominate trees with an overestimated CPA and CD, but that may not be the case for the majority of the trees in the plot. It could also be that the balance from the underestimated and overestimated trees favour the final result. Another reason could be that the crown boundaries of the mixed plot could be better recognisable from the image. Further analysis would be needed on this point.

Dominant broadleaves plots resulted with an R^2= 0.46 and RMSE= 101.77 ton/ha on AGB DBH-CPA and R^2= 0.71 and RMSE= 74.56 ton/ha on AGB DBH-CD. To find an explanation from the results on this plot type, we did a deeper analysis on section 5.5.2 on the plots whose estimations differ the most with the biometric AGB/AGC.

Previous studies on mixed temperate forest like the one that was reported by Jayathunga et al., (2018), they estimate AGC on plots with different characteristics about tree-age, species dominance and management activities. The accuracy variations between plot types were between 7.6% RMSE on young conifers and 35.8% on reserve forest plots. The young broadleaves plot presented 22.9% while the dominant broadleaves plots reported a 10.7 RMSE% and the dominant conifer reported 14.5% (on the last two plot types, harvesting and silvicultural activities are done).

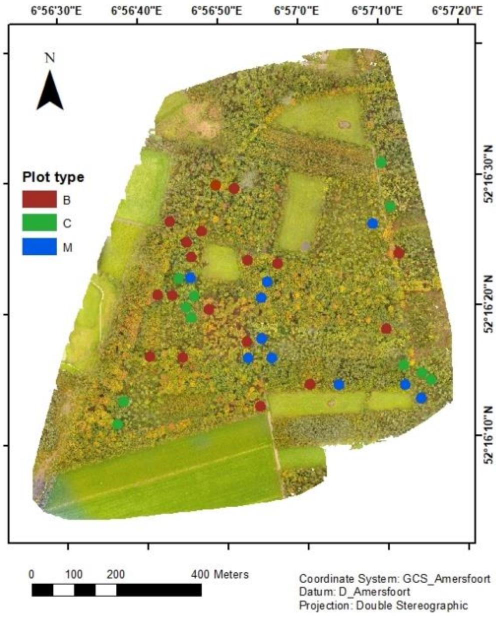

Figure 31. Location of plots types within the study area.

5.4.2. Extreme plot cases

Extreme cases happened only in six plots (i.e., 2, 7, 10, 14, 17 and 27) in the issue of estimating AGB, more particularly on the low accuracy in dominant broadleaves plots which was due to error propagation from individual tree AGB estimations into tons/ha. Therefore, we did a linear regression for each tree species.

When there is a high density, the crown size would be smaller than expected by the DBH-CPA model and this lead to an underestimation of the DBH and therefore an underestimation on the AGB/AGC (i.e. plot 7, 14, 17 and 27). On the contrary, when there is a crown without any space restriction, an overestimation of the DBH and therefore also in AGB/AGC would happen. This is the case of plot 2 and 10, composed by mainly Beech open-grown trees with an outstandingly big canopy size in relation to their DBH compared to other plots. The effect is similar to the DBH estimations from DBH-CD relationship but, their DBH estimations lead to an AGB/AGC values with less difference compare to the biometric AGB/AGC.

The mentioned plots situation is extreme cases, where the difference between estimated and observed value are high (except for plot 17). In all of the plots, Beech is the most frequent tree within the plots. We did the AGB/AGC accuracy using linear regression on a tree base (Figure 32 and Figure 33) and verify that the RMSE and RMSD of Beech AGB estimations are higher than any other species (Table 32 and Table 33). As an example of its high sensitivity, we include an extra linear regression of Beech without the trees within plots two and ten (which are mainly stand-alone trees), the results change prominently.

Table 32. Linear regression results from the AGB Accuracy assessment on a tree base from the DBH-CPA relationship.

Species	N	R	R^2	RMSE [kg/tree]	RMSE %	RMSD [kg/tree]
Spruce	78	0.94	0.89	172.87	19.32	179.42
Douglas	81	0.91	0.84	345.91	31.02	347.84
Pine	52	0.81	0.66	201.86	28.26	212.07
Birch	44	0.74	0.55	125.07	42.34	131.94
Oak	91	0.93	0.87	300.48	25.91	318.47
Beech	85	0.68	0.47	1206.29	52.54	1674.01
Beech without p2 and p10	78	0.88	0.78	788.26	35.75	790.43

Table 33. Linear regression results from the AGB Accuracy assessment on a tree base from the DBH-CD relationship.

Species	N	R	R^2	RMSE [kg/tree]	RMSE %	RMSD [kg/tree]
Spruce	78	0.94	0.89	175.34	19.60	180.56
Douglas	81	0.91	0.83	353.19	31.68	356.76
Pine	52	0.81	0.66	201.86	28.26	212.07
Birch	44	0.74	0.55	125.07	42.34	131.94
Oak	91	0.93	0.86	304.34	26.24	313.84
Beech	85	0.68	0.47	1206.29	52.54	1674.03
Beech without p2 and p10	78	0.88	0.78	788.26	35.75	790.43

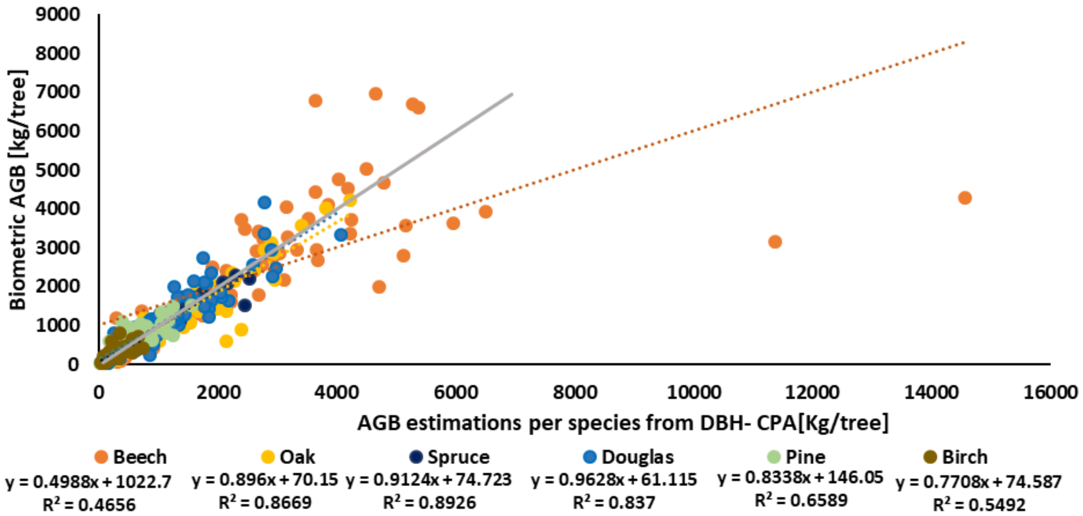

Figure 32. Scatter plot of AGB estimations from each species DBH estimation models, DBH-CPA compared against the biometric AGB[kg/tree].

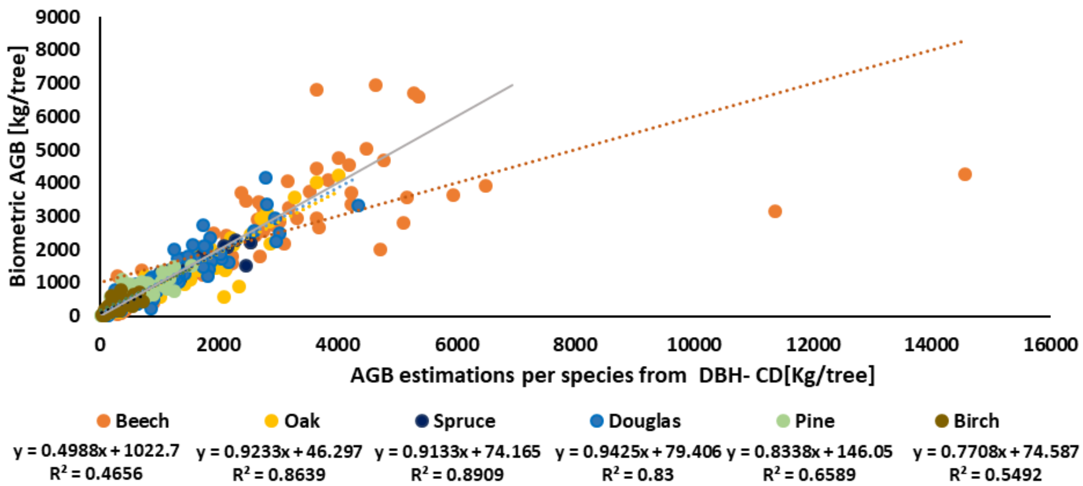

Figure 33. Scatter plot of AGB estimations from each species DBH estimation models, DBH-CD models compared against the biometric AGB[kg/tree].

In summary, Beech species-specific models (DBH-CPA and DBH-CD) are more sensitive to tree density and space availability, which is related to its high plasticity, hence limiting the model application. When focussing on the extreme underestimation plots, the AGB estimations from the general DBH-CD model results are closer to the biometric than the species-specific models.

Due to the crown morphology and their species plasticity, the dominant broadleaves deal with higher variation and, therefore, the AGB using DBH-CPA model have lower accuracy than the DBH-CD model. In this study, we have proved that it was caused mainly by the effect of Beech species. In those cases, the species-specific DBH-CD relationship can better overcome the broadleaves crown size variation and estimate the AGB/AGC with higher accuracy than DBH-CPA.

This study considers that although all DBH models lead to results with no significant differences from field measure DBH, the DBH estimations from the species-specific DBH-CD has proven to be able to better describe and overcome the variations from exogenous environmental factors. Only in the case of Beech, it is advised to use the general DBH-CD model to better estimate AGB rather than the species-specific. Nevertheless, further analysis needs to be done on Beech species to improve the applicability of the DBH estimations.

5.5. Recommendations

To improve the DTM accuracy is advisable to use more and well-distributed GCPs using markers and also to consider the manual or semi-manual classification of the point cloud to ensure that all points classified as “ground” are at ground level.

6. CONCLUSION

The main objective of this research was to analyse the effect of the shape and size of the crown area of temperate forest tree species and how they affect the AGB and AGC estimations when UAV images are used. It was done by using UAV-RGB images to build DBH estimation models from the DBH-CPA and DBH-CD relationships of six species. Further, this study analysed the effect of these models to estimate above-ground biomass (AGB) and aboveground carbon stock (AGC). To our knowledge, there is no previous study with this approach.

The original contribution of this research is based not only on its novelty but also in the following: The DBH estimations models were able to efficiently simplify the variations that affect the DBH-CPA and DBH-CD relationship to make practical and applicable prediction of DBH and further the ABG/AGC estimations using UAV RGB images. Both relationships estimate DBH with no significantly different from field measure DBH. Nevertheless, the DBH estimations from the species-specific DBH-CD was proved to be able to better describe and overcome the variations from exogenous environmental factors. However, in the case of Beech species, further analysis is needed to improve the DBH estimations. The conclusions are organised in answering the research questions of this study:

RQ. 1.1 What is the relationship between CPA and field measured DBH of conifers and broadleaves species in general categories and specific species?

By manually on-screen digitised CPA from Orthomosaic, this study found that the quadratic and power functions models are the best explaining the relationship between CPA and DBH. In the case of Spruce, Douglas Fir, Oak and the general Broadleaves, the quadratic model is the best. While in the case of Pine, Birch, Beech, and general Conifers is the power model. The models showed high accuracy (R^2 >80 i.e., 0.93, 0.91, 0.89, 0.85), except for Pine (R^2 =78) and Birch (R^2 =71).

RQ. 1.2 Which specific specie presents the highest accuracy in assessing DBH through CPA?

The model validation was done using an independent dataset. All species-specific DBH models and general species category models, the t-test showed no significant difference between the estimated values and the biometric DBH (< t-Critical (P > 0.05). Spruce was the species with highest accuracy results (R^2 = 0.92, RMSE = 3.95cm). In the case of the broadleaves, Oak presented the highest results between the species-specific models (R2 = 0.92, RMSE = 3.83 cm).

However, there is no significance difference between the estimations of Spruce – Douglas (t(48)= 0.94 , p= 0.35, p > 0.05), Spruce- Pine (t(39)= 0.83, p= 0.41, p > 0.05), and Pine-Douglas (t(41)= 0.18, p= 0.86, p > 0.05). In the case of broadleaves species, between Oak and Beech the estimation results showed no significant difference (t(49)= 1.172, p= 0.25, p > 0.05). The comparison between the estimations from Birch-Oak and Birch-Beech was found significantly different (t(38)= -5.73, p= 1.33E-06, p< 0.05) and (t(37)= -4.036, p= 2.63E-04, p < 0.05) respectively.

RQ. 2.1 What is the relationship between CD and field measured DBH of conifers and broadleaves species in general categories and specific species?

The tree CD was derived from the CPA and plotted against DBH to build the DBH-CD relationship. Power and Quadratic were the types of functions that best describe the relationship between variables (with the highest R^2 and lower RMSE and RMSD). With the exception of Pine (R^2 =78) and Birch species (R^2 =71), the selected model showed high accuracy (R^2 >80 i.e. 0.93, 0.91, 0.89, 0.86). The quadratic model fiction was the best on Spruce, Douglas Fir, Oak and the general Broadleaves. While Pine, Birch, Beech and general Conifers were the power model. In this sense, the selected function type for all cases were on agreement with the DBH-CPA models. Moreover, the accuracy results were very similar between the two models with slightly better accuracy results by the DBH-CD models.

RQ. 2.2 Which specie shows the highest accuracy in assessing DBH from CD?

The model validation was done using the independent dataset, for all species-specific models and general species category models, the t-test showed no significant difference between the estimated values and the biometric DBH (< t-Critical ($P > 0.05$). In the case of conifers species, Spruce was the species with the highest accuracy results ($R^2 = 0.93$, RMSE = 3.90 cm). In the case of the broadleaves species, Oak presented the highest results between the species-specific models ($R^2 = 0.92$, RMSE = 3.76 cm).

As in the case of DBH-CPA, there was no significance difference between the estimations of Spruce – Douglas Fir (t(48)= 0.94 , p= 0.35, $p > 0.05$), Spruce- Pine (t(39)= 0.83, p= 0.41, $p > 0.05$), and Pine-Douglas Fir (t(41)= 0.19, p= 0.85, $p > 0.05$). With the broadleaves species, Between Oak and Beech the estimation results showed no significant difference (t(49)= 1.12, p= 0.27, $p > 0.05$). While, the comparison between the estimations from Birch-Oak and Birch-Beech was found significantly different (t(38)= -5.68, p= 1.59E-06, $p < 0.05$) and (t(37)= -4.04, p= 2.62E-04, $p < 0.05$) respectively.

RQ. 3.1 What is the accuracy of modelled AGB and AGC derived from UAV images compared to field measurements?

The AGB estimation results both from general and species-specific models showed very similar accuracy results. The t-test showed no significant difference between the estimations of AGB and AGC from each of the models and the biometric AGB/AGC ($p > 0.05$). When comparing between the statistical indicators from the linear regression, the AGB estimations from species-specific DBH-CD models can explain a higher variance with the lowest RMSE ($R^2 = 0.81$; RMSE = 62.04 ton/ha). It also got the highest p-value = 0.74. The species-specific estimations from the DBH-CPA model ($R^2 = 0.65$) got the highest RMSE (84.15 tons/ha), which is slightly higher than the general DBH-CPA model [tons/ha].

Since we have used uniform conversion factor, AGC results showed the same behaviour as in AGB estimations with an RMSE reduced around half. the estimations from the species-specific DBH-CD models explained higher variance with the lowest RMSE ($R^2 = 0.81$; RMSE = 31.02 ton/ha).

RQ. 3.2 Which plot type (broadleaved, conifers or mixed) specie shows high accuracy in estimating its AGB/ AGC?

By applying the species-specific DBH models. Mixed plots presented the highest accuracy (R2 = 0.91; RMSE = 51.69 ton/ha from DBH-CD and R2 = 0.88; RMSE = 57.57ton/ha from DBH-CPA). It was followed by the conifers plots (R2 = 0.83; RMSE = 29.77 ton/ha from DBH-CD and R2 = 0.79; RMSE = 33.58 ton/ha from DBH-CPA). Broadleaves plots got the lowest accuracy results with R2 = 0. 46; RMSE = 101.77 ton/ha from DBH-CD and R2 = 0.71; RMSE = 74.56 ton/ha from DBH-CPA).

In the case of AGC, the results were similar, the mixed plots resulted with the highest accuracy $R2 = 0.91$; RMSE = 25.84 ton/ha from DBH-CD and $R2 = 0.88$; RMSE = 28.78 ton/ha from DBH-CPA). It was followed by the conifers plots: $R2 = 0.83$; RMSE = 14.89 ton/ha from DBH-CD and $R2 = 0.79$; RMSE = 16.79 ton/ha from DBH-CPA. Broadleaves plots have also got the lowest accuracy results with R2 = 0. 46; RMSE = 50.88 ton/ha from DBH-CD and $R2 = 0.71$; RMSE = 37.28 ton/ha from DBH-CPA.

RQ. 3.3 Which DBH estimation model performed better on the AGB and AGC estimations?

Species-specific DBH-CD was the one that best performed on the estimation of AGB and AGC of all the plots measured according to the accuracy assessment. Moreover, the study site has variations in tree density and canopy density. It was found that Species-specific DBH-CD was the best overshoot the extreme cases. In this research, Beech was found to have some high extreme outliers, due to its high plasticity, that resulted in hight variation is the model. Beech DBH was the only species which was described best by the general category of broadleaves model. We consider than this species might need further research with a more robust and wider range of canopy density.

7. LIST OF REFERENCES

Ali, A., Ashraf, M. I., Gulzar, S., & Akmal, M. (2020). Estimation of forest carbon stocks in temperate and subtropical mountain systems of Pakistan: implications for REDD+ and climate change mitigation. Environmental Monitoring and Assessment, 192(3), 1–13. https://doi.org/10.1007/s10661-020-8157-x

Alonzo, M., Andersen, H.-E., Morton, D., & Cook, B. (2018). Quantifying Boreal Forest Structure and Composition Using UAV Structure from Motion. Forests, 9(3), 119. https://doi.org/10.3390/f9030119

Avenza Systems. (2020). Avenza Maps. Retrieved July 24, 2020, from https://www.avenza.com/avenza-maps/

Bauhus, J., Forrester, D. J., Gardiner, B., Jactel, H., Vallejo, R., & Pretzsch, H. (2017). Mixed-species forests: ecology and management.

Bayer, D., & Pretzsch, H. (2017). Reactions to gap emergence: Norway spruce increases growth while European beech features horizontal space occupation–evidence by repeated 3D TLS measurements. Silva Fennica, 51(5).

Blanchard, E., Birnbaum, P., Ibanez, T., Boutreux, T., Antin, C., Ploton, P., … Couteron, P. (2016). Contrasted allometries between stem diameter, crown area, and tree height in five tropical biogeographic areas. Trees, 30(6), 1953–1968. https://doi.org/10.1007/s00468-016-1424-3

Bonham, C. D. (2013, May 17). Front Matter. Measurements for Terrestrial Vegetation, pp. i–xiii. https://doi.org/doi:10.1002/9781118534540.fmatter

Bouillon, S., Borges, A. V., Castañeda-Moya, E., Diele, K., Dittmar, T., Duke, N. C., … Twilley, R. R. (2008). Mangrove production and carbon sinks: A revision of global budget estimates. Global Biogeochemical Cycles, 22(2), 1–12. https://doi.org/10.1029/2007GB003052

Brown, S. (2002). Measuring carbon in forests: Current status and future challenges. Environmental Pollution, 116(3), 363–372. https://doi.org/10.1016/S0269-7491(01)00212-3

BU, B. U. S. of P. H. (2016). Regression Diagnostics. Retrieved July 24, 2020, from https://sphweb.bumc.bu.edu/otlt/MPH-Modules/BS/R/R5_Correlation-Regression/R5_Correlation-Regression7.html

Chave, J., Andalo, C., Brown, S., Cairns, M. A., Chambers, J. Q., Eamus, D., … Yamakura, T. (2005). Tree allometry and improved estimation of carbon stocks and balance in tropical forests. Oecologia, 145(1), 87–99. https://doi.org/10.1007/s00442-005-0100-x

Ciesla, W. M. (2002). An overview of temperate broadleaf forests. In Non-wood forest products from temperate broad-leaved trees. Retrieved from http://www.fao.org/3/y4351e/y4351e05.htm#bm05

Clough, B. F., Dixon, P., & Dalhaus, O. (1997). Allometric Relationships for Estimating Biomass in Multi-stemmed Mangrove Trees. Australian Journal of Botany, 45(6), 1023. https://doi.org/10.1071/BT96075

D'Annunzio, R., Lindquist, E. J., & MacDicken, K. G. (2017). Global forest land-use change from 1990 to 2010: an update to a global remote sensing survey of forests. Retrieved from http://www.fao.org/3/a-i5098e.pdf

Dandois, J. P., & Ellis, E. C. (2013). High spatial resolution three-dimensional mapping of vegetation spectral dynamics using computer vision. Remote Sensing of Environment, 136, 259–276. https://doi.org/10.1016/j.rse.2013.04.005

Dempewolf, J., Nagol, J., Hein, S., Thiel, C., & Zimmermann, R. (2017). Measurement of Within-Season Tree Height Growth in a Mixed Forest Stand Using UAV Imagery. Forests, 8(7), 231. https://doi.org/10.3390/f8070231

Disney, M. I., Kalogirou, V., Lewis, P., Prieto-Blanco, A., Hancock, S., & Pfeifer, M. (2010). Simulating the impact of discrete-return lidar system and survey characteristics over young conifer and broadleaf forests. Remote Sensing of Environment, 114(7), 1546–1560.

Dittmann, S., Thiessen, E., & Hartung, E. (2017). Applicability of different non-invasive methods for tree mass estimation: A review. Forest Ecology and Management, 398, 208–215. https://doi.org/10.1016/j.foreco.2017.05.013

Ecology Pocket Guide. (2018). Temperate, Tropical, and Subtropical Coniferous Forest. Retrieved March 30, 2020, from http://www.ecologypocketguide.com/temperate-coniferous-forest

Erb, K. H., Kastner, T., Plutzar, C., Bais, A. L. S., Carvalhais, N., Fetzel, T., … Luyssaert, S. (2018). Unexpectedly large impact of forest management and grazing on global vegetation biomass. Nature, 553(7686), 73–76. https://doi.org/10.1038/nature25138

FAO. (1993). The Challenge of sustainable forest management : what future for the world's forests?. Food and Agriculture Organization of the United Nations.

FAO. (2010). Netherlands Country Report Global Forest Resources Assesment. Retrieved from http://www.fao.org/3/al580E/al580E.pdf

FAO. (2015a). Global Forest Resources Assessments. Retrieved March 30, 2020, from Food and Agriculture Organization of the United Nations, Rome, Italy website: http://www.fao.org/forest-resources-assessment/current-assessment/maps-and-figures/en/

FAO. (2015b). Netherlands Global Forest Resources Assessment 2015 Country Resport. Retrieved from http://www.fao.org/3/a-au190e.pdf

FAO. (2018). REDD+ Reducing Emissions from Deforestation and Forest Degradation. Retrieved July 23, 2020, from http://www.fao.org/redd/en/#:~:text=It is estimated that globally,later implementation phase of REDD%2B.

Frazer, G. W., Magnussen, S., Wulder, M. A., & Niemann, K. O. (2011). Simulated impact of sample plot size and co-registration error on the accuracy and uncertainty of LiDAR-derived estimates of forest stand biomass. Remote Sensing of Environment, 115(2), 636–649. https://doi.org/10.1016/J.RSE.2010.10.008

Frey, J., Kovach, K., Stemmler, S., & Koch, B. (2018). UAV photogrammetry of forests as a vulnerable process. A sensitivity analysis for a structure from motion RGB-image pipeline. Remote Sensing, 10(6), 912.

Fritz, A., Kattenborn, T., & Koch, B. (2013). UAV-Based photogrammetric point clouds – tree stem mapping in open stands in comparison to terrestrial laser scanner point clouds.

Gering, L. R., & May, D. M. (1995). The relationship of diameter at breast height and crown diameter for four species groups in Hardin County, Tennessee. Southern Journal of Applied Forestry, 19(4), 177–181.

Getzin, S., & Wiegand, K. (2007). Asymmetric tree growth at the stand level: random crown patterns and the response to slope. Forest Ecology and Management, 242(2–3), 165–174.

Ghasemi, N., Sahebi, M. R., & Mohammadzadeh, A. (2011). A review on biomass estimation methods using synthetic aperture radar data. International journal ofgeomatics and geosciences, 1(4), 776–788.

Gibbs, H. K., Brown, S., Niles, J. O., & Foley, J. A. (2007). Monitoring and estimating tropical forest carbon stocks: making REDD a reality. Environmental Research Letters, 2(4), 045023. https://doi.org/10.1088/1748-9326/2/4/045023

Gibbs, H. K., & Herold, M. (2007). Tropical deforestation and greenhouse gas emissions. Environmental Research Letters, 2(4), 045021. https://doi.org/10.1088/1748-9326/2/4/045021

Gilliam, F. S. (2016). Forest ecosystems of temperate climatic regions: from ancient use to climate change. New Phytologist, 212(4), 871–887. https://doi.org/10.1111/nph.14255

Giri, C., Ochieng, E., Tieszen, L. L., Zhu, Z., Singh, A., Loveland, T., … Duke, N. (2011). Status and distribution of mangrove forests of the world using earth observation satellite data. Global Ecology and Biogeography, 20(1), 154–159. https://doi.org/10.1111/j.1466-8238.2010.00584.x

Global Climate Observing System, G. (2020.). GCOS | WMO. Retrieved February 26, 2020, from https://gcos.wmo.int/en/essential-climate-variables/about

Gobakken, T., & Næsset, E. (2008). Assessing effects of laser point density, ground sampling intensity, and field sample plot size on biophysical stand properties derived from airborne laser scanner data. Canadian Journal of Forest Research, 38(5), 1095–1109. https://doi.org/10.1139/X07-219

Goodbody, T. R. H., Coops, N. C., Marshall, P. L., Tompalski, P., & Crawford, P. (2017). Unmanned aerial systems for precision forest inventory purposes: A review and case study. Forestry Chronicle, 93(1), 71–81. https://doi.org/10.5558/tfc2017-012

Google Earth (2019). Enchede, Netherlands. Image published on Feb 06 2019. 358605.92 m E, 5789250.67 m N, Eye alt 13.86km. Retrieved Jun 10 2020.

Grznárová, A., Mokros, M., Surovy, P., Slavík, M., Pondelík, M., & Merganič, J. (2019). The crown diameter estimation from fixed wing type of UAV imagery. ISPRS - International Archives of the Photogrammetry, Remote Sensing and Spatial Information Sciences, XLII-2/W13, 337–341. https://doi.org/10.5194/isprs-archives-XLII-2-W13-337-2019

Gschwantner, T., Schadauer, K., Vidal, C., Lanz, A., Tomppo, E., Di Cosmo, L., … Lawrence, M. (2009). Common tree definitions for national forest inventories in Europe.

IGISMAP. (2020). Netherlands Province Shapefile . Retrieved September 5, 2020, from Netherlands Province Shapefile website: https://www.igismap.com/download-free-netherland-shapefile-boundary-polygon/

Heath, L. S., Kauppi, P. E., Burschel, P., Gregor, H. D., Guderian, R., Kohlmaier, G. H., … Weber, M. (1993). Contribution of temperate forests to the world's carbon budget. Water, Air, & Soil Pollution, 70(1–4), 55–69. https://doi.org/10.1007/BF01104988

Hemery, G. E., Savill, P. S., & Pryor, S. N. (2005). Applications of the crown diameter–stem diameter relationship for different species of broadleaved trees. Forest Ecology and Management, 215(1–3), 285–294.

Hirata, Y., Takao, G., Sato, T., & Toriyama, J. (2012). REDD-plus Cookbook Reducing Emissions from Deforestation and forest Degradation and the Role of Conservation, Sustainable Management of Forests and Enhancement. Retrieved from https://www.ffpri.affrc.go.jp/redd-rdc/en/reference/cookbook/redd_cookbook_all_high_en.pdf

Huang, H., He, S., & Chen, C. (2019). Leaf abundance affects tree height estimation derived from UAV images. Forests, 10(10). https://doi.org/10.3390/f10100931

IPCC. (2018). An IPCC Special Report on the impacts of global warming of 1.5°C above pre-industrial levels and related global greenhouse gas emission pathways, in the context of strengthening the global response to the threat of climate change, sustainable development,. Retrieved from https://www.ipcc.ch/site/assets/uploads/sites/2/2019/06/SR15_Full_Report_High_Res.pdf

IPPC. (2018). Global Warming of 1.5°C, Summary for Policy Makers. Retrieved from https://www.ipcc.ch/sr15/chapter/summary-for-policy-makers/

Ishii, H. T., Tanabe, S., & Hiura, T. (2004). Exploring the Relationships Among Canopy Structure, Stand Productivity, and Biodiversity of Temperate Forest Ecosystems. Forest Science, 50(3), 342–355. https://doi.org/10.1093/FORESTSCIENCE/50.3.342

Jayathunga, S., Owari, T., & Tsuyuki, S. (2018). The use of fixed–wing UAV photogrammetry with LiDAR DTM to estimate merchantable volume and carbon stock in living biomass over a mixed conifer–broadleaf forest. International Journal of Applied Earth Observation and Geoinformation, 73, 767–777. https://doi.org/10.1016/j.jag.2018.08.017

Jucker, T., Caspersen, J., Chave, J., Antin, C., Barbier, N., Bongers, F., … Coomes, D. A. (2017). Allometric equations for integrating remote sensing imagery into forest monitoring programmes. Global Change Biology, 23(1), 177–190. https://doi.org/10.1111/gcb.13388

Kachamba, D., Ørka, H., Gobakken, T., Eid, T., & Mwase, W. (2016). Biomass Estimation Using 3D Data from Unmanned Aerial Vehicle Imagery in a Tropical Woodland. Remote Sensing, 8(11), 968. https://doi.org/10.3390/rs8110968

Ketterings, Q. M., Coe, R., van Noordwijk, M., & Palm, C. A. (2001). Reducing uncertainty in the use of allometric biomass equations for predicting above-ground tree biomass in mixed secondary forests. Forest Ecology and Management, 146(1–3), 199–209.

Kikuzawa, K., & Umeki, K. (1996). Effect of canopy structure on degree of asymmetry of competition in two forest stands in northern Japan. Annals of Botany, 77(6), 565–571.

Kloek, N. (2014). Baronnenpad Enschede . Retrieved June 14, 2020, from https://wandelfotosite.nl/landgoederenroute-textielbaronnen-enschede/

Konôpka, B., Pajtík, J., Moravčík, M., & Lukac, M. (2010). Biomass partitioning and growth efficiency in four naturally regenerated forest tree species. Basic and Applied Ecology, 11(3), 234–243.

Kraus, K. (2007). Photogrammetry : geometry from images and laser scans. Retrieved from https://books.google.nl/books?id=tTf8MUhY29IC&printsec=frontcover#v=snippet&q=sigma&f=false

Lal, R., & Lorenz, K. (2012). Carbon sequestration in temperate forests. In Recarbonization of the Biosphere: Ecosystems and the Global Carbon Cycle (pp. 187–202). https://doi.org/10.1007/978-94-007-4159-1_9

Lenard, E. (2008). Habits of trees and shrubs in landscape design. Architecture, Civil Engineering, Environment (ACEE), 4, 13–20.

Lisein, J., Michez, A., Claessens, H., & Lejeune, P. (2015). Discrimination of Deciduous Tree Species from Time Series of Unmanned Aerial System Imagery. plos one, 10(11), e0141006. https://doi.org/10.1371/journal.pone.0141006

Lisein, J., Pierrot-Deseilligny, M., Bonnet, S., & Lejeune, P. (2013). A Photogrammetric Workflow for the Creation of a Forest Canopy Height Model from Small Unmanned Aerial System Imagery. Forests, 4(4), 922–944. https://doi.org/10.3390/f4040922

Loehle, C. (2016). Biomechanical constraints on tree architecture. Trees, 30(6), 2061–2070. https://doi.org/10.1007/s00468-016-1433-2

Loreti, F., & Pisani, P. L. (1990). Structural manipulation for improved performance in woody plants. HortScience, 25(1), 64–70.

Lu, D. (2006). The potential and challenge of remote sensing-based biomass estimation. International Journal of Remote Sensing, 27(7), 1297–1328. https://doi.org/10.1080/01431160500486732

Lumen. (2020). Introduction to Statistics: Outliers . Retrieved July 24, 2020, from https://courses.lumenlearning.com/introstats1/chapter/outliers/

Magnussen, S., & Reed, D. (2015). Modelling for estimation and monitoring. Knowledge Reference for National Forest Assessments, 111–136. Retrieved from http://www.fao.org/forestry/fma/73411/en/

Messinger, M., Asner, G., & Silman, M. (2016). Rapid Assessments of Amazon Forest Structure and Biomass Using Small Unmanned Aerial Systems. Remote Sensing, 8(8), 615. https://doi.org/10.3390/rs8080615

Morin, D., Planells, M., Guyon, D., Villard, L., Mermoz, S., Bouvet, A., … Dedieu, G. (2019). Estimation and Mapping of Forest Structure Parameters from Open Access Satellite Images: Development of a

Generic Method with a Study Case on Coniferous Plantation. Remote Sensing, 11(11), 1275. https://doi.org/10.3390/rs11111275

Musselman, R. C., & Fox, D. G. (1991). A Review of the Role of Temperate Forests in the Global Co2 Balance. Journal of the Air and Waste Management Association, 41(6), 798–807. https://doi.org/10.1080/10473289.1991.10466876

Nasrullah, A. (2016). Systematic Analysis of Unmanned Aerial Vehicle (UAV) Derived Product Quality. https://doi.org/10.13140/RG.2.1.3132.0729

Natuurmonumenten. (2020). Nature reserve Natural monuments: Haagse Bos. Retrieved June 14, 2020, from https://www.natuurmonumenten.nl/natuurgebieden/haagse-bos#r=1

Nex, F., & Remondino, F. (2014). UAV for 3D mapping applications: A review. Applied Geomatics, 6(1), 1–15. https://doi.org/10.1007/s12518-013-0120-x

Niklas, K. J. (1992). Plant biomechanics: an engineering approach to plant form and function. University of Chicago press.

Novak, J., Slodicak, M., & Dušek, D. (2011). Aboveground biomass of substitute tree species stand with respect to thinning–European larch (Larix decidua Mill.). Journal of Forest Science, 57(57), 8–15. Retrieved from https://www.researchgate.net/publication/228854840_Aboveground_biomass_of_substitute_tree_species_stand_with_respect_to_thinning-European_larch_Larix_decidua_Mill

Offwell Woodland & Wildlife Trust. (2000). An Introduction to British Woodlands and their Management. Retrieved March 31, 2020, from Offwell Woodland & Wildlife Trust website: http://www.countrysideinfo.co.uk/woodland_manage/index.htm

Otero, V., Van De Kerchove, R., Satyanarayana, B., Martínez-Espinosa, C., Fisol, M. A. Bin, Ibrahim, M. R. Bin, … Dahdouh-Guebas, F. (2018). Managing mangrove forests from the sky: Forest inventory using field data and Unmanned Aerial Vehicle (UAV) imagery in the Matang Mangrove Forest Reserve, peninsular Malaysia. Forest Ecology and Management, 411, 35–45. https://doi.org/10.1016/J.FORECO.2017.12.049

Paganová, V., Maceková, M., & Bakay, L. (2015). A quantitative analysis of dendrometric data on Sorbus domestica L. phenotypes for urban greenery. Urban Forestry & Urban Greening, 14(3), 599–606.

Pallardy, S. G. (2010). Physiology of woody plants. Academic Press.

Panagiotidis, D., Abdollahnejad, A., Surový, P., & Chiteculo, V. (2017). Determining tree height and crown diameter from high-resolution UAV imagery. International Journal of Remote Sensing, 38(8–10), 2392–2410. https://doi.org/10.1080/01431161.2016.1264028

Perko, R., Raggam, H., Gutjahr, K., & Schardt, M. (2010). The capabilities of TerraSAR-X imagery for retrieval of forest parameters. na.

Pham, T. D., Yokoya, N., Bui, D. T., Yoshino, K., & Friess, D. A. (2019). Remote sensing approaches for monitoring mangrove species, structure, and biomass: Opportunities and challenges. Remote Sensing, 11(3), 1–24. https://doi.org/10.3390/rs11030230

Picard, N. (2012). Manual for building a tree volume and biomass allometric equations.

Piñeiro, G., Perelman, S., Guerschman, J. P., & Paruelo, J. M. (2008). How to evaluate models: Observed vs. predicted or predicted vs. observed? Ecological Modelling, 216(3–4), 316–322. https://doi.org/10.1016/j.ecolmodel.2008.05.006

Pix4D. (2020a). Ground sampling distance (GSD) . Retrieved August 1, 2020, from https://support.pix4d.com/hc/en-us/articles/202559809-Ground-sampling-distance-GSD

Pix4D. (2020b). Processing Options. Retrieved August 1, 2020, from Pix4D website: https://support.pix4d.com/hc/en-us/articles/202557759-Menu-Process-Processing-Options-1-Initial-Processing-General

Pommerening, A. (2007). Forest structures. Retrieved from http://www.pommerening.org/wiki/images/f/fc/GeneralTextOnStructure.pdf

Pommerening, Arne. (2015). Basic tree variables, forestry summary characteristics and biodiversity measures . Retrieved from http://www.pommerening.org/wiki/images/e/eb/ForestrySummaryCharacteristics.pdf

Poole, M. A., & O'Farrell, P. N. (1971). The assumptions of the linear regression model. Transactions of the Institute of British Geographers, 145–158.

Potapov, P. (2009). Gross forest cover loss in temperate forests: biome-wide monitoring results using MODIS and Landsat data. Journal of Applied Remote Sensing, 3(1), 033569. https://doi.org/10.1117/1.3283904

Pretzsch, H. (2010). Re-evaluation of allometry: state-of-the-art and perspective regarding individuals and stands of woody plants. In Progress in botany 71 (pp. 339-369). Springer, Berlin, Heidelberg.

Pretzsch, H. (2014, September 1). Canopy space filling and tree crown morphology in mixed-species stands compared with monocultures. Forest Ecology and Management, Vol. 327, pp. 251–264. https://doi.org/10.1016/j.foreco.2014.04.027

Primasatya, R. F., Hussin, Y. A., & Van Leeuwen, L. M. (2016). Terrestrial Laser scanning to support carbon estimation in nature conservation area: A case study of Haagse Bos and Snippert Forest, Netherlands. 37th Asian Conference on Remote Sensing, ACRS 2016: Spatial Data Infrastructure for Sustainable Development.

Puliti, S., Ene, L. T., Gobakken, T., & Næsset, E. (2017). Use of partial-coverage UAV data in sampling for large scale forest inventories. Remote Sensing of Environment, 194, 115–126. https://doi.org/10.1016/j.rse.2017.03.019

RFS, R. F. S. (2015). Tree Classification. Retrieved July 22, 2020, from https://www.rfs.org.uk/learning/forestry-knowledge-hub/trees-biology/tree-classification/

Rodríguez-Veiga, P., Wheeler, J., Louis, V., Tansey, K., & Balzter, H. (2017). Quantifying Forest Biomass Carbon Stocks From Space. Current Forestry Reports, 3(1), 1–18. https://doi.org/10.1007/s40725-017-0052-5

Ruiz, L., Hermosilla, T., Mauro, F., & Godino, M. (2014). Analysis of the Influence of Plot Size and LiDAR Density on Forest Structure Attribute Estimates. Forests, 5(5), 936–951. https://doi.org/10.3390/f5050936

Ruxton, G. D. (2006). The unequal variance t-test is an underused alternative to Student's t-test and the Mann–Whitney U test. Behavioral Ecology, 17(4), 688–690. https://doi.org/10.1093/beheco/ark016

Salach, A., Bakuła, K., Pilarska, M., Ostrowski, W., Górski, K., & Kurczyński, Z. (2018). Accuracy assessment of point clouds from LidaR and dense image matching acquired using the UAV platform for DTM creation. ISPRS International Journal of Geo-Information, 7(9), 342.

Samanthi. (2011). Difference Between Deciduous and Coniferous Trees. Retrieved June 14, 2020, from https://www.differencebetween.com/difference-between-deciduous-and-vs-coniferous-trees/

Sanderson, M., Santini, M., Valentini, R., & Pope, E. (2012). Relationships between forests and weather.

Schröter, M., Härdtle, W., & von Oheimb, G. (2012). Crown plasticity and neighborhood interactions of European beech (Fagus sylvatica L.) in an old-growth forest. European Journal of Forest Research, 131(3), 787–798.

Sedjo, R. A. (1992). Temperate forest ecosystems in the global carbon cycle. Ambio, 21(4), 274–277. https://doi.org/10.2307/4313942

Seidel, D., Leuschner, C., Müller, A., & Krause, B. (2011). Crown plasticity in mixed forests—quantifying asymmetry as a measure of competition using terrestrial laser scanning. Forest Ecology and Management, 261(11), 2123–2132.

Seidel, D., Ruzicka, K. J., & Puettmann, K. (2016). Canopy gaps affect the shape of Douglas-fir crowns in the western Cascades, Oregon. Forest Ecology and Management, 363, 31–38.

Sharma, R. P., Bílek, L., Vacek, Z., & Vacek, S. (2017). Modelling crown width–diameter relationship for Scots pine in the central Europe. Trees - Structure and Function, 31(6), 1875–1889. https://doi.org/10.1007/s00468-017-1593-8

Shimano, K. (1997). Analysis of the Relationship between DBH and Crown Projection Area Using a New Model. Journal of Forest Research, 2(4), 237–242. https://doi.org/10.1007/BF02348322

Sinha, S., Jeganathan, C., Sharma, L. K., & Nathawat, M. S. (2015). A review of radar remote sensing for biomass estimation. International Journal of Environmental Science and Technology, 12(5), 1779–1792. https://doi.org/10.1007/s13762-015-0750-0

Smith, J. M. B. (2020). Temperate forest | ecology | Britannica. Retrieved June 13, 2020, from Enciclopedia Britannica website: https://www.britannica.com/science/temperate-forest

Song, C., Dickinson, M. B., Su, L., Zhang, S., & Yaussey, D. (2010). Estimating average tree crown size using spatial information from Ikonos and QuickBird images: Across-sensor and across-site comparisons. Remote Sensing of Environment, 114(5), 1099–1107. https://doi.org/10.1016/j.rse.2009.12.022

Sousa, A. M. O., Gonçalves, A. C., & da Silva, J. R. M. (2017). Above-Ground Biomass Estimation with High Spatial Resolution Satellite Images. In Biomass Volume Estimation and Valorization for Energy. https://doi.org/10.5772/65665

Suchomel, C., Pyttel, P., Becker, G., & Bauhus, J. (2012). Biomass equations for sessile oak (Quercus petraea (Matt.) Liebl.) and hornbeam (Carpinus betulus L.) in aged coppiced forests in southwest Germany. Biomass and Bioenergy, 46, 722–730. https://doi.org/10.1016/j.biombioe.2012.06.021

Tenaw Geremew, W. (2011). Assessment of aboveground carbon stock in coniferous and broadleaf forests, using high spatial resolution satellite images. University of Twente.

Torresan, C., & Wallace, L. (2016). Forestry applications of UAVs in Europe: a review. International Journal of Remote Sensing.

Miller, G. T. (George T., Spoolman, S., Cengage Learning), & National Geographic Learning. (2019). Environmental science (16th ed.; G. Tyler Miller & S. Spoolman, Eds.). Cengage Learning.

United Nations, D. and S. A. (2018). Goal 15: Protect, restore and promote sustainable use of terrestrial ecosystems, sustainably manage forests, combat desertification, and halt and reverse land degradation and halt biodiversity loss — SDG Indicators. Retrieved February 26, 2020, from https://unstats.un.org/sdgs/report/2018/goal-15/

Uria-Diez, J., & Pommerening, A. (2017). Crown plasticity in Scots pine (Pinus sylvestris L.) as a strategy of adaptation to competition and environmental factors. Ecological Modelling, 356, 117–126.

van der Maatek-Theunissen, M., & Schuck, A. (2013). Integration of Nature Protection in Forest Policy in the Netherlands .

Vincent, G., & Harja, D. (2008). Exploring ecological significance of tree crown plasticity through three-dimensional modelling. Annals of Botany, 101(8), 1221–1231. https://doi.org/10.1093/aob/mcm189

Walker, D. J., & Kenkel, N. C. (2000). The adaptive geometry of boreal conifers. Community Ecology, 1(1), 13–23. https://doi.org/10.1556/comec.1.2000.1.4

Wanga, J., & Lindenbergha, R. (2018). Validating a workflow for tree inventory updating with 3d point clouds obtained by mobile laser scanning. International Archives of the Photogrammetry, Remote Sensing and Spatial Information Sciences, 42, 2.

Wang, G. (Ed.), Weng, Q. (Ed.). (2014). Remote Sensing of Natural Resources. Boca Raton: CRC Press, https://doi.org/10.1201/b15159

Westoby, M. J., Brasington, J., Glasser, N. F., Hambrey, M. J., & Reynolds, J. M. (2012). 'Structure- from-Motion' photogrammetry: A low- cost, effective tool for geoscience applications. Geomorphology, 179, 300–314. https://doi.org/10.1016/j.geomorph.2012.08.021

White, J., Wulder, M. A., Varhola, A., Vastaranta, M., Coops, N. ., Cook, B. D., & Pitt, D. (2013). A best practices guide for generating forest inventory attributes from airborne laser scanning data using the area-based approach. Retrieved from https://cfs.nrcan.gc.ca/publications?id=34887

William M. Ciesla. (1995). Non-Wood Forest Products from Temperate Broad-Leaved Trees. Retrieved from http://www.fao.org/3/y4351e/y4351e00.htm#Contents

Wilson, E. O. (Eds.). (1988). Biodiversity. https://doi.org/10.17226/989

WWF. (2020). Temperate Coniferous Forest. Retrieved June 13, 2020, from 2020 website: https://www.worldwildlife.org/biomes/temperate-coniferous-forest

Yap, B. W., & Sim, C. H. (2011). Comparisons of various types of normality tests. Journal of Statistical Computation and Simulation, 81(12), 2141–2155. https://doi.org/10.1080/00949655.2010.520163

Zarco-Tejada, P. J., Diaz-Varela, R., Angileri, V., & Loudjani, P. (2014). Tree height quantification using very high resolution imagery acquired from an unmanned aerial vehicle (UAV) and automatic 3D photo-reconstruction methods. European Journal of Agronomy, 55, 89–99. https://doi.org/10.1016/j.eja.2014.01.004

Zaiontz, C. (2020). Real Statistics Software using Excel . Retrieved July 24, 2020, from https://www.real-statistics.com/appendix/citation-real-statistics-software-website/

Zianis, D., & Mencuccini, M. (2004). On simplifying allometric analyses of forest biomass. Forest Ecology and Management, 187(2–3), 311–332.

8. APPENDIX A. Table sheet of fieldwork data collection

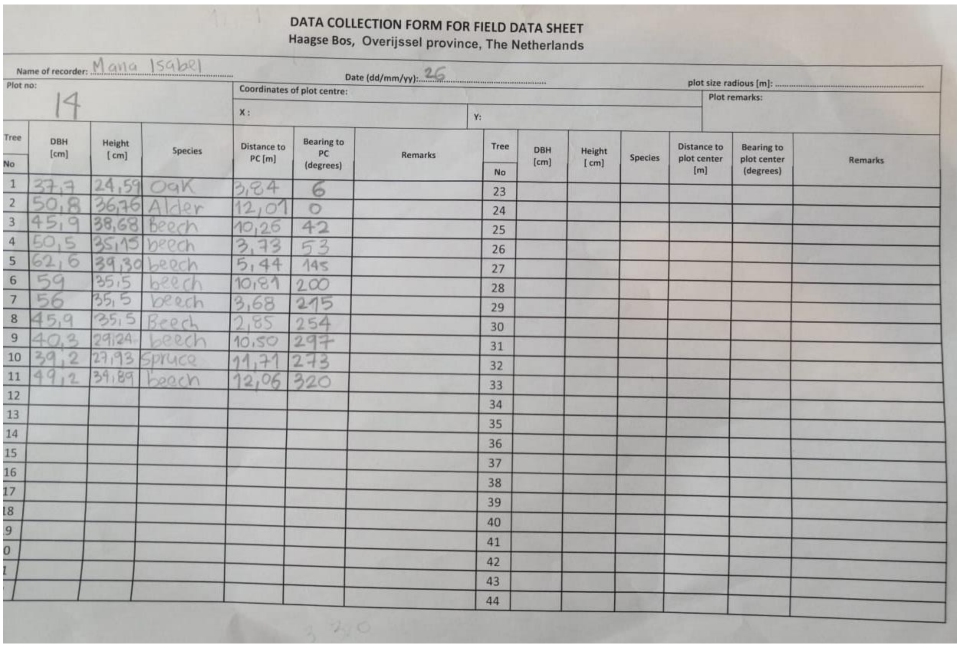

DATA COLLECTION FORM FOR FIELD DATA SHEET
Haagse Bos, Overijssel province, The Netherlands

Name of recorder: Maria Isabel
Date (dd/mm/yy): 26
plot size radious [m]:
Plot no: 14
Coordinates of plot centre:
X :
Y:
Plot remarks:

Tree No	DBH [cm]	Height [cm]	Species	Distance to PC [m]	Bearing to PC (degrees)	Remarks	Tree No	DBH [cm]	Height [cm]	Species	Distance to plot center [m]	Bearing to plot center (degrees)	Remarks
1	37,7	24,59	Oak	3,84	6		23						
2	50,8	36,76	Alder	12,01	0		24						
3	45,9	38,68	Beech	10,26	42		25						
4	50,5	35,15	beech	3,73	53		26						
5	62,6	39,30	beech	5,44	145		27						
6	59	35,5	beech	10,81	200		28						
7	56	35,5	beech	3,68	215		29						
8	45,9	35,5	Beech	2,85	254		30						
9	40,3	29,24	beech	10,50	297		31						
10	39,2	27,93	Spruce	11,71	273		32						
11	49,2	34,89	beech	12,06	320		33						
12							34						
13							35						
14							36						
15							37						
16							38						
17							39						
18							40						
9							41						
0							42						
1							43						
							44						

Figure 34: Fieldwork datasheet

9. APPENDIX B. UAV camera settings and quality report

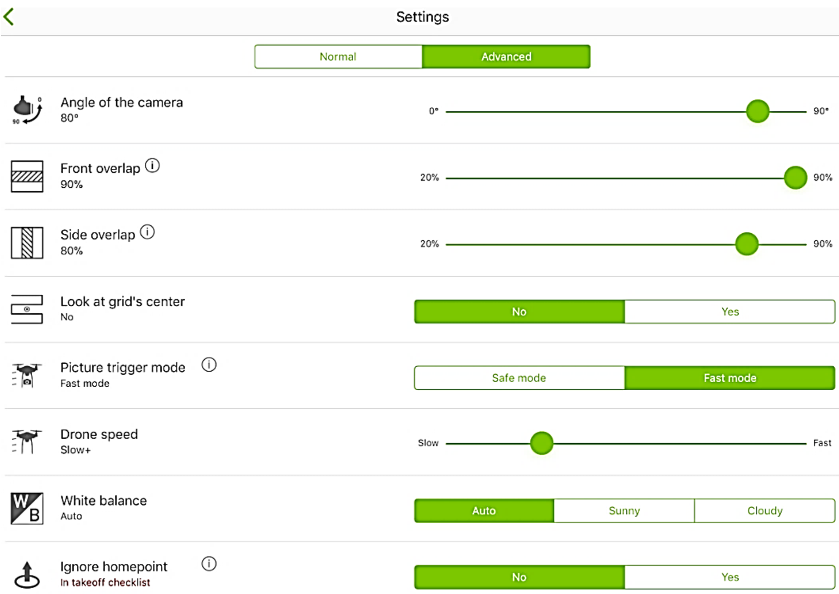

Figure 35: Camera and drone images setting onPix4Dcapture application.

Summary

Project	S_result
Processed	2020-04-04 00:15:14
Camera Model Name(s)	FC330_3.6_4000x3000 (RGB)
Average Ground Sampling Distance (GSD)	4.64 cm / 1.83 in
Area Covered	0.790 km^2 / 79.0145 ha / 0.31 sq. mi. / 195.3501 acres
Time for Initial Processing (without report)	01h:02m:18s

Quality Check

Images	median of 57568 keypoints per image	
Dataset	807 out of 807 images calibrated (100%), all images enabled	
Camera Optimization	0.08% relative difference between initial and optimized internal camera parameters	
Matching	median of 3122.71 matches per calibrated image	
Georeferencing	yes, 3 GCPs (3 3D), mean RMS error = 0 m	

Preview

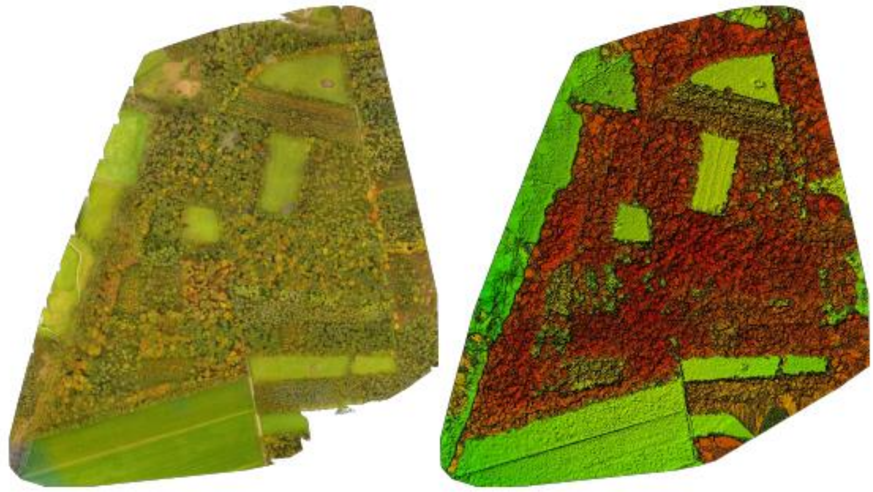

Figure 1: Orthomosaic and the corresponding sparse Digital Surface Model (DSM) before densification.

Figure 36. Summary of the UAV quality report

10. APPENDIX C. Plots characteristics configuration

* Plot 24 was eliminated because the bad weather didn't allow to finalize the measurements.

Plot No.	Total tree No.	B no	C no	Dominant species	Plot type
1	7	4	3	Oak/Spruce	Mixed
2	6	4	2	Beech/Spruce	Broadleaves
3	8	4	4	Pine	Mixed
4	15	14	1	Birch	Broadleaves
5	13	13	0	Beech	Broadleaves
6	8	8	0	Beech	Broadleaves
7	14	14	0	Beech	Broadleaves
8	14	0	14	Douglas	Broadleaves
9	13	1	12	Spruce	Conifers
10	7	7	0	Oak/Beech	Broadleaves
11	6	4	2	Oak	Broadleaves
12	15	14	1	Birch/Oak	Broadleaves
13	10	10	0	Beech/Oak	Broadleaves
14	11	10	1	Beech	Broadleaves
15	9	2	7	Douglas	Broadleaves
16	16	3	13	Douglas	Conifers
17	17	8	9	Douglas/Beech	Mixed
18	19	11	8	Pine/Oak	Mixed
19	17	12	5	Beech/Birch	Broadleaves
20	14	8	6	Pine/Birch	Mixed
21	20	15	5	Birch	Broadleaves
22	11	0	11	Douglas	Conifers
23	7	0	7	Douglas	Conifers
25	13	4	9	Spruce/Oak	Mixed
26	15	1	14	Douglas/Larch	Conifers
27	9	9	0	Beech	Broadleaves
28	9	0	9	Spruce	Conifers
29	14	1	13	Spruce	Conifers
30	8	4	4	Oak/Spruce	Mixed
31	12	5	7	Spruce	Mixed
32	11	8	3	Oak	Broadleaves
33	12	0	12	Pine	Conifers
34	8	4	4	Oak/Pine	Mixed
35	11	2	9	Pine	Conifers
36	12	1	11	Douglas	Conifers
37	8	6	2	Oak	Broadleaves
38	8	7	1	Oak	Broadleaves
39	11	0	11	Pine/Larch	Conifers
40	6	3	3	Oak/Pine	Mixed

11. APPENDIX D. Residuals variance from DBH estimation models and validation

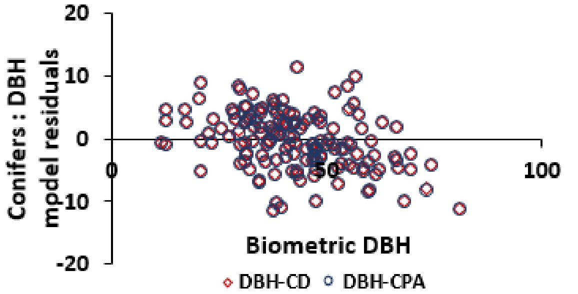

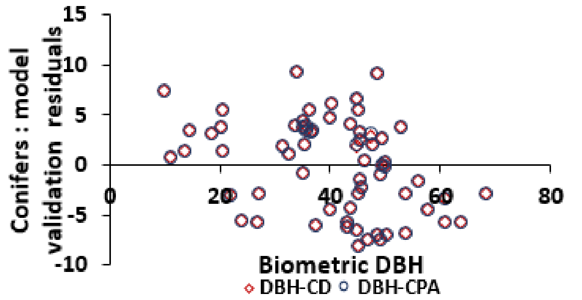

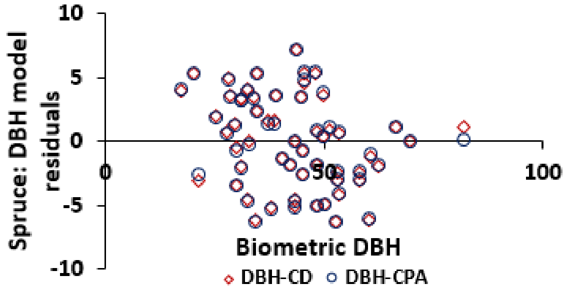

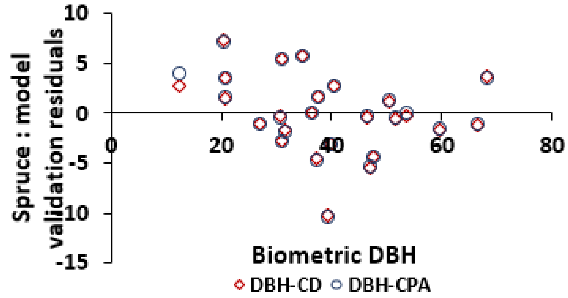

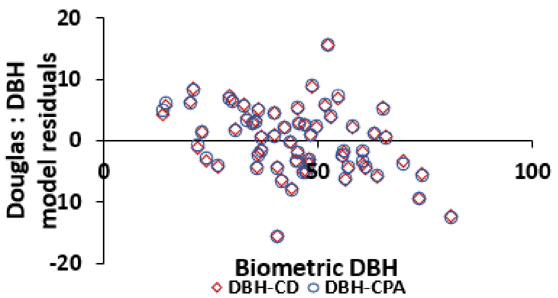

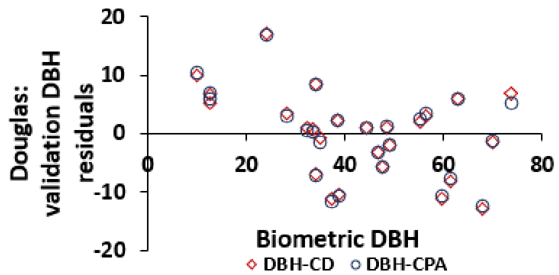

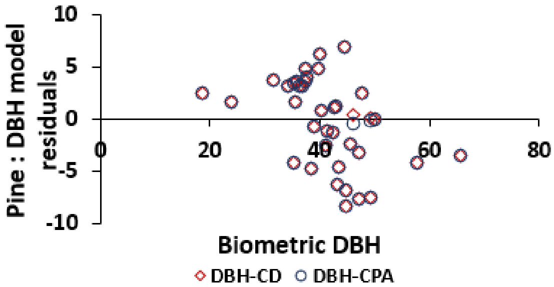

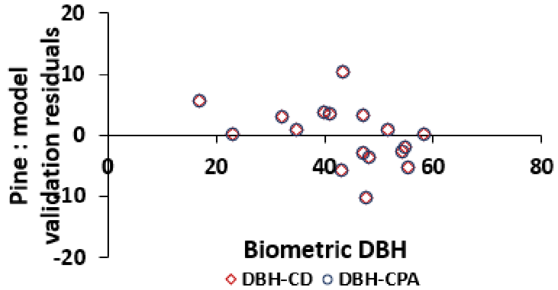

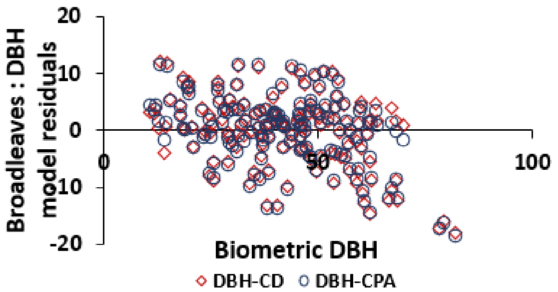

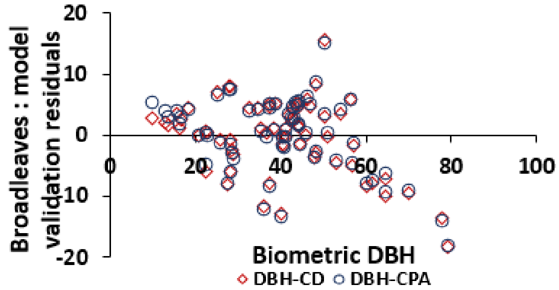

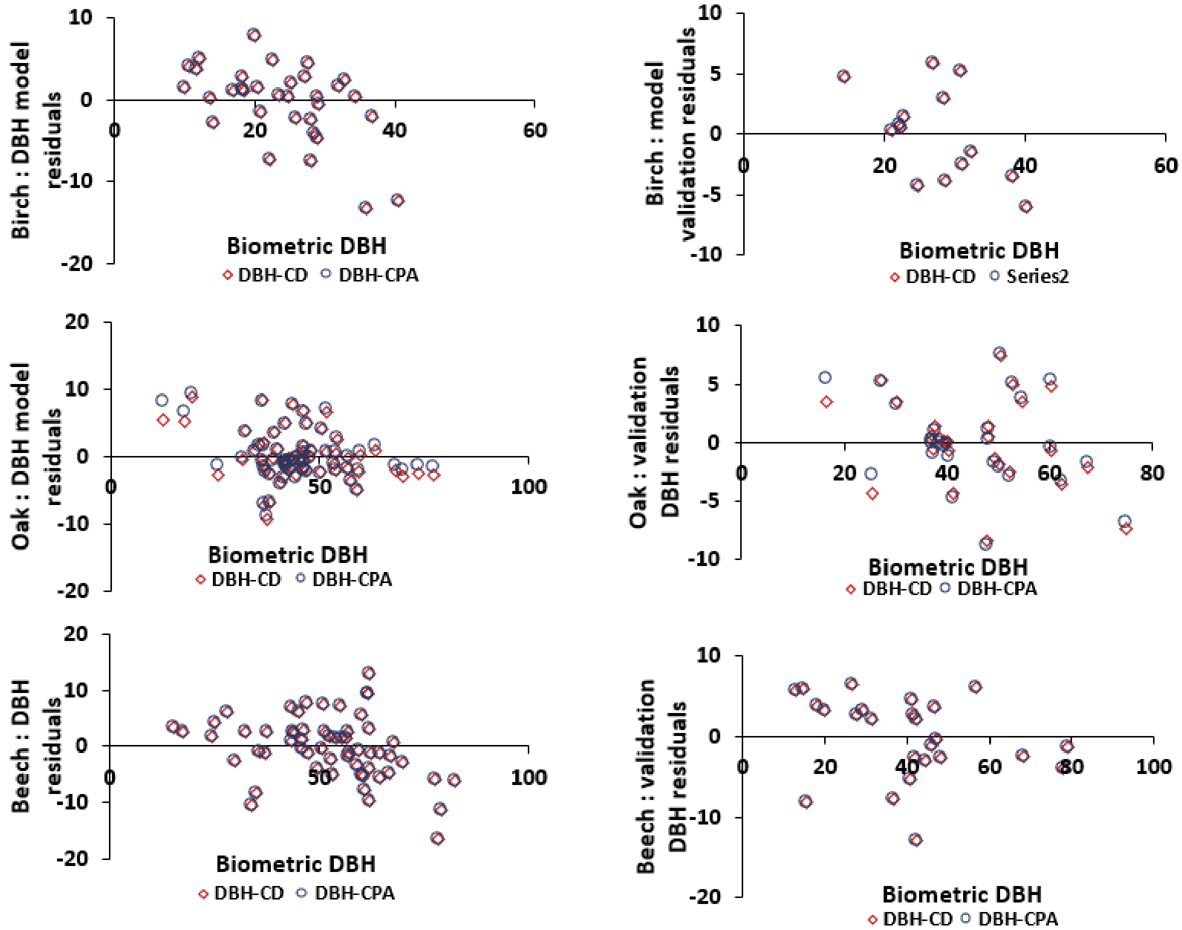

Figure 37. Residual variance from the DBH model building(left) and validation right).

12. APPENDIX E. AGB and AGC residuals variance

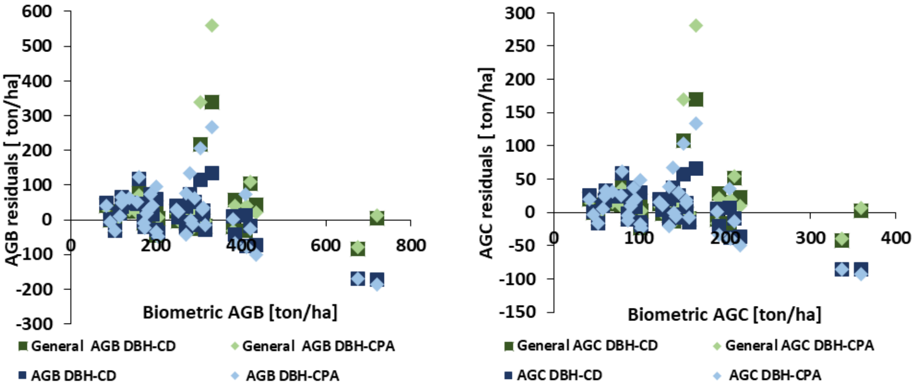

Figure 38. AGB and AGC Residual variance from linear regression.

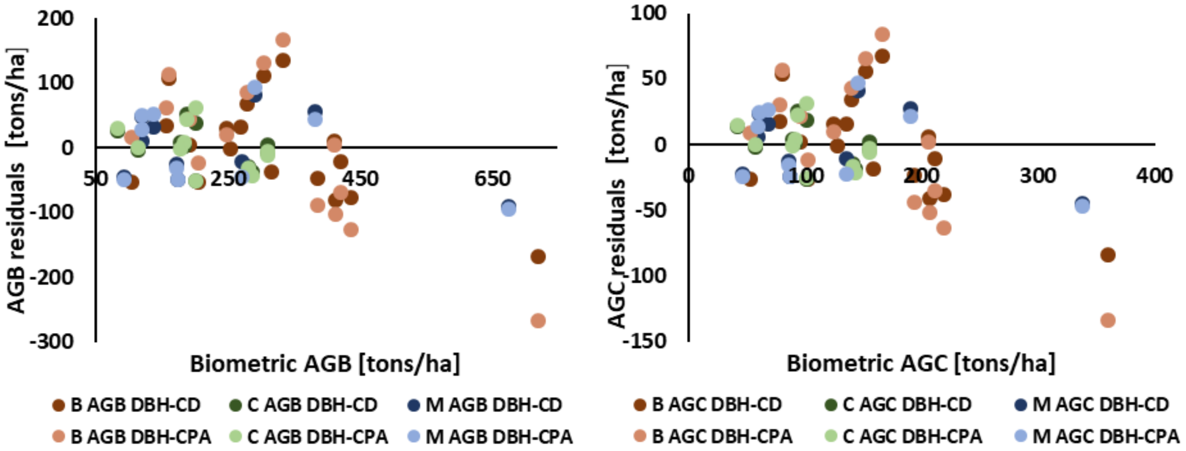

Figure 39. linear regression residuals from AGB and AGC for plot type.

13. APPENDIX F. AGB and AGC results per plot

Table 34. AGB/AGC biometric and estimation results of each plot.

Plot No	Tree No.	B No.	C No.	Dominant species	Plot type	Biometric AGB [tons/ha]	AGB DBH-CPA[tons/ha]	AGB DBH-CD[tons/ha]	General AGB DBH-CPA[tons/ha]	General AGB DBH-CD[tons/ha]	Biometric AGC [tons/ha]	AGC DBH-CPA[tons/ha]	AGC DBH-CD[tons/ha]	General AGC DBH-CPA[tons/ha]	General AGC DBH-CD[tons/ha]
1	7	4	3	Oak/Spruce	M	92.56	86.74	93.93	89.55	90.81	46.28	43.37	46.97	44.77	45.40
2	6	4	2	Beech/Spruce	B	333.44	600.88	466.64	894.17	672.68	166.72	300.44	233.32	447.08	336.34
3	8	4	4	Pine	M	120.12	167.60	157.54	153.50	145.45	60.06	83.80	78.77	76.75	72.73
4	15	14	1	Birch	B	105.08	73.62	72.26	89.40	89.05	52.54	36.81	36.13	44.70	44.53
5	13	13	0	Beech	B	386.73	319.77	344.77	428.37	443.54	193.37	159.88	172.39	214.18	221.77
6	8	8	0	Beech	B	413.63	336.14	338.17	453.44	443.60	206.81	168.07	169.08	226.72	221.80
7	14	14	0	Beech	B	719.76	533.41	547.27	732.50	724.94	359.88	266.71	273.64	366.25	362.47
8	14	0	14	Douglas	B	412.42	484.57	424.73	416.83	380.50	206.21	242.29	212.37	208.42	190.25
9	13	1	12	Spruce	C	286.95	275.00	272.99	288.00	283.34	143.47	137.50	136.50	144.00	141.67
10	7	7	0	Oak/Beech	B	304.49	511.32	418.29	643.24	520.88	152.24	255.66	209.15	321.62	260.44
11	6	4	2	Oak	B	157.05	208.18	204.11	177.65	180.15	78.53	104.09	102.06	88.83	90.08
12	15	14	1	Birch/Oak	B	248.53	278.55	287.52	267.53	272.88	124.27	139.27	143.76	133.76	136.44
13	10	10	0	Beech/Oak	B	279.64	412.97	353.06	321.05	299.08	139.82	206.49	176.53	160.53	149.54
14	11	10	1	Beech	B	422.09	395.30	403.95	531.60	525.75	211.04	197.65	201.98	265.80	262.87
15	9	2	7	Douglas	B	160.48	284.13	277.29	230.37	237.84	80.24	142.07	138.64	115.18	118.92
16	16	3	13	Douglas	C	187.46	260.89	261.60	218.28	229.09	93.73	130.45	130.80	109.14	114.55
17	17	8	9	Douglas/Beech	M	674.57	503.78	504.11	595.34	589.27	337.28	251.89	252.06	297.67	294.64
18	19	11	8	Pine/Oak	M	381.48	382.80	391.70	349.34	359.88	190.74	191.40	195.85	174.67	179.94
19	17	12	5	Beech/Birch	B	205.75	158.56	167.86	211.51	210.87	102.87	79.28	83.93	105.76	105.43
20	14	8	6	Pine/Birch	M	172.71	163.55	169.73	162.12	164.53	86.36	81.77	84.86	81.06	82.27
21	20	15	5	Birch	B	191.84	231.35	208.63	255.37	224.36	95.92	115.67	104.32	127.68	112.18
22	11	0	11	Douglas	C	282.07	281.98	275.76	254.61	255.97	141.04	140.99	137.88	127.30	127.98
23	7	0	7	Douglas	C	202.26	298.65	262.42	257.15	235.89	101.13	149.33	131.21	128.57	117.94
25	13	4	9	Spruce/Oak	M	291.65	352.71	342.67	324.67	321.58	145.83	176.36	171.34	162.34	160.79
26	15	1	14	Douglas/Larch	C	310.34	338.66	325.99	309.76	304.26	155.17	169.33	162.99	154.88	152.13
27	9	9	0	Beech	B	437.18	336.87	365.50	457.17	481.60	218.59	168.43	182.75	228.59	240.80
28	9	0	9	Spruce	Ci	115.23	126.22	134.13	133.17	137.85	57.61	63.11	67.07	66.58	68.92
29	14	1	13	Spruce	C	183.89	214.41	209.42	198.76	197.06	91.95	107.20	104.71	99.38	98.53
30	8	4	4	Oak/Spruce	M	174.41	151.10	153.63	157.13	155.56	87.21	75.55	76.81	78.56	77.78
31	12	5	7	Spruce	M	270.95	229.06	248.64	249.63	264.29	135.48	114.53	124.32	124.82	132.15
32	11	8	3	Oak	B	317.39	303.16	288.90	314.74	299.59	158.69	151.58	144.45	157.37	149.79
33	12	0	12	Pine	C	201.79	166.45	173.20	156.14	155.29	100.90	83.23	86.60	78.07	77.64
34	8	4	4	Oak/Pine	M	121.03	185.26	186.12	175.76	171.33	60.51	92.63	93.06	87.88	85.67
35	11	2	9	Pine	C	179.37	198.11	210.33	180.78	186.99	89.69	99.06	105.17	90.39	93.50
36	12	1	11	Douglas	C	311.04	347.12	337.78	309.13	307.46	155.52	173.56	168.89	154.57	153.73
37	8	6	2	Oak	B	270.46	346.66	309.35	271.32	262.77	135.23	173.33	154.67	135.66	131.39
38	8	7	1	Oak	B	254.54	277.73	262.27	253.72	251.12	127.27	138.87	131.14	126.86	125.56
39	11	0	11	Pine/Larch	C	83.14	122.18	132.85	118.18	123.89	41.57	61.09	66.42	59.09	61.95
40	6	3	3	Oak/Pine	M	137.55	200.52	186.73	168.05	161.86	68.78	100.26	93.36	84.03	80.93